**University of Alberta**

# Development and Modeling of an Impact Test to Determine the Bone-Implant Interface Properties of Osseointegrated Implants

by

**Ryan Clair Swain**



A thesis submitted to the Faculty of Graduate Studies and Research in partial fulfillment of the requirements for the degree of **Doctor of Philosophy**.

Department of Mechanical Engineering

Edmonton, Alberta
Fall 2006

*Your file Votre référence*
*ISBN: 978-0-494-23114-2*
*Our file Notre référence*
*ISBN: 978-0-494-23114-2*

# Abstract

The ongoing need for a clinically effective, non-invasive technique for monitoring implant stability has led to a number of testing methods based on the concept of resonant frequency. Resonant frequency measurements provide an indirect measure of the bone-implant interface. To date, these measurements do not provide specific detail of the changes occurring due to modeling/remodeling at the interface.

In this study an impact testing method based on the Periotest® handpiece has been developed and with the use of a four degree of freedom analytical model has led to a method of directly estimating the bone-implant interface properties. The technique is applied in a variety of *in vitro* tests to gain an understanding of the parameters influencing the measurements and to provide a measurement protocol. The impact technique, protocol and model are then used *in vivo* to evaluate the interface properties of Bone Anchored Hearing Aid (BAHA®) implants in twelve patients at installation, 1, 2, 3, 6 and 12 month intervals.

Analytical model estimates of the interface stiffness *in vitro* found the interface stiffness of FRB-10 modeling material to be 7.5–7.7 GPa which is comparable to the 9.3 GPa modulus of elasticity. *In vivo*, the average interface stiffness for the patients at implant placement was 5.0 GPa which increased to 7.9 GPa by the twelfth month. Individual interface stiffness values showed a great deal of variation within the first three months, with changes up to 7 GPa

occurring.

The developed impact testing technique is shown to be accurate and sensitive in the measurement of interface properties both *in vitro* and *in vivo*. The analytical model provides a method to extract basic mechanical properties of the interface from the impact measurements. Ultimately, the testing method is shown to have clinical significance as it provides a means to track the mechanical properties of the bone-implant interface in a noninvasive way in patients.

This is dedicated to those who have given me the strength to continually move forward throughout my life. To my friends, my supervisors, and most importantly, my parents.

# Table of Contents

# List of Tables

# List of Figures

# Nomenclature

| | |
|---|---|
| CT | Contact time. |
| PTV | Periotest® value. |
| ISQ | Inter Stability Quotient used with the Osstell®. |
| $\omega_r$ | Measured frequency of impact for each mode. |
| $\omega_1$ | Measured first mode frequency of impact. |
| $p_r$ | Model frequency of impact for each mode. |
| $p_1$ | Model first mode frequency of impact. |
| $m_R$ | Mass of Periotest® impacting rod. |
| $m_I$ | Mass of the implant. |
| $m_A$ | Mass of the abutment. |
| $J_I$ | Centroidal mass moment of inertia of the implant. |
| $J_A$ | Centroidal mass moment of inertia of the abutment. |
| $K_S$ | Stiffness of the Periotest® impact rod. |
| $K_D$ | Stiffness of the abutment (local deformations). |
| $K_T$ | Torsional spring at the implant-abutment joint. |
| $K_F$ | Stiffness provided by implant flange. |
| $k$ | Stiffness of bone-implant interface (per unit length.) |
| $X_1$ | Variable describing horizontal position of impacting rod. |
| $X_2$ | Variable describing horizontal position of implant-abutment. |
| $\Theta_1$ | Variable describing angular rotation of the abutment. |
| $\Theta_2$ | Variable describing angular rotation of the implant. |
| $O$ | Position along abutment longitudinal axis that crosses the line of impact. |
| $G_1$ | Location of abutment center of gravity. |
| $G_2$ | Location of implant center of gravity. |
| $L_A$ | Length of the abutment. |
| $L_I$ | Length of the implant. |
| $L_O$ | Distance from the top of the abutment to the Periotest® rod striking position. |
| $L_C$ | Distance implant top is above the supporting material surface. |
| $b$ | Radius of implant-abutment system. |
| $h_1$ | Vertical distance from $O$ to $G_1$. |
| BAHA® | Bone anchored hearing aid. |
| $\beta$ | Damping proportionality constant. |
| $\nu_r$ | Damping ratio for each mode. |

# Chapter 1

# Introduction

The use of oral mucosa penetrating (permucosal) implants to replace lost teeth has a long history, dating back to the Maya Indians (100–1500 AD) who reportedly constructed root shaped implants out of obsidian. Despite the early start, dental implants did not see common clinical use until the 1960s. Through this period dental implants were of a wide variety of designs such as subperiosteal, blade, and cylindrical designs. Many of the implants were seldom based on scientific design. Moreover, the implants were introduced into clinical use with little or no scientific scrutiny. While some patients reportedly experienced benefits from these implants, many patients experienced implant failure. Some implant failures resulted in extensive bone loss and produced irreversible defects and complications. In 1978 the National Institutes of Health (NIH) sponsored a conference to provide the dental consumer, practitioner and researcher with defined criteria for implant success (NIH, 1978). The conference recommendations included the criteria that a dental implant should provide functional service for five years in 75% of the cases. The conference evaluated subperiosteal, staple/transosteal, vitreous carbon and blade implants and concluded from the data presented that there was no statistically valid reason to support the use of these implants.

In May 1982 a meeting held in Toronto, Canada presented a new type of implant technology based on the work of Professor Per-Ingvar Brånemark, a Swedish medical researcher. Professor Brånemark realized that bone adhered to titanium optical chambers while studying bone healing. Brånemark then performed a number of animal and clinical trials implanting various shapes and sizes of titanium into bone. In some cases the bone adhered so well to the titanium implant that it could not be removed without causing fractures in the surrounding bone, while the interface between the implant and bone remained intact. An example of an implant with the bone adhered to the titanium

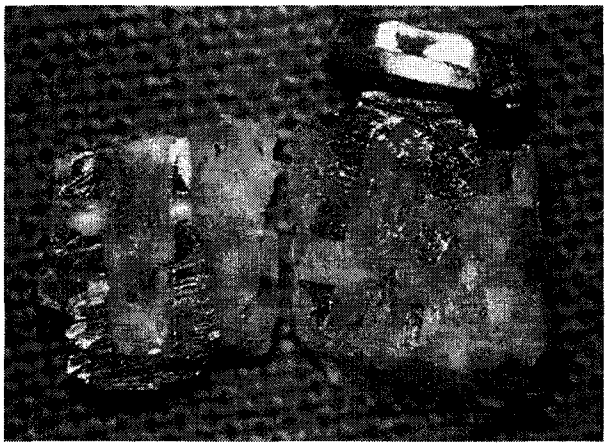

Figure 1.1: Titanium fixture removed and cut into two halves with bone tissue firmly-and inseparably-adhering to the titanium surface (from Brånemark, P-I. et al. 1985).

surface is shown in Figure 1.1. Brånemark referred to this direct structural and functional connection between the bone and the titanium implant surface as *osseointegration* (Brånemark, P-I. et al., 1985). Brånemark found that what was needed to achieve osseointegration included a biocompatible material, minimum surgical trauma to the bone with drilling temperatures below 44°C and an immobile healing phase (Brånemark, P-I. et al., 1985). In support of the concept of osseointegration Adell, R. et al. (1981) released a study of "osseointegrated" titanium implants which achieved a 91% success rate in the human mandible for more than 15 years. Unlike previous implant designs, the osseointegrated titanium implants were developed using meticulous scientific work. Furthermore, the titanium implants could satisfy the criteria set forth at the 1978 NIH conference.

Due to the high success rates and longer retention time of the osseointegrated titanium implants presented at the 1982 Toronto meeting, the number of intraoral and extraoral treatment options utilizing this technology has steadily increased. Titanium implants are currently utilized in a variety of different clinical applications such as:

1. tooth replacement (single tooth, multiple tooth, full arch),
2. for use in maxillofacial rehabilitation (jaw defects due to cancer or trauma),
3. anchorage in orthodontic treatment,

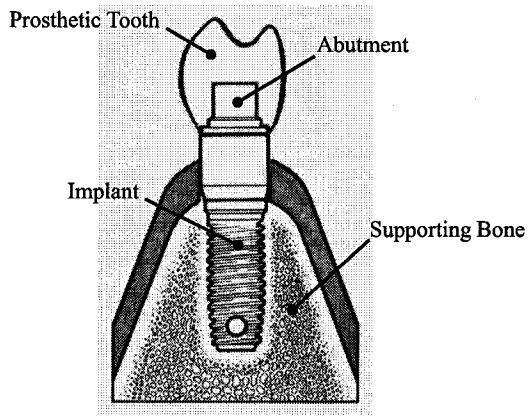


Figure 1.2: Percutaneous implant-abutment system used for tooth replacement (modified from Brånemark, P-I. et al. 1985).

4. facial prosthesis retention,

5. as an anchor and transmission path for Bone Anchored Hearing Aids (BAHA®),

6. orthopedic applications (arthroplasty, amputations).

A typical implant and abutment system used for tooth replacement is shown in Figure 1.2.

Today, osseointegrated implants are typically installed in either a one-stage or two-stage surgery. During implant installation a hole is drilled and gradually deepened and widened until it reaches the appropriate diameter. The hole is then tapped and the implant is placed (the tapping step is not always completed, as some implants are self tapping). After installation the implant is covered and left to heal between 3-6 months, depending on the quality of the bone (longer healing times may be required for patients with poor or irradiated bone). The second stage of the surgery occurs after the healing period, where the implant is uncovered and an external component termed an abutment is attached. In one-stage surgeries the abutment is immediately attached after implant installation. It is generally recommended that after a one-stage procedure the implant is left unloaded for at least three months post surgery to allow osseointegration to take place. Changes to the timing of loading have recently been introduced with loading now being categorized as delayed, delayed-immediate or immediate loading.

Professor Brånemark's aim for osseointegrated implants was to provide stable, safe and reliable anchorage with a predictable duration-without significant complications-for the patient's lifetime (Brånemark, P-I. et al., 1985). The success of these implants is dependant on the quality of the bone-implant interface. To help ensure treatment success there is an ongoing need for a non-destructive and non-invasive technique to monitor the quality of the bone-implant interface to assist clinicians in diagnosing any changes in the status of the interface. Monitoring the interface would allow for decisions to be made on when an implant may be loaded and for any remedial action to be initiated to prevent loss of the implant. It is estimated that more than 500,000 dental implants are used annually in the United States alone. Estimations of the worldwide market for implant-based dental reconstruction products will top $3.5 billion by 2010. As a result of the growing implant market, a number of different implant testing techniques have been developed. Difficulties associated with each of the measurement methods has prevented any one measurement technique from gaining widespread acceptance within the clinical community providing implant care. For the methods presently in use, system models have not been extensively employed leading to incomplete interpretations of the measurement results. This has led to an overall lack of understanding of how implant measurement systems function and how the measurements relate to events at the bone-implant interface.

## 1.1 Literature Review

There are currently a number of methods employed to attempt to evaluate bone-implant quality and quantity. Histology and histomorphometry require specimens of the bone-implant interface to be removed and prepared. Removal torque measures the torsional moment required to rupture the interface of a threaded implant. The invasive or destructive nature of these tests are not well suited for clinical application on patients. This has prompted the development of non-invasive tests that are non-destructive and relatively convenient to employ in a clinical setting. The following provides information on some of the non-invasive, non-destructive techniques that have been developed to evaluate the status of the bone-implant interface. These techniques are reviewed and comments are made on some of the challenges encountered with their use.

### 1.1.1 Radiography and Magnetic Resonance Imaging

Conventional diagnostic techniques, such as radiography and magnetic resonance imaging, are generally able to evaluate bone quantity and in some cases may provide parameters that relate to bone quality (eg. Hounsfield units). These techniques are limited in their ability to monitor the actual bone-implant interface as the implant tends to shield this region resulting in poor image resolution in this vital area (Sundén, S. et al., 1995). Furthermore, images obtained in this manner are costly and high quality radiographs carry the risk of radiation exposure (van Steenberghe, D. and Quirynen, M., 1993).

### 1.1.2 Mechanical Measurement Methods

The need for an inexpensive and non-invasive monitoring technique has spurred the development of dynamic mechanical testing methods. Biological changes to the bone-implant interface are believed to be strongly related to its stiffness and damping properties (Meredith, N., 1997). A well integrated implant is thought to be stiffer and have less damping than one in which osseointegration is lacking or incomplete . The mechanical techniques developed to date, although different in the manner of measurement, are based on determining the resonant frequency of the bone-implant system. These measurements are often carried out with other restorative components (such as attached abutments) or components of the measurement system that require attachment to the implant which affect this measured frequency. Changes in the dynamic response measurements can then be theoretically linked to changes in the stiffness and damping of the implant interface. This, of course, assumes that there are no other changes in the system that may mask those of the interface. For example, Faulkner, G. et al. (1999b) found measurable changes caused by loosening between components.

#### 1.1.2.1 Impedance Head Hammer

Elias, J. et al. (1996) developed a dynamic modal testing technique for the assessment of the bone-implant interface. This technique used an impedance head hammer to measure the implant vibration. The device was hinged at the non-contact end to allow the hammer to swing in a pendulum-like manner. Upon impact, the piezoelectric crystal in the impact hammer head produced a voltage proportional to the force at the hammer tip. Figure 1.3 illustrates an ideal force time curve of a strike where $F_p$ is the peak force, $T_c$ is the time of contact and the area under the curve represents the impulse of the

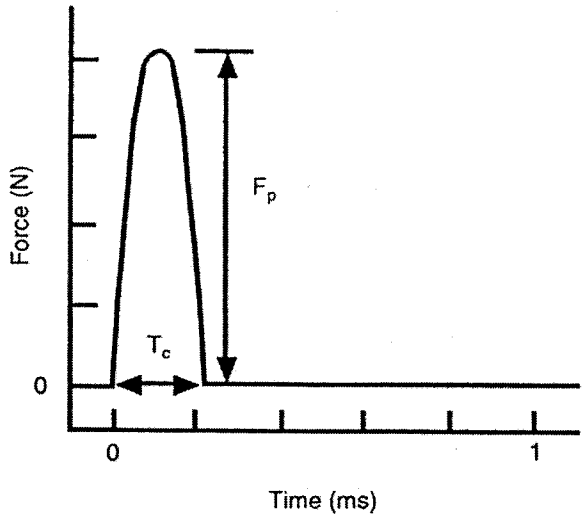


Figure 1.3: Ideal force time curve for a dynamic modal test (from Elias, J. et al. 1996).

strike. The force curve was also displayed in the frequency domain as the force power spectrum, the power spectrum representing the root-mean-square (RMS) average of the fast Fourier transform (FFT).

A theoretical model of the system shown in Figure 1.4 was developed in which the implant was supported by a translational spring and a rotational spring. Since the impedance hammer and components of the implant system were assumed to be significantly stiffer than the interface surrounding the implant, the implant and hammer were assumed to be rigid bodies. The theoretical model was compared to an experimental impact to validate the model. From the comparison, it was determined that the implant primarily rotated within the interface, which indicated that the rotational spring governed the motion. A modified rotation-only model was then developed. From this model when the force-time curve resembles a sinusoid, the peak force of the force-time curve is proportional to the 6 dB roll-off of the power spectrum. The 6 dB roll-off frequency is the frequency at which the power spectrum has decreased 6 dB from the maximum value. At this frequency, the RMS amplitude of vibration is one-half of the maximum value. According to the analysis presented, both the 6 dB roll-off and the peak force are proportional to the square root of the rotational stiffness of the interface. Therefore, both these

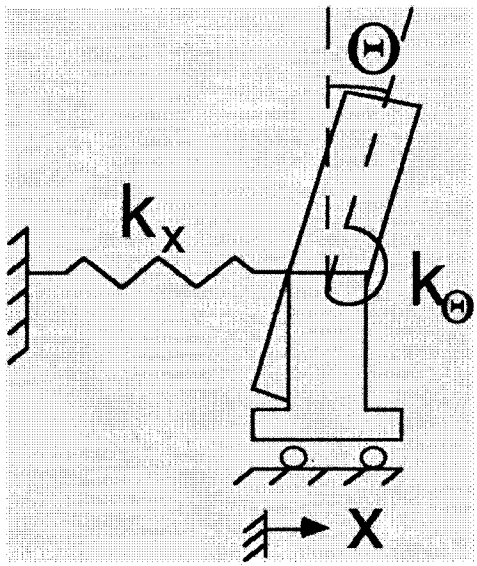


Figure 1.4: Two degree of freedom model developed by Elias, J. 1994.

parameters could be used to assess the rotational stiffness of the interface.

The authors measured the 6 dB roll-off frequencies in two *in vitro* tests. In the first test, eight Ø3.75 x 7 mm long Brånemark implants were installed into four cubes of cortical bone and four cubes of trabecular bone. The 6 dB roll-off frequency was then determined to be from 2.27 to 3.72 kHz for the trabecular samples and from 4.17 to 6.15 kHz for the cortical samples. The authors claimed the differences between the cortical and trabecular frequency readings supported the theory that the 6 dB roll-off frequency could be used to distinguish different interface properties of bone.

The second *in vitro* study was performed using the same trabecular bone samples as the previous test, but this time the implants were cemented into the bone samples. The cemented interfaces were tested at time intervals between 10 to 90 minutes as the cement cured to determine the sensitivity of the testing technique to direct changes in the interface stiffness. The authors determined that as the cement cured the 6 dB roll-off frequency rapidly increased and reached a maximum value similar to that found for cortical bone.

The developed modal testing technique was shown *in vitro* to be capable of assessing frequency changes of implants in different supporting bone structures. Further, the theoretical analysis done could relate the frequency measurements directly to a rotational stiffness of the interface. The *in vitro* success of this testing technique, however, did not translate into clinical success. This may have been due to limitations caused from the inherent geometry, size and method of testing with the impedance head hammer.

#### 1.1.2.2 Impact Head with Acoustic Pickup

Another resonant frequency technique has been presented by Huang, H.-M. et al. (2002) which also utilizes an impulse force hammer. In this technique the impulse force hammer is used to impact an implant-abutment system and the vibration signal is recorded by a non-contacting microphone. The acoustic signal is then analyzed to determine the resonant frequency of the implant-abutment system. The experimental set-up used is shown in Figure 1.5.

To test the reliability of the testing technique the resonant frequency of seven Ø3.75 x 10 mm long implants placed into cubic bone blocks was determined. The measured resonant frequency values were then compared to finite element simulations of the experiments. The authors determined that the finite element simulated results were similar to the measurements. The finite element model was then used to predict how bone quality and density affect the measured resonant frequency. The bone quality simulations used different elastic modulus values to determine how the modulus values relate to the

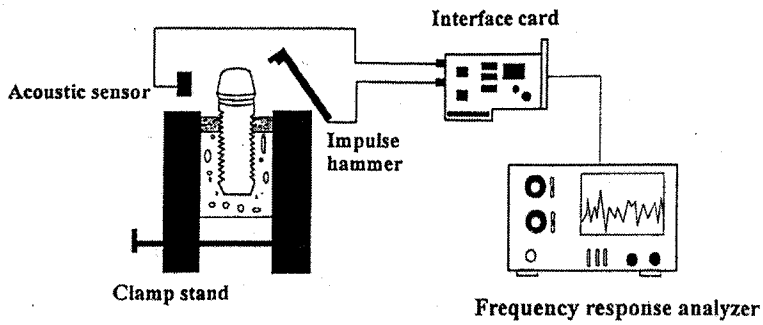


Figure 1.5: Device set-up used for resonant frequency experiments (from Huang, H.-M. et al. 2002).

resonant frequency. For these simulations, the properties of the interface were assumed to be the same as the surrounding bone. The authors determined that higher modulus bone provides higher resonant frequencies than lower modulus bone. The simulations also determined that as the bone density was reduced that resonant frequency decreased in a linear manner.

In a follow up study Huang, H.-M. et al. (2003) tested the impact head with acoustic pickup method *in vivo* by installing six Ø3.75 x 10 mm long implants in six rabbit tibias. The implants were installed using two different methods, three of the rabbits had a 3.75 mm hole drilled while the other three rabbits had larger 5 mm hole drilled. The oversized 5 mm holes were drilled to simulate poor initial starting stability. During implant installation a rabbit with a 3.75 mm drilled hole was removed from the study because the tibia fractured. Resonant frequency measurements were then taken every week for 14 weeks as the implants healed. Two of the implants placed in the oversized 5 mm holes showed a decrease in the resonant frequency at the one week measurement before failing in the second week. The remaining implants showed increases in the resonant frequency until reaching a plateau. Based on the findings the authors concluded that their technique is a reliable and accurate method for the early assessment of the osseointegration process.

Although this technique has been tested and modeled with a finite element analysis *in vitro* followed by *in vivo* tests there are currently no reports of the use of this method in clinical trials.

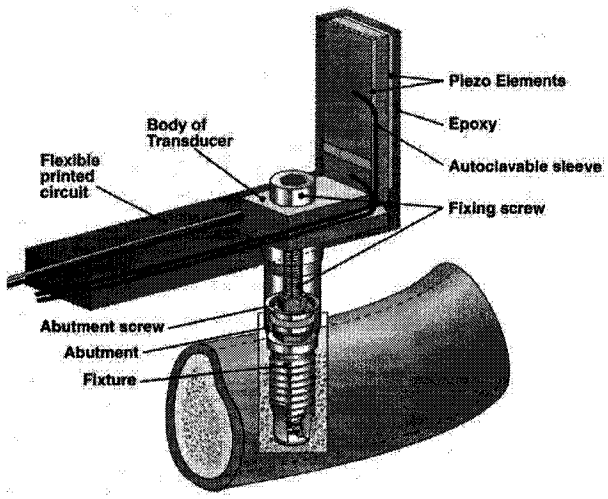


Figure 1.6: Schematic of resonance frequency transducer-abutment-implant system (from Meredith, N. 1997).

#### 1.1.2.3 Osstell®

The only commercially available system designed specifically for the assessment of implants is the Osstell® which was developed by Professor Neil Meredith. The Osstell® consists of a transducer which is attached to the implant or abutment as shown in Figure 1.6. The transducer consists of two piezoceramic elements attached to a cantilever beam. One of the piezocermaic elements is excited over a range of frequencies with a sinusoidal signal and the other measures the frequency response of the system. At system resonance there is a marked increase in amplitude and change in phase of the received signal which is illustrated in Figure 1.7.

Meredith, N. et al. (1996a) tested the sensitivity of the Osstell® to the effects of different length implants, torque between the transducer-implant and interface stiffness changes *in vitro*. The different length implants were mounted in an aluminum block with different heights of the implants left exposed. Epoxy was used to ensure as uniform an interface as possible between the implant and the aluminum. The *in vitro* testing found that the resonant frequency of the implants decreased as the exposed height increased. The system resonant frequency appeared insensitive to the torque values of 10, 20, 32 and 45 Ncm tested. Sensitivity to changes in interface stiffness was

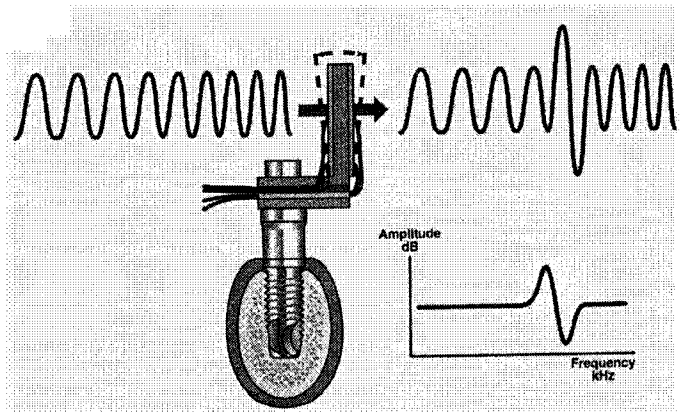


Figure 1.7: Schematic of resonance frequency transducer-implant system showing input signal, output signal and frequency response curve (modified from Meredith, N. 1997).

tested by taking resonant frequency measurements over time on an implant placed in self polymerizing acrylic resin. As the resin cured the resonant frequency increased demonstrating that the resonant frequency measurement was sensitive to changes in interface stiffness.

The Osstell® was first tested *in vivo* by Meredith, N. et al. (1997). In a group of 9 patients who had a total of 56 implants placed, resonant frequency measurements were taken at implant installation and then repeated 8 months later. It was found that implant stability increased over the 8 month period for all except for two failed and one rotationally mobile implant. In a more recent study including 36 patients Bischof, M. et al. (2004) found that implants placed in the mandible had higher readings than those planted in the maxilla and that measurements were higher in better quality bone.

The Osstell® has been used to evaluate the effect on implant stability of an one-stage approach with the implants being immediately loaded (Friberg, B. et al., 1999). The results showed that a small but statistically significant reduction of implant stability occurred during the first 15 weeks. The patients were brought back for measurements after one year of loading and no further changes could be seen. These results have led to a number of studies, some of which show no difference between immediate and delayed loaded implants in the jaw (Bischof, M. et al., 2004) and others which show an increased failure rate over one year of immediate loading (Glauser, R. et al., 2004).

Further testing with the Osstell® to determine if measurements at implant installation can predict the level of osseointegration have been completed. Glauser, R. et al. (2004) found no significant difference between implants that failed and those that did not from the initial readings. Measurements by Friberg, B. et al. (1999) and Glauser, R. et al. (2004) do, however, show that failing implants demonstrate a decrease in stability at measurements prior to failure.

It appears that there have been relatively few studies modeling the Osstell® numerically. In Meredith, N. (1997) it is mentioned that the resonant frequencies and corresponding mode shapes of the original transducer were investigated using finite element analysis. While the mode shape data is provided, the frequency data is not present. Further, the finite element simulations were done for a fixed transducer and comparisons of the finite element simulation to *in vitro* or *in vivo* experiments were not completed. Another finite element study was more recently completed which determined that the Osstell® transducer is suited for follow-up in time stability measurements on a single implant but not for quantitative comparison of the stability of implants (Pattijn, V. et al., 2006). In essence, the resonant frequency values of different implants cannot be directly compared due to geometry differences such as length and diameter. Further, according to the finite element study by Pattijn, V. et al. (2006) the Osstell® transducer does not always measure the first bending mode of the system as stated by Meredith, N. (1997). The finite element simulations by Pattijn, V. et al. (2006) did not compare simulation results with *in vitro* or *in vivo* Osstell® measurements, so the claims have not been tested. However, if the Osstell® is indeed measuring different modes of vibration unbeknownst to operators the resonant frequency data may be miss-interpreted. This may explain why in Nedir, R. et al. (2004) only 8.7% of the measurements on mobile implants (as determined by movement by hand) by the Osstell® registered low readings.

One of the main goals cited by Meredith in developing the Osstell® was to provide a quantitative measure of implant stability and osseointegration (Meredith, N., 1997). While the Osstell® does provide a quantitative measure of the resonant frequency of an implant-abutment-transducer system, it does not provide a quantitative measure of the bone-implant interface properties. Increases or decreases in resonant frequency over time (assuming no changes in the measurement system) are believed to be related to changes in the interface properties. However, there is currently no method to directly relate the resonant frequency to the interface properties. Determining this relationship experimentally is further complicated by the way the Osstell® presents the resonant frequency measurement. The commercially available Osstell® converts

the resonant frequency into a unique measurement scale called the "Implant Stability Quotient" or ISQ. The ISQ is meant to be a more user-friendly scale, having integer values between 0 and 100. The Osstell® uses a set of calibration constants that are unique to each transducer lead to convert the resonant frequency to an ISQ (Hurst, S., 2002). By converting the resonant frequency into an ISQ in this manner the Osstell® may be artificially influencing the relationship between the measurements and the interface properties.

With so many clinical trials utilizing the Osstell® more numerical work needs to be completed and compared to *in vitro* and *in vivo* testing. This will provide a better understanding of the information the resonant frequency measurements provide such as:

- which frequency modes the system is measuring,
- how internal components affect the resonant frequency readings,
- how the resonant frequencies can be related to the interface stiffness.

While the Osstell® has been clinically effective in identifying implants in danger of failing, a large majority of implant restorations used for dental applications are cemented/non-retrievable prostheses and the Osstell® cannot be attached once the prosthesis is in place.

#### 1.1.2.4 Periotest®

One of the earliest and most widely published mechanical techniques is the Periotest®, which utilizes a handpiece to accelerate a small metal rod towards an implant-abutment system and initiate an impact. The Periotest® was originally developed to provide a quantitative measure of the mobility of teeth (Lukas, D. and Schulte, W., 1990). The authors describe the operation of the Periotest® in detail.

> The impact rod, which has a mass of 8 g, moves along an almost frictionless guide. The impact rod is drawn by a magnetic coil into the inside of the handpiece against the rear stop. When the dentist pushes the starting button, the impact rod is accelerated by a propulsion coil. Before the front of the impact rod comes out of the handpiece, the propulsion field is turned off. The velocity of the impact rod remains constant after this time, and the distance between the handpiece and the tooth under percussion can vary within a certain range without affecting the results of the measurement. This feature is important for the free-hand application

> of the Periotest®. The deceleration of the impact rod on impact with the tooth is measured by an accelerometer installed in the impacting rod. This operation is repeated for each tooth 16 times in 4 seconds.
>
> from Lukas, D. and Schulte, W. (1990)

To relate the impact accelerometer signal to tooth mobility, the signal was put through a low-pass filter and a number of signal characteristics were identified. Figure 1.8 shows a filtered accelerometer signal and the characteristics that were evaluated for a single tooth impact. The nine characteristics examined were:

- $t_o$, time from the beginning of the impact until the zero crossing (the time of contact);
- $s(t_o)$, the standard deviation of $t_o$;
- $t_{min}$, the time until the first minimum;
- $t_{max}$, the time to the maximum;
- $s(t_{min})$, the standard deviation of $t_{min}$;
- $s(t_{max})$, the standard deviation of $t_{max}$;
- $A_{min}$, minimum amplitude;
- $A_{max}$, maximum amplitude;
- $A_{max}/A_{min}$, the ratio of these two amplitudes.

The signal characteristics were then correlated to the clinical mobility of the teeth as defined by the authors (Lukas, D. and Schulte, W., 1990). The correlation determined that $t_o$ - the contact time, provided the best correlation with tooth mobility.

The relationship between contact time, $t_o$, and the clinical tooth mobility was represented as a formula. The degrees of mobility were broken down into a range of convenient values called Periotest® values or PTVs. The contact time (in seconds) was then directly related to the Periotest® values.

For PTV > 13

$$\text{PTV} = 10 \cdot \sqrt{\left(\frac{\text{contact time}}{6\text{x}10^{-5}} - 8.493\right)} - 4.17$$

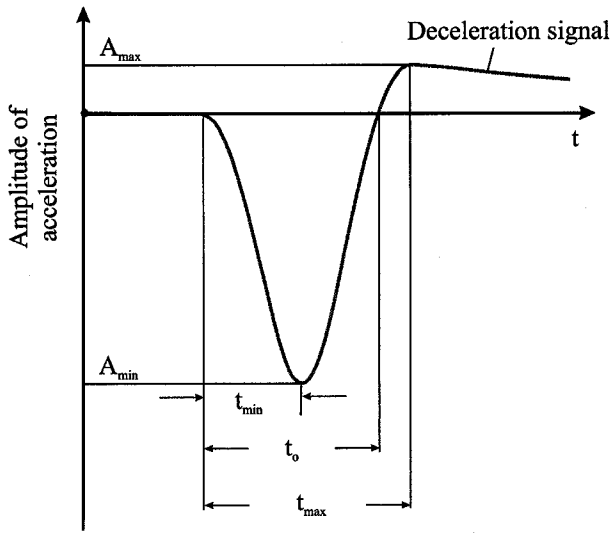


Figure 1.8: Impact accelerometer signal and identified characteristics (modified from Lukas, D. and Schulte, W. 1990).

For PTV < 13

$$\text{PTV} = \frac{\text{contact time}}{2\text{x}10^{-5}} - 21.3$$

The relationship between mobility and PTV is such that an increase in PTV corresponds to an increase in mobility. Stiffer teeth would have a lower PTV value and more mobile teeth would have a higher PTV value. The relationship between contact time, PTV and degree of mobility is shown in Table 1.1. While the table shows PTV values from -8 to 30 the Periotest® device has a range from -8 to 50 PTV.

While the Periotest® was originally developed to measure the mobility of teeth, numerous investigators have considered its use for implants with varying degrees of success (Olivé, J. and Aparicio, C., 1990; van Steenberghe, D. et al., 1995; Carr, A.B. et al., 1995). To test an implant with the Periotest® an abutment is connected and measurements are taken on the abutment. While initial testing by Olivé, J. and Aparicio, C. (1990) suggested the Periotest® was an objective and easily applied measurement technique for stability assessment there are a number of problems associated with its use. Derhami, K. et al. (1995) found that while inter-operator and inter-instrumental variability did not influence PTVs, the vertical measurement point on the abutment proved to have a strong effect on PTV readings. Faulkner, G. et al. (2001) also noted

Table 1.1: The relation between contact time, Periotest value and degrees of mobility. The Periotest values are the degrees of mobility multiplied by ten (from Lukas, D. and Schulte, W. 1990)

| Contact time (ms) | Periotest value | Degree of mobility |
|---|---|---|
| 1.21 | 30 | III can be moved with labial pressure |
| 0.86 | 20 | II mobility can be seen |
| 0.65 | 10 | I mobility can be felt |
| 0.502 | 4 | 0 stable anchored |
| 0.426 | 0 | Ankylosis (without periodontium) |
| 0.266 | -8 | |

that the PTV is very sensitive to the position at which the Periotest® impacts the abutment but also found it to be sensitive to angulation of the handpiece.

While some researchers were suggesting that the PTV is sensitive to clinical parameters, others found that the Periotest® lacked the sensitivity to measure implants. Aparicio, C. (1997) found that in a study of 1182 Brånemark implants the PTV values range between -7 and 0 in the mandible and -7 to +1 in the maxilla. As the Periotest® only provides integer values this range of implant PTV values in the mandible and maxilla is quite limited. The reduced range for implants as compared to teeth (which can have PTV values between -8 and 50) indicates that the Periotest® may lack the resolution required to monitor subtle but important changes in the bone-implant interface.

## 1.2 Development of an Improved Impact Technique Based on the Periotest®

While there are a number of difficulties associated with the Periotest®, the Periotest® handpiece does provide a convenient means to dynamically excite the implant-abutment system in areas that may be inaccessible to the Osstell® or impact hammer devices. An impact technique based on the use of this handpiece also has the distinct advantage that it can be used on implant-abutment systems with non-retrievable or cemented restorations.

Some of the difficulties associated with the Periotest® may be due to the history of the device. As previously mentioned, the Periotest® was originally developed to measure tooth mobility and had been used clinically for this pur-

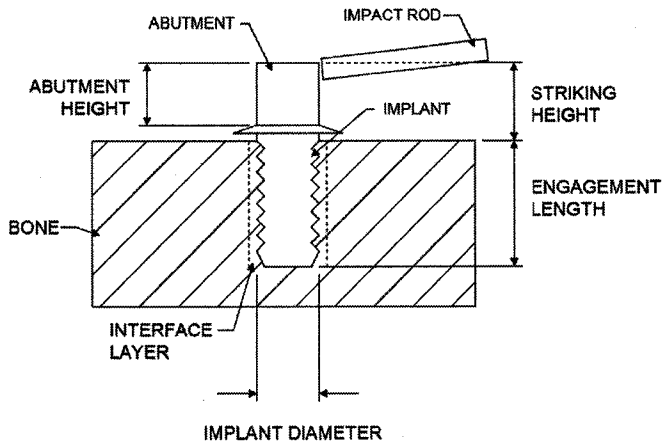


Figure 1.9: Typical implant-abutment system being impact tested by the Periotest®

pose. When the Periotest® was suggested for use on implants the first studies immediately applied it clinically. The Periotest® device did not have the *in vitro*, *in vivo*, numerical and analytical evaluations required for an understanding of how the measurement results relate to the bone-implant interface. It is important to remember that the Periotest® measurements are not based on an understanding of the impact response, but are from a correlation of signal parameters to tooth mobility as defined by Lukas, D. and Schulte, W. (1990).

After the Periotest® was introduced for use in implant measurements one of the first researchers to attempt to model the system to better understand the measurement technique was Kaneko, T.M. (1994). The system shown in Figure 1.9 was modeled analytically as a single degree of freedom system in which the implant-abutment was assumed to be a rigid body pinned at the implant base. The model was used to estimate the force of the impact and relate PTV to an equivalent interface stiffness. However, analytical results were not compared directly to *in vitro* or *in vivo* experiments.

More recently, Giannitsios, D. (2001) developed a two degree of freedom analytical model which is shown in Figure 1.10. In this model the implant and abutment were considered as one rigid body which was modeled as a uniform solid cylinder. Since the Periotest® impact rod is restricted to a linear path by the handpiece it was modeled as a particle. The bone-implant interface was modeled as a series of springs acting along the length of the implant as shown.

The springs were arranged in both the vertical, and horizontal directions with each direction having a different stiffness value represented as a stiffness per unit length. The damping effects of bone were modeled as a viscous damping per unit length shown with dashpots in Figure 1.10. The model provided rotation and horizontal translation and model results were correlated to *in vitro* measurements for extraoral implant-abutment systems. The accelerometer signal from the Periotest® unit (which had been passed through a low-pass filter) was collected and analyzed separately allowing non-integer PTV values to be determined, thereby increasing the resolution of the Periotest® for implants. Giannitsios found that for the extraoral implant-abutment systems the two degree of freedom model could be reduced to a single degree of freedom system if the mass of the implant and abutment are assumed to be negligible compared to that of the impacting rod. The *in vitro* testing and model results determined that implant diameter, length of engagement between bone and implant, angulation of Periotest® handpiece and striking height along abutment all influenced the output of the Periotest®. An *in vivo* patient study was also attempted, however, results were inconclusive due to what the authors believed was a poor understanding of the effects due to measurement parameters and lack of a rigorous clinical testing protocol. To reduce these effects a strict measurement protocol was developed based on the *in vitro* testing. In a follow up study, Hurst, S. (2002) applied the improved protocol and resolution of the testing technique *in vitro* and *in vivo*. The results indicated that due to the strict protocol and improved Periotest® resolution obtained by analyzing the accelerometer signal separately the enhanced Periotest® exhibited the same abilities to measure changes in implant geometric parameters as the Osstell®.

While improvements to the PTV resolution and strict protocols for the instrument use are important, it is possible that some of the inconsistencies in the reported Periotest® results are also due to a lack of understanding of how the system being measured responds when excited. Further, all the testing results utilizing PTVs use the low-pass filtered accelerometer signal described by Lukas, D. and Schulte, W. (1990). An un-filtered or "raw" accelerometer signal collected directly from the Periotest® handpiece is compared to the low-pass filtered (conditioned) accelerometer signal in Figure 1.11. There are significant differences between the two signals shown. The raw signal has a very visible higher frequency component that is removed in the conditioned signal. The conditioned signal also noticeably increases the apparent contact time, which is taken to be the time required for the acceleration signal to return to zero after the impact has been initiated. The filtering process may be removing important information about the response of the implant-abutment system, as well as significantly affecting the contact time which is subsequently used to

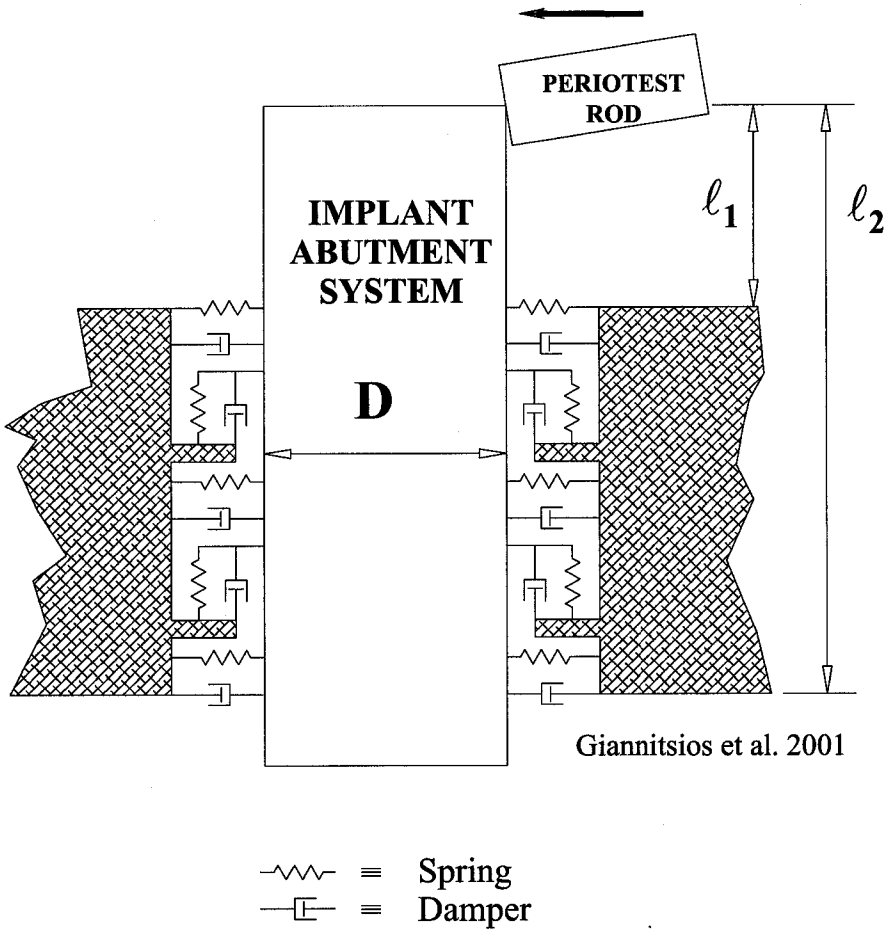


Figure 1.10: Proposed model in Giannitsios, D. (2001).

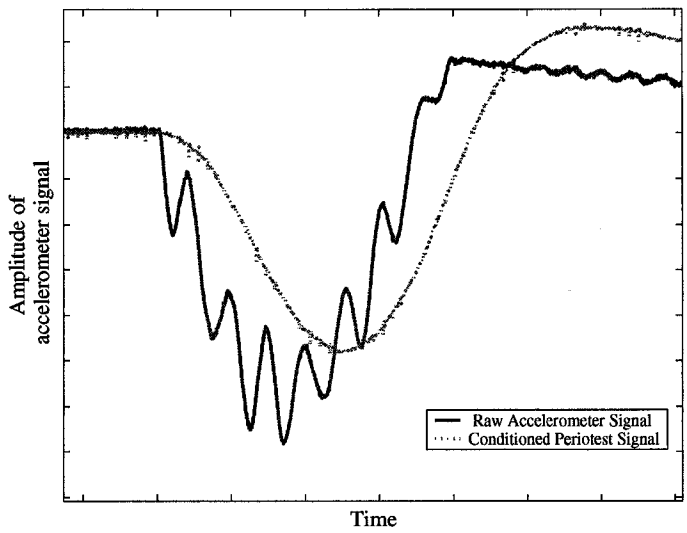


Figure 1.11: Raw accelerometer signal collected from the Periotest® handpiece and conditioned accelerometer signal used to calculate PTV.

calculate the Periotest® value (PTV). This calls into question previous model results by Kaneko, T.M. (1994) and Giannitsios, D. (2001) which make use of the PTV, as the filtered signal (and subsequent PTV calculation) does not appear to represent the true dynamics of the impact.

The high frequency component in the raw accelerometer signal has been shown in Periotest® measurements conducted by Meredith, N. (1997). However, Meredith did not provide any explanation for its appearance or of its significance. Impedance hammer measurements by Elias, J. et al. (1996) also had a higher frequency component which can be seen in Figure 1.12. Elias, J. et al. (1996) suggested that the high frequency term was the result of the hammer losing contact with the abutment.

Studies by Hurst, S. (2002) and Jones, S. (2005) have attempted to explain the high frequency component found in the raw acceleromter signal by modeling the Periotest® system. Hurst, S. (2002) used the raw accelerometer signal with a two-degree of freedom model based on the model developed by Giannitsios, D. (2001). Hurst, S. (2002) included the mass of the implant and abutment in the Giannitsios, D. (2001) model. The model then remained a two-degree of freedom system and returned two natural frequencies. Hurst, S. (2002) theorized that the two natural frequencies from the model could

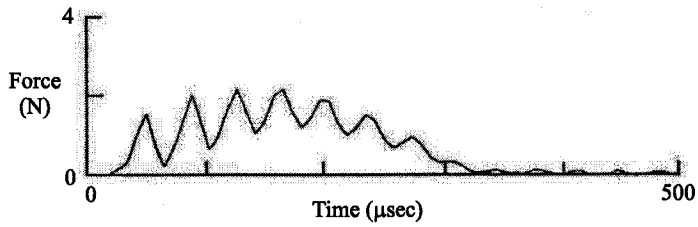


Figure 1.12: Typical force curve produced for a lateral tap of a Brånemark implant in a cube of trabecular bone with the impedance head hammer (modified from Elias, J. et al. 1996).

Table 1.2: Natural frequencies of Ø3.75 x 10 mm intraoral implant with 10 mm abutment as reported by Hurst, S. (2002).

| Mode | Theoretical Frequency (Hz) | Empirical Frequency (Hz) |
|---|---|---|
| 1 | 1000 | ~1070 |
| 2 | 14000 | ~17000 |

explain the two frequencies found in the raw accelerometer signal. *In vitro* testing by Hurst, S. (2002) on a Ø3.75 x 10 mm intraoral implant with 10 mm abutment resulted in measurement and model results as shown in Table 1.2. While the results from Hurst, S. (2002) are promising, the model first and second mode results were compared to a single implant-abutment system *in vitro*. A more detailed study with a range of different length implants is required to verify these results. A finite element analysis (FEA) for the system shown in Figure 1.9 was completed and the transient simulation of the impact by the rod was compared to the raw accelerometer signal by Jones, S. (2005). FEA simulations provided additional evidence that the higher frequency term was a second mode of vibration of the system during impact. It was shown that the stiffness of the components affects the overall response including the higher frequency component in the raw accelerometer signal. One difficulty in using the finite element technique was the very long processing time required and the necessity of doing a somewhat imprecise frequency analysis on the transient response.

Based on the work by Hurst, S. (2002) and Jones, S. (2005) the high frequency component in the raw accelerometer signal may be a second mode of vibration occurring during impact. Developing an impact technique based

on the Periotest® un-filtered raw accelerometer signal would have three main benefits over the existing Periotest®:

1. The measurement would more accurately reflect the true dynamics of the impact.
2. The poor resolution of the current PTV scale could be improved.
3. The higher frequency component in the signal may give additional information about the system.

Further modeling of the system could then relate the raw accelerometer response to the bone-implant interface properties.

## 1.3 Thesis Goal

The present thesis is concerned with the development and modeling of an impact technique utilizing the accelerometer data provided by the Periotest® handpiece in order to determine the bone-implant interface stiffness and damping properties of percutaneous titanium implants. A measurement technique was developed based on the raw accelerometer impact response with the aims of providing a reliable, non-invasive, rapid and relatively inexpensive measurement system that is suitable for use with a variety of different implant-abutment applications including non-retrievable systems. A theoretical model of the dynamics during impact was used to directly relate the measured impact response to the implant interface properties. The impact testing technique and model were tested *in vitro* using two general types of percutaneous implants, intraoral implants used in orthodontic treatments and flanged extraoral implants for use with bone anchored hearing aids (BAHA®). Further, the impact test and model were used to determine the bone-implant interface properties of BAHA® patients *in vivo*.

## 1.4 Thesis Outline

Chapter 2 describes some of the experimental equipment and procedures used in the *in vitro* testing to determine the impact response of implant-abutment systems. The methods of calculating the fundamental frequency from the Periotest® rod impact as well as higher frequency components found in the raw accelerometer signal are discussed. Experiments comparing the raw and filtered accelerometer signal contact times to the contact time of a strain gauged

abutment are outlined. The measurements used in evaluating the different clinical variables used in determining a measurement protocol are then presented.

In Chapter 3 results from the *in vitro* testing described in Chapter 2 are presented. The first set of results is used to compare the raw and conditioned accelerometer signals to determine the effects of filtering. The effects of different clinical variables on the fundamental frequency are then presented. Finally, a measurement protocol based on the *in vitro* testing is presented.

The analytical model of the impact from the Periotest® is presented in Chapter 4. The development of the model and the tests used to determine model parameters are presented. The model is then used to estimate the interface stiffness of intraoral and extraoral implants placed in a modeling material based on the measured impact response. Model predictions using the determined interface stiffness are compared to *in vitro* tests over a range of implant-abutment geometries as outlined in Chapter 2.

In Chapter 5 the analytical model is used to investigate changes in the resonant frequencies of implants due to simulated changes in the bone-implant interface. Two changes in the bone structure are modeled, changes in supporting bone stiffness and marginal bone losses around the neck of the implant. The model is then used to predict the influence of a flange on the raw accelerometer response at different interface stiffnesses.

Chapter 6 presents *in vivo* impact test results. Twelve patients treated with Bone Anchored Hearing Aid (BAHA®) implants had longitudinal measurements on the implants at installation, 1, 2, 3, 6 and 12 months. The analytical model is used to determine the stiffness and damping properties of the bone-implant interface over time.

Chapter 7 summarizes the results of the work, presenting the advantages and limitations of the developed impact technique and analytical model. Conclusions and recommendations for future work are also discussed.

# Chapter 2

# *In Vitro* Testing Methods

This chapter outlines the *in vitro* experimental equipment and procedures that were developed in order to gain a better understanding of the accelerometer impact response that occurs during a Periotest® measurement. The basic equipment used for all the *in vitro* tests is described in the first section of this chapter. The methods of calculation of the fundamental frequency, along with higher frequency components present in the raw accelerometer signal are described in the next section. Following that, experiments done to evaluate the accuracy of the present Periotest® calculation of the contact time used for calculation of the so called Periotest® value (PTV) are outlined. Finally, tests to determine the effect of various clinical variables on the raw accelerometer signal contact time are outlined.

## 2.1 General Testing Equipment

### 2.1.1 Modifications to the Periotest®

A Periotest® unit was modified as shown in Figure 2.1 to allow collection of two different accelerometer signals. One signal corresponds to the conditioned signal that the Periotest® uses in determining the so called PTV. This signal is measured directly from pin #1 of the M8930 Lf 442CN integrated circuit (located at Position A in Figure 2.1) as described in Giannitsios, D. (2001). The raw accelerometer signal is collected prior to the signal entering the circuit board at Position B. The purpose of collecting the two signals is to compare the conditioned accelerometer signal used in the calculation of the Periotest® value (PTV) with the raw accelerometer signal collected before any signal processing is done. The data acquisition systems that collect the accelerometer signal data utilize the port at Position C.

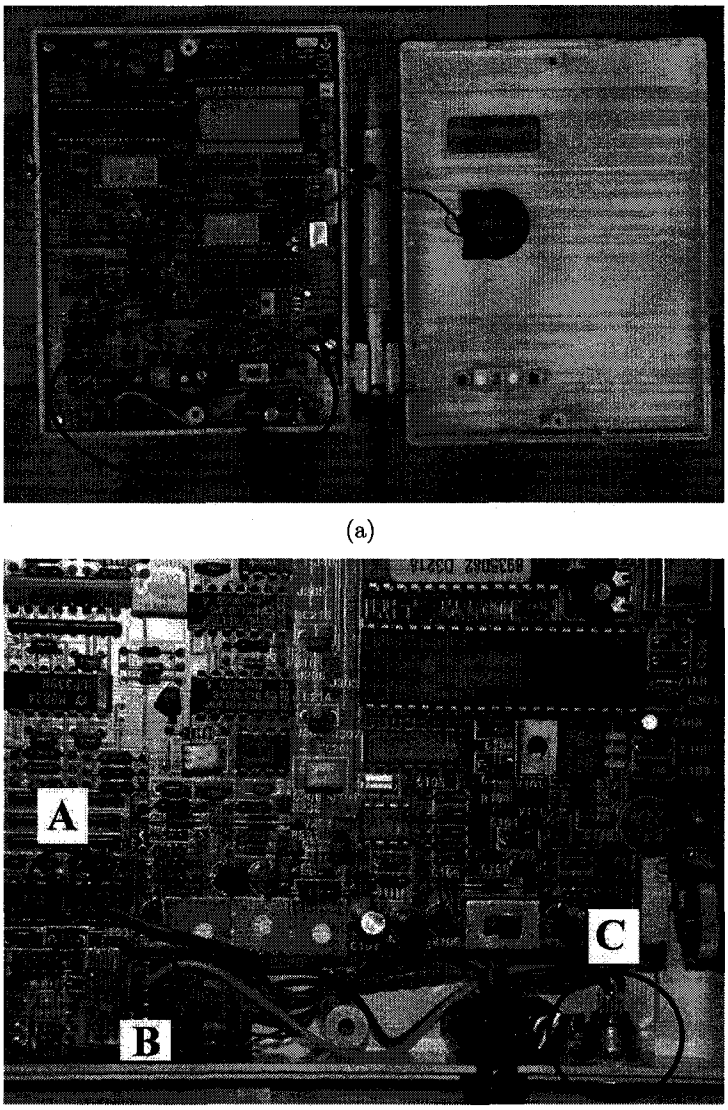


(a)

(b)

Figure 2.1: a) Modifications to the Periotest®. b) Close-up view of the modifications. The conditioned signal is from Position A, the raw signal is from Position B, and the coupling to the data acquisition systems attaches at Position C.

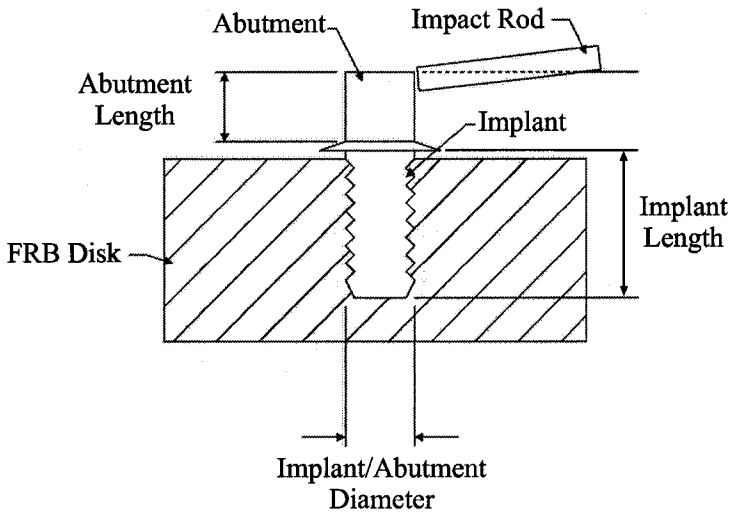


Figure 2.2: Implant-abutment System.

### 2.1.2 *In-Vitro* Implants and Abutments

Three different implant-abutment models were used to simulate a range of bone-anchored implant applications. The *in vitro* models were previously developed for use in measurements with the Periotest® and Osstell® (Giannitsios, D., 2001; Hurst, S., 2002). A set of three different implants (a Ø3.75 x 4 mm flanged extraoral implant and two Ø4 x 10 mm intraoral implants, Brånemark system, Nobel Biocare, Canada) were mounted in 41 mm diameter disks of Photoelastic FRB-10 plastic (Measurements Group Inc, Raleigh North Carolina, USA). FRB-10 was chosen as its elastic modulus of 9.3 GPa is of the same order as that reported for cortical bone and for dense cancellous bone (1.3 - 25.8 GPa) (Cowin, S. and Guo, X., 2001). A schematic of the implant-abutment system is shown in Figure 2.2.

The implants were installed into the disks using drills and taps equivalent to the *in vivo* installation protocol. However, one of the 10 mm implants was not completely threaded into the FRB disk, and was left with the head being 3 mm above the FRB surface as shown in Figure 2.3. Implants were secured to the disks with epoxy cement (5 Minute Epoxy, Devcon, Danvers, MA, USA) to ensure as uniform an interface as possible.

Standard abutments with lengths of 4, 5.5, 7, and 10 mm (Nobel Biocare, Toronto, Ontario, Canada) were coupled to the implants as required with

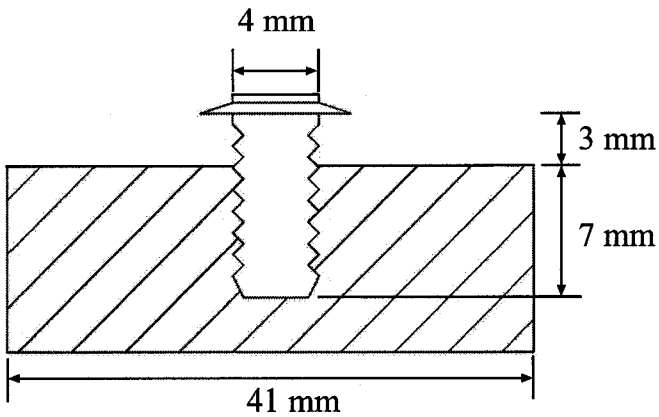


Figure 2.3: Ø4 x 10 mm implant 3 mm proud.

either a hand torque (DIB 038, Nobel Biocare, Toronto, Ontario, Canada) or an electric torque controller (Nobel Biocare, Götenborg, Sweden) with a torque of 20 Ncm unless otherwise specified.

### 2.1.3 Periotest® Handpiece Stand

*In vitro* testing utilized the same testing apparatus (shown in Figure 2.4) previously used by Derhami, K. et al. (1995), Giannitsios, D. (2001) and Hurst, S. (2002). The FRB implant disks were mounted in a circular steel base that was in turn mounted to a stand which also held the Periotest® handpiece. The stand allowed for vertical and horizontal positioning of the handpiece as well as the ability to control its angulation in the vertical plane. The holder had two micrometer attachments (Vickers Instrument Ltd., England) to control the horizontal and vertical displacements. Angulation of the handpiece was set with the use of a standard bevel gauge.

The Periotest® handpiece was aligned so that the striking rod would impact the superior corner of the abutment being measured. The horizontal distance between the tip of the Periotest® and the abutment was set to 1.5 mm, within the recommended 0.5 to 2.0 mm range specified in the Periotest® operating instructions. The handpiece was given a slight inclination so as to ensure only one point of contact between the Periotest® striking rod and abutment as recommended in Giannitsios, D. (2001).

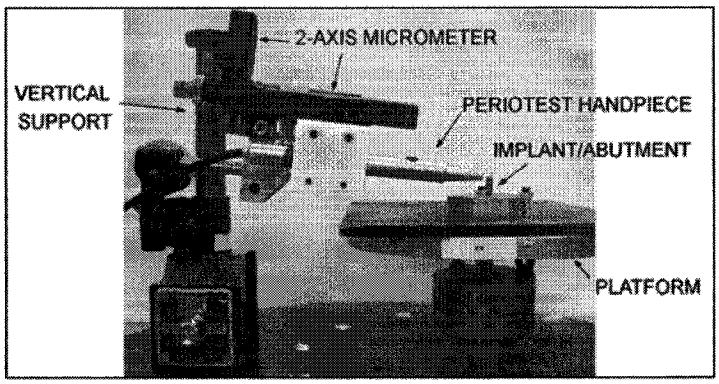


Figure 2.4: Experimental Setup

### 2.1.4 Strain Gauged Abutment

To independently monitor the motion of the implant-abutment system, a strain gauge was mounted on a separate abutment to measure the bending strain during the impact by the Periotest® rod. A linear strain gauge, type EA-06-015EH-120 (Micro-Measurements, Measurements Group Inc., Raleigh, North Carolina, USA), was mounted vertically on the exterior surface of a 5.5 mm abutment (as shown in Figure 2.5) on the side impacted by the rod . The strain gauge was attached using M-Bond 200 (Micro-Measurements) adhesive and then coated with M-Coat D acrylic (Micro-Measurements). The lead wires from the strain gauge were 0.005-inch diameter type 7X00157 (California Fine Wire, California, USA).

The strain gauge lead wires were connected to an Intertechnology 2150 System multi-channel signal conditioner/amplifier (Intertechnology Inc., Don Mills, Ontario, Canada) whose output was subsequently read by the data acquisition system.

### 2.1.5 Data Acquisition Systems

#### 2.1.5.1 Microstar Data Acquisition System

The data acquisition system utilized for multi-channel measurements (such as for simultaneous measurements of strain abutment, raw accelerometer and conditioned accelerometer data) was a DAP 5400a sampling card (Microstar Laboratories, Bellevue, WA, USA) connected to an Intel Pentium 4, 2.20 GHz

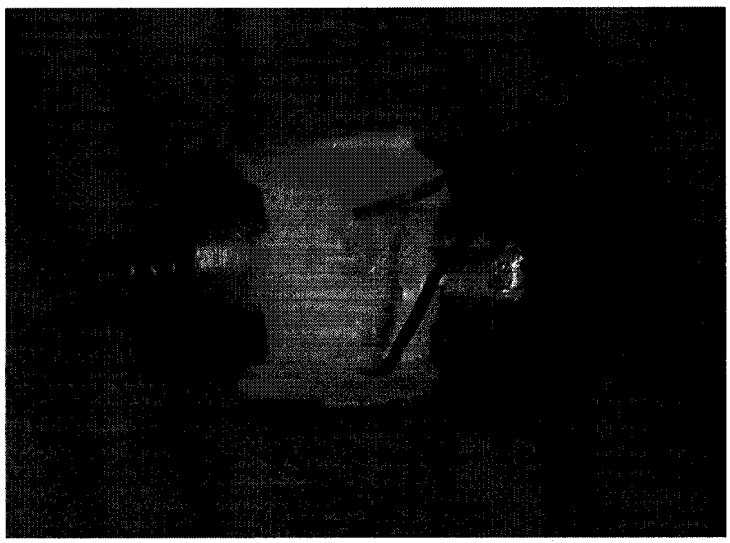

Figure 2.5: A 5.5 mm abutment with strain gauge attached.

desktop computer. Custom software was used to collect and save the data from the measurements.

The data acquisition system was set with a sampling rate of 2 MHz for each of three channels, which could simultaneously monitor the strain gauge signal, the raw accelerometer signal and the Periotest® conditioned acceleration signal.

#### 2.1.5.2 Instrunet Data Acquisition System

Not all measurements required multiple channel signal sampling with the Microstar system, and the desktop setup provided very limited mobility with the testing apparatus. To provide mobility and ease of measurement setup, single channel raw accelerometer data was collected with an Instrunet analog/digital model 100 sampling system (set to its maximum sampling rate of 167 kHz) connected to a Toshiba Satellite A10 laptop computer. Custom software described in Giannitsios, D. (2001) and Hurst, S. (2002) collected and saved the raw accelerometer data to the laptop.

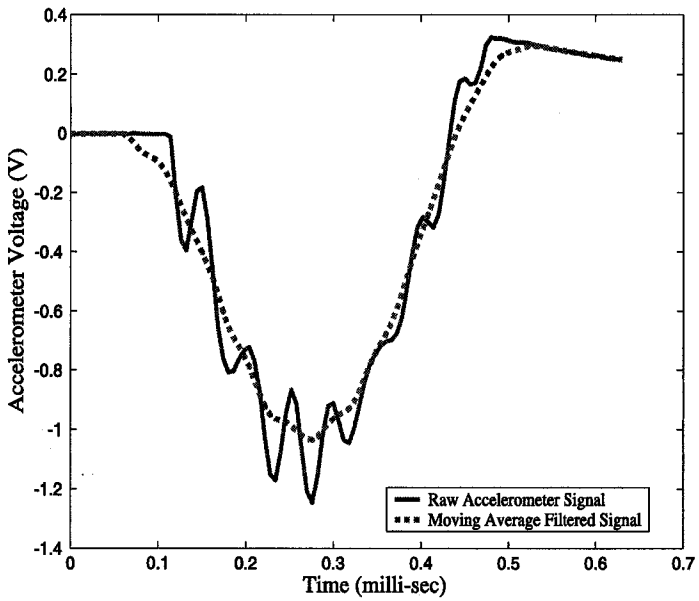


Figure 2.6: Raw accelerometer signal collected from the Periotest® handpiece filtered with a moving average filter.

## 2.2 Measured Signal Analysis

The data collected was analyzed and plotted using Matlab (Mathworks, Natick, Massachusetts, USA). An example of a typical impact plot is shown in Figure 2.6.

### 2.2.1 Accelerometer Signal Analysis of Data Collected with the Microstar Sampling System

#### 2.2.1.1 Moving Average Filter to Remove High Frequency Components

The raw accelerometer signal was shown in Hurst, S. (2002) to have a high frequency component in the signal which can be seen in Figure 2.6. To determine the contact time from this signal, the raw acceleration signal was filtered by a moving average filter to remove higher frequency terms without introducing a phase shift and distortion of the contact time (Oppenheim, A.V. et al., 1983). The signal was post-processed with the use of a custom Matlab pro-

gram. The moving average filter used smooths the data as shown in Figure 2.6 by replacing each data point with the average of the point and eighteen of the neighboring data points (ie. nine points ahead and nine points behind).

#### 2.2.1.2 Comparison of Contact Times

To determine the contact times of the different accelerometer signals collected, an algorithm was developed in Matlab to calculate the contact time (CT) of the impact. Contact times were compared for the conditioned Periotest® signals and the raw accelerometer signals (processed with the moving average filter).

For the conditioned Periotest® accelerometer signal, the algorithm would identify an impact in the signal by detecting a large amplitude disturbance. This occurred at an accelerometer voltage value less than or equal to -0.2 V (ie. if the absolute value of the voltage was greater than or equal to 0.2 V). The algorithm would then step backward until the start of impact corresponding to Point A on Figure 2.7 was found and the voltage value and time was recorded. This point was determined when two conditions were met; the voltage value had to be greater than -0.04 V and the absolute value of the difference between two neighboring points had to be less than $5x10^{-4}$ V. The algorithm would then step forward and record the time corresponding to Point C, which occurred when the voltage value of the signal was greater than or equal to the voltage value recorded at Point A. The contact time, CT, was then calculated as the difference between the times of these two points. The contact time was then averaged over the 16 strikes to give the final contact time.

The algorithm for the raw accelerometer signal also identified an impact as occurring when the accelerometer voltage was less than or equal to -0.2 V. However, to accurately determine the value of the contact time, the effects of the high frequency component were reduced with a moving average filter as outlined in Section 2.2.1.1. This had two main effects: first it made identifying the start of the impact less difficult due to the smoothing effect of the filter, and second it helped to remove the high frequency component in the signal making it easier to identify the end of the impact.

The algorithm determined the start of contact in the moving average filtered signal corresponding to Point A on Figure 2.8 and the end (Point C) the same way as was found in the conditioned signal case. However, as can be seen in Figure 2.8 the moving average filtered signal starts to decrease before the raw accelerometer signal does (ie. Point A on the moving average filter and Point A' on the raw accelerometer signal).

It was previously stated that the moving average filter does not cause a phase shift or distortion in the contact time. However, the contact Point A

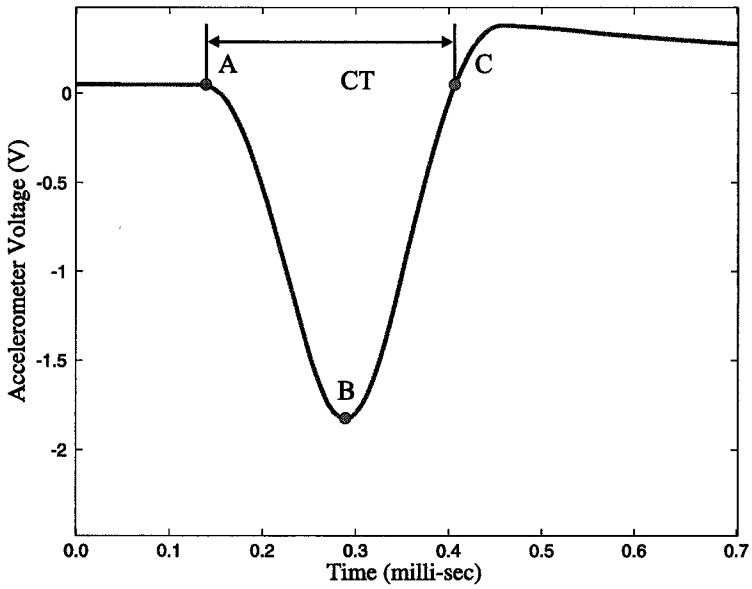


Figure 2.7: Conditioned Periotest® accelerometer signal.

and Point A' do not match when the moving average filter is used. This occurs when the moving average filter first encounters a changing signal. As the filter averages neighboring points before and after, the points after in the raw accelerometer signal start to decrease during the impact so the average of the neighboring values start to decrease. This can be thought of as the moving average filtered signal "foreshadowing" what is going to occur in the raw signal. Once all the points being averaged are part of the impact signal (and not occurring before impact is initiated) there will be no phase shift in the signal.

Since the number of neighboring points the moving average filter uses is known (in this case nine), it is also known that the moving average predicted decrease at Point A' will occur precisely nine time steps after Point A. This identifies Point A' as the start of contact. The end of the impact time is taken from the moving average filtered signal at Point C and the contact time is the time difference between Points A' and C. The contact time for each strike was then averaged over the 16 strikes to give the final contact time.

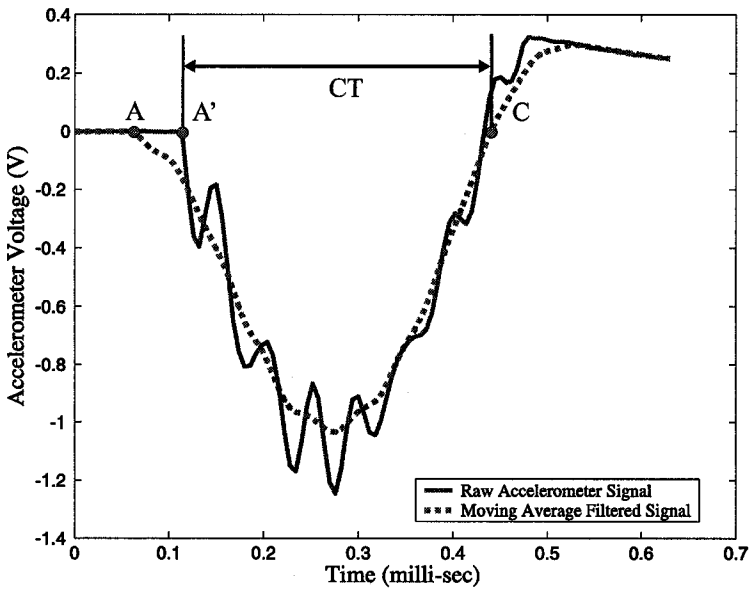


Figure 2.8: Determining contact time of raw accelerometer signal using a moving average filter.

### 2.2.2 Calculation of Fundamental Frequency of Impact from Data Collected with the Instrunet Sampling System

The fundamental frequency of impact of a raw accelerometer signal such as the one shown in Figure 2.6 was found based on the contact time, CT. A Fast Fourier Transform (FFT) analysis was not used to determine the fundamental frequency as the impact consists of only a half period of vibration of the system. Without a full cycle the frequency domain content of the FFT will contain a number of spurious frequency components. To avoid this effect, the fundamental frequency is determined from the contact time of the signal.

The contact time with the Instrunet system was determined in the same manner as described in Section 2.2.1.2 for the Microstar system. However, some modifications to this method were required when used with the Instrunet system. When measuring stiff implant-abutment systems, such as a 10 mm implant with a 3 mm abutment, the moving average filter of the raw signal diverged significantly from the raw signal which can be seen around Point C' on Figure 2.9a. The moving average filter signal shifts to the right of the measured raw signal because the neighboring data points used in the average are well after the rod has lost contact with the abutment. This error becomes significant in this case due to the combination of the short contact time along with the lower sampling speed of the Instrunet system compared to the Microstar system (167 kHz compared to 2 MHz). To reduce the error from averaging points too far from where the rod loses contact, the number of data points used in the moving average filter was based on the minimum number of data points between C' and D' (as shown in Figure 2.9a) for the measurement. For the signal shown in Figure 2.9a, there are three data points between C' and D' therefore the moving average filter used seven data points (the average of the point, three points ahead and three points behind). This reduced the error between the moving average filtered signal and the raw accelerometer signal contact times as shown in Figure 2.9b. For less stiff systems, such as a 4 mm implant with a 10 mm abutment, the number of neighboring points used in the moving average filter was eighteen (the same number of points used with the Microstar system). To increase the precision of the Matlab code for all the Instrunet measurements, the end point (Point C) was determined using linear interpolation between two voltage values bracketing to the starting voltage at Point B.

Once the contact time is determined, the measured fundamental resonant

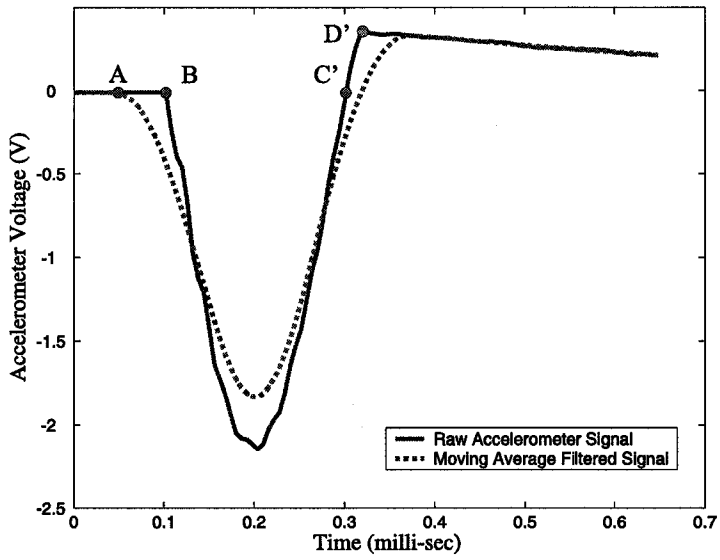


(a)

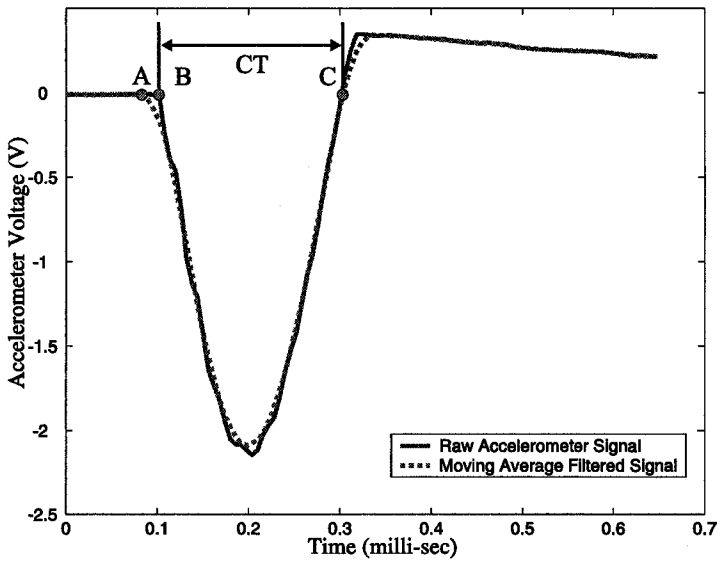


(b)

Figure 2.9: a) The moving average filtered signal diverged from the raw signal at Point C' when the moving average filter was initially used with the Instrunet system. b) The error was reduced by using fewer data points in the moving average filter.

frequency ($\omega_1$) of the system is given by

$$\omega_1 = \frac{1}{2\,(\mathrm{CT})}. \tag{2.1}$$

This measured fundamental frequency calculation was used over a variety of different implant and abutment geometries. During testing, it was found that occasionally during a test of sixteen strikes, an individual strike frequency would be significantly different than the others. To remove outliers, the Matlab code would first immediately remove any strike frequency under 700 Hz, as measured implant frequencies were found to be between 1200-2800 Hz. The code would then calculate an average of the remaining points, and remove any strike frequency more than two standard deviations from the average. If any strikes were removed, the average would be re-calculated and the remaining frequencies would be re-checked. This would continue until all remaining strike frequencies were within the two standard deviations of the average. It should be noted that having one of the sixteen strikes removed was not uncommon. However, it was rare that three or more strikes were removed.

## 2.3 Comparison of Contact Times Between Collected Strain and Acceleration Signals

In this section the measurements to evaluate the Periotest® raw and conditioned signals are outlined. This was done to evaluate the effects filtering has on PTV calculations. The Microstar data acquisition system was used to collect the data for the strain measurements, and for the simultaneous comparison of the raw and conditioned accelerometer signals.

### 2.3.1 Strain Gauge Measurements

Measurements using the strain gauge were completed using the testing apparatus described in Section 2.1.3. The strain abutment was coupled to the 4 mm implant disk with a torque of 20 Ncm. The Periotest® was then used to take an impact measurement by striking the top corner of the abutment.

### 2.3.2 Comparison of Raw and Conditioned Accelerometer Signals

To measure the difference between the raw accelerometer signal and the Periotest® conditioned signal the contact times for three different systems were evaluated:

- 4 mm implant with a 10 mm abutment to simulate a more flexible system (longer contact time),
- 10 mm implant with a 3 mm abutment to simulate a stiffer system (shorter contact time),
- 10 mm implant with a 10 mm abutment to evaluate an intermediate case.

The measurement setup was as described in Section 2.1.3, with impacts occurring on the superior rim of the abutments. Contact times were calculated using the Matlab code outlined in Section 2.2.1.2.

## 2.4 Measurements Utilizing Raw Accelerometer Signals

This section outlines the procedures for the remaining *in vitro* tests completed measuring only the raw accelerometer signal with the smaller, more mobile Instrunet data acquisition system. The measurements were done to develop a measurement protocol and test the measurement system over a range of different implant and abutment geometries. Tests were completed using the different implant systems and abutments outlined in Section 2.1.2 placed into the testing stand outlined in Section 2.1.3. Frequencies of the impacts were determined using the Matlab code outlined in Section 2.2.2.

### 2.4.1 Repeatability and Reproducibility of the Measurement System

To evaluate the repeatability and reproducibility of the measurement system, seven sets of five consecutive measurements were taken on the flanged Ø3.75 x 4 mm implant with a 5.5 mm abutment. The handpiece was set at an angle of 5° from an axis perpendicular to the implant-abutment system. The distance between the end of the handpiece and the abutment was set to 1.5 mm. The vertical micrometer was set so that the Periotest® rod would strike the rim of the 5.5 mm abutment. Between each set of five readings the stand was moved and then re-aligned to strike the rim of the abutment in an attempt to replicate the previous set of readings.

### 2.4.2 Evaluation of Clinical Variables

The experimental apparatus was used to evaluate several clinical variables that potentially could affect the readings. These variables include:

1. Handpiece distance from abutment,
2. Abutment torque,
3. Striking height (position along the abutment where contact is made),
4. Angulation of handpiece.

To evaluate the effect of these variables, one variable was changed while attempting to hold all other variables constant. Figure 2.10 illustrates the tests done on handpiece distance, striking height and handpiece angulation. Unless stated otherwise, measurements were done on the Ø3.75 x 4 mm flanged extraoral implant by striking the top rim of a 5.5 mm abutment torqued to 20 Ncm.

#### 2.4.2.1 Handpiece Distance

The Periotest® instructions recommend that the handpiece be held a distance of 0.5 to 2.0 mm from the object being measured. To determine the effect of variations in this distance, measurements were taken at distances of 0.5, 1.0, 1.5, 2.0, and 2.5 mm from the 4 mm implant/5.5 mm abutment system. Five readings were taken at each of these distances.

#### 2.4.2.2 Abutment Torque

To determine the effect of abutment torque on the resonant frequency, the 5.5 mm abutment was torqued to the 4 mm implant system at 5, 10, 15, 20, and 25 Ncm. Five consecutive measurements were done at each of these values. Torque values were measured with a TorsionMaster Testing System (MTS Systems Corp, Eden Prairie, Minnesota, USA).

#### 2.4.2.3 Striking Height

For these readings, a 10 mm abutment replaced the 5.5 mm abutment used in previous measurements, as the 10 mm abutment allowed for a greater variation of the striking height. The abutment was attached to the implant with a torque of 20 Ncm. Measurements were taken striking the top of the abutment and then lowering the handpiece distances of 0.5, 1, 1.5, 2, 3, 4, 5, and 6 mm. Five readings were taken at each height.

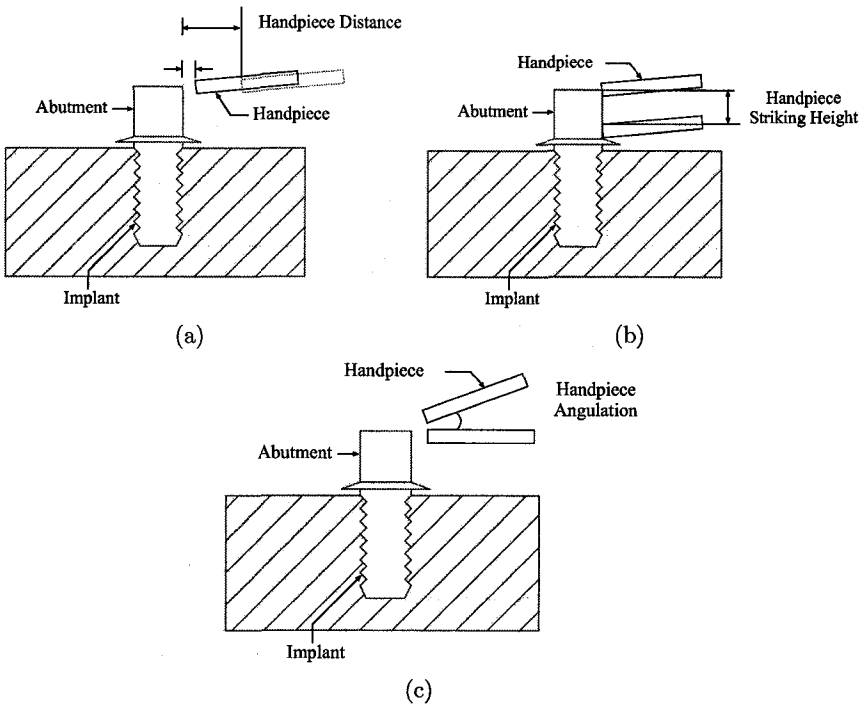


Figure 2.10: Clinical variables. a) Handpiece distance from the abutment. b) Handpiece striking height. c) Angulation of the handpiece.

#### 2.4.2.4 Angulation of the Handpiece

The Periotest® instructions recommend an angulation of ±20° from the horizontal. To determine the effects of angulation, five consecutive readings were done at 0, 1, 2, 3, 4, 5, 10, 15, and 20° (0° corresponding to when the handpiece is perpendicular to the abutment). The angulation of the handpiece was controlled using a standard bevel gauge (Figure 2.4 shows the Periotest® handpiece with a 5° angulation). Measurements were done on the 4 mm implant with the 5.5 mm abutment.

### 2.4.3 Measurements On Different Implant/Abutment Geometries

The following sections include the procedures for a number of measurements on a Ø3.75 x 4 mm flanged extraoral implant and two Ø4 x 10 mm intraoral implants (one of which was set 3 mm proud to the disk surface). For all measurements the horizontal distance of the handpiece was set at 1.5 mm and angulation of the handpiece was set to 3°.

#### 2.4.3.1 Striking Height

Measurements at different striking heights along a 10 mm abutment for the Ø3.75 x 4 mm flanged extraoral implant and fully engaged Ø4 x 10 mm intraoral implant cases were done. The measurements were taken by striking the top corner of the abutments and then lowering the handpiece 0.5 mm until a significant change in the first mode frequency was determined. The handpiece was then lowered 1, 2, 3, and 4 mm from this point and readings were recorded. Five readings were taken at each height.

#### 2.4.3.2 Abutment Sizes

Both the Ø3.75 x 4 mm flanged extraoral implant and fully engaged Ø4 x 10 mm intraoral implant had 4, 5.5, 7 and 10 mm abutments connected to 20 Ncm. Each implant then had a set of five measurements on the top rim of each abutment.

#### 2.4.3.3 Changes in Engagement Length

To test the effects of changes to the amount of implant supporting material (engagement length), measurements were done on the 10 mm implant that was 3 mm proud (shown in Figure 2.11). Five resonant frequency measurements

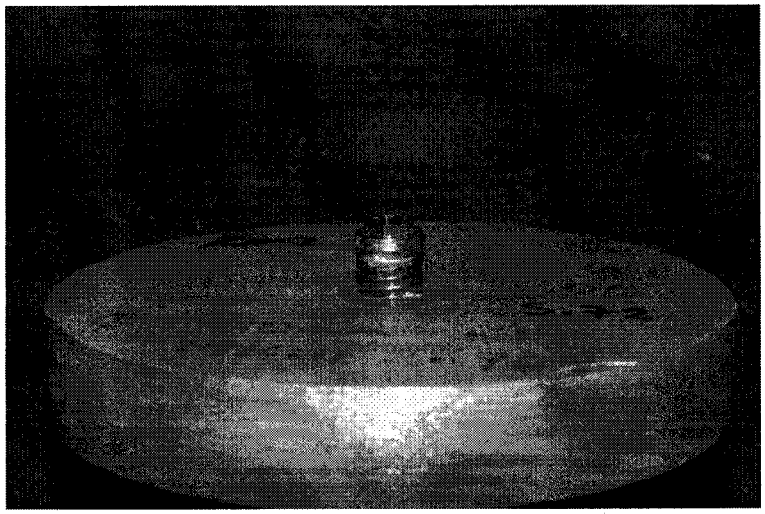

Figure 2.11: Ø4 x 10 mm implant set 3 mm proud.

were taken on the top rim of 4, 5.5, 7 and 10 mm length abutments which were torqued to the implant with 20 Ncm.

# Chapter 3

# Development of a Measurement Protocol For Impact Testing of Percutaneous Implant Integrity

Part of the process in developing an improved impact technique is determining the limitations of the Periotest® handpiece as well as the entire system and to consider modifications which may make its use more appropriate. This chapter presents the results from a number of the experiments described in Chapter 2 to reduce errors associated with the impact measurements. The first set of results compare the raw and conditioned accelerometer signals. The following section presents fundamental frequency measurement results based on the raw accelerometer signal. The *in vitro* measurement results lead to the development of a handpiece measurement protocol to minimize measurement errors by improving measurement precision. While an improved measurement protocol will aid in minimizing measurement errors, some variation in the measurements will persist. To quantify the clinical variation that may be present in measurements the results from tests by four experienced clinicians utilizing the developed protocol are presented.

## 3.1 *In Vitro* Periotest® Signal Analysis

The strain gauged abutment described in Section 2.1.4 and the tests outlined in Section 2.3.1 were used to provide measurements in which both the accelerometer and strain gauge outputs could be simultaneously monitored. The strain gauge was used as an independent measure of the time the impact rod was in contact with the abutment, permitting a direct comparison of the contact

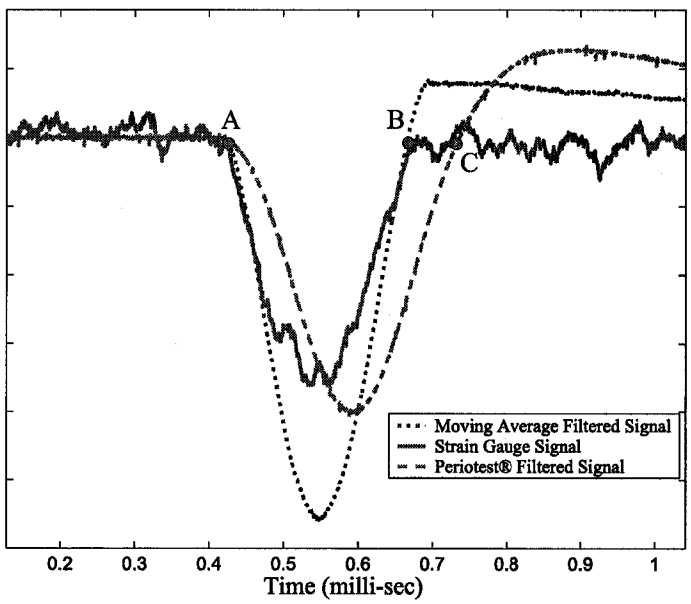


Figure 3.1: Strain gauge, moving average filtered and conditioned Periotest® signal readings for a 4 mm implant with 5.5 mm abutment.

time between the different methods. The raw accelerometer signal was filtered with the moving-average filter to remove the higher frequency component as described in Section 2.2.1.1.

The results of the simultaneous strain gauge, moving average filtered accelerometer signal and conditioned Periotest® signal measurements for a typical impact event are illustrated in Figure 3.1. The Periotest® rod begins contact with the abutment at Point A, as indicated by all three signals. The contact time based on the strain gauge signal matches the moving average accelerometer signal almost identically (difference between Point A and Point B), while the Periotest® conditioned signal shows a significantly longer contact time shown as Point C. The difference between Point B and Point C was measured to be 0.07 milli-sec. While this value may not seem large, the contact time between Point A and Point B for this strike was 0.25 milli-sec, resulting in a 28% longer contact time between points A and C. In terms of PTV, the Periotest® conditioned signal produces PTV value of -5 while the contact time based on the moving average and strain gauge signals produces a PTV value of -9.

One explanation for the difference between the moving average filtered accelerometer signal and the conditioned Periotest® signal contact time is the filtering method used. The moving average filter minimizes any distortion to the contact time as discussed in Section 2.2.1.1. Many common filters, such as a Butterworth or Chebyshev filters, have a phase shift that can affect the contact time. Furthermore, the amount of phase shift is dependant on the frequency of the signal, at different frequencies there will be different amounts of phase shift. The higher the measured frequency, the more phase shift is present. This means for measurement systems with greater mobility (less stiff) there may be little phase shift due to filtering. Since the Periotest® was originally developed to measure tooth mobility (with teeth having much more mobility than implants) the developers may not have been concerned with the effects of filtering on the accelerometer signal.

The strain gauge signal was not filtered so there is no distortion in the contact time from the strain data. The agreement between the strain gauge signal and the moving average filtered signal provides evidence that the actual contact time is between Points A and B in Figure 3.1.

Once it was determined that the Periotest® conditioned signal could be significantly different from the raw accelerometer signal, measurements to quantify the extent of the difference were done on different implant-abutment geometries as described in Section 2.3.2. The results of the measurements are shown in Figure 3.2. The largest difference in contact time was 88 $\mu$s (the 10 mm implant with a 3 mm abutment), which is over 40% of the moving average filtered value.

The analysis of the accelerometer signal from the handpiece, coupled with that from the strain gauge mounted on the abutment (Figure 3.1), showed that the moving average filtered signal based on the raw accelerometer signal is closer to the actual contact time of the implant-abutment system. Therefore it provides a more representative measure of the first mode resonant frequency (and thus the stiffness) of the system. In addition, it was found that the differences between the conditioned signal used by the Periotest® to calculate the PTV and the true signal can be significant - especially for stiffer implant-abutment systems. The results in Figure 3.2 show that as the stiffness of the overall system increases the difference between the Periotest® conditioned signal and the moving average filtered signal increases. The difference was 8% for a 4 mm implant and a 10 mm abutment, while for the 10 mm implant with a 3 mm abutment this difference increased to 40%. As a result, to be as effective as possible in detecting clinically relevant changes in the implant interface the raw accelerometer signal should be used.

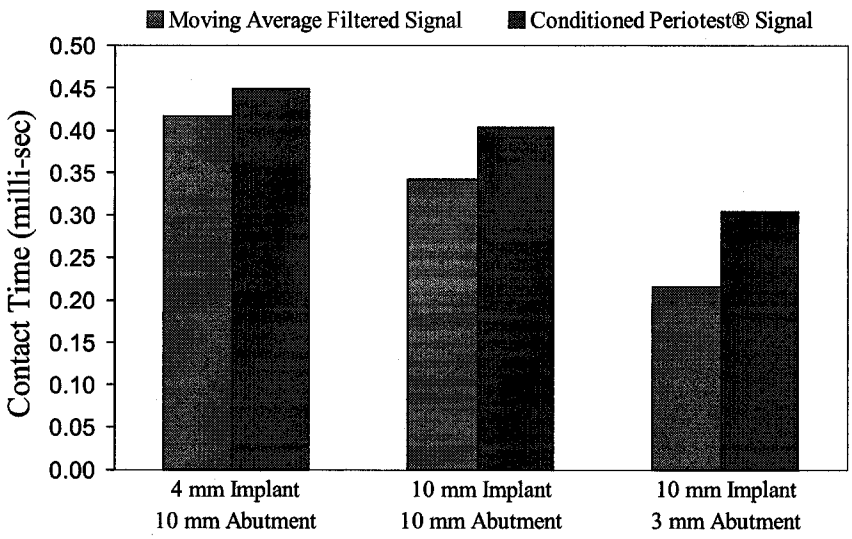


Figure 3.2: Comparison of contact times in milli-seconds of the moving average filtered signal to the conditioned Periotest® signal.

Previous results from Giannitsios, D. (2001) indicated that the conditioned Periotest® signal matched early strain gauge data collected. However, the strain abutment used for this testing was a 10 mm abutment, coupled to an 4 mm extraoral implant. This "less stiff" system minimized the difference between the strain gauge and conditioned accelerometer signal, and without knowledge of a raw accelerometer signal, further testing was not completed. The strain gauge data presented in this section was for a shorter abutment simulating a "more stiff" system, which more clearly demonstrates the difference between the conditioned Periotest® signal and the collected strain data.

## 3.2 Development of an Improved Measurement Method Based on the Raw Accelerometer Signal

Periotest® measurements on implants have PTV's which are significantly lower than for natural teeth due to bone being a much stiffer supporting structure than periodontal ligaments. Since the Periotest® has a built in lower PTV limit of -8 and only produces integer values, there is a limited range of PTV readings available for a typical implant application. This limited range does not provide enough resolution to monitor subtle changes in the bone-implant interface over time. To overcome this, Giannitsios, D. (2001) and Hurst, S. (2002) outlined a method to increase the resolution of the Periotest® based on the contact time of the conditioned Periotest® signal. In addition, it was previously shown that the conditioned Periotest® signal introduces a significant phase shift in the accelerometer signal which produces a distortion of the contact time. While this distortion may not be important for natural teeth with relatively long contact times, it becomes very significant for the smaller contact times associated with implant measurements.

This section concentrates on an improved method of measuring implant stability based on the raw accelerometer signal. The results are reported in terms of the fundamental frequency of the impact, obtained from the raw accelerometer data as outlined in Section 2.2.2.

### 3.2.1 Repeatability and Reproducibility of the Measurement System

The repeatability and reproducibility measurements discussed in Section 2.4.1 are shown in Figure 3.3. As discussed in Section 2.4.1, between each trial of five readings the stand was moved and then re-aligned to strike the rim of the abutment in an attempt to replicate the previous set of readings. Each column in Figure 3.3 represents the average of five readings with each reading consisting of sixteen impacts. The error bar on each column represents the standard deviation of the readings. The mean resonant frequency across all columns (7 trials of 5 readings for each trial) was found to be 2083 $\pm$ 12 Hz. Within a single column the largest standard deviation was 12 Hz. Of the seven trials, the lowest average value was 2070 $\pm$ 12 Hz (Trial 7) and the highest average reading was 2095 $\pm$ 3 Hz (Trial 1).

The results shown in Figure 3.3 demonstrate that when handpiece measurement variables (such as striking height and handpiece angulation) are

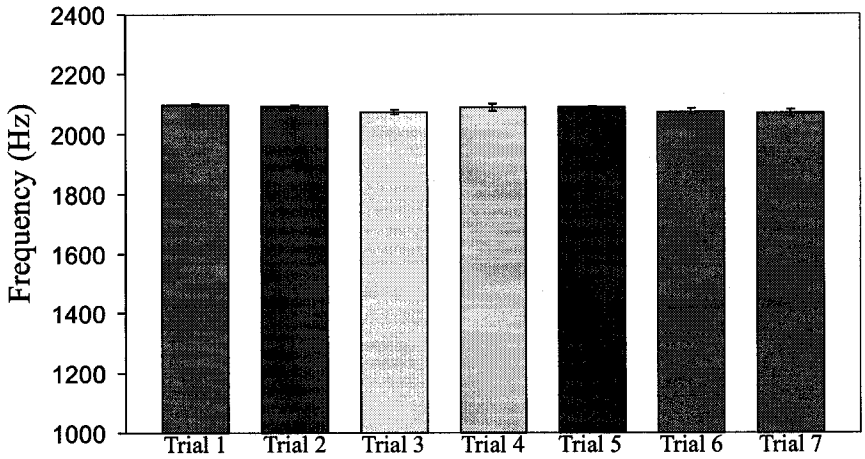


Figure 3.3: Measurements on the repeatability and reproducibility of a Ø3.75 x 4 mm implant with a 5.5 mm abutment.

controlled with the Periotest® handpiece stand the standard deviation across multiple measurements was 12 Hz. Two standard deviations (95% confidence interval) of this value could then represent a minimum resolution for a single impact measurement. This could then be used as a quick check to see if two measurements are the same, if they are more than 48 Hz apart($\pm$ 24 Hz for each measurement) then there is likely a difference in the readings.

### 3.2.2 Evaluation of Clinical Variables

In the previous section, Figure 3.3 demonstrated the degree of repeatability and reproducibility that can be achieved if the clinical variables are held constant. When the Periotest® handpiece is held by hand, these variables become much more difficult to control. This section concentrates on identifying how each of these clinical variables affect the measurements so that a measurement protocol can be developed.

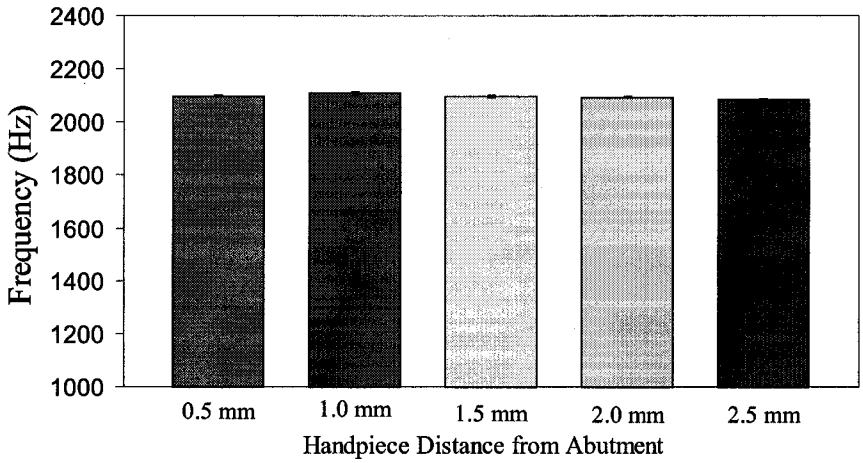


Figure 3.4: Effect of handpiece distance on measurements with a 5.5 mm abutment connected to a Ø3.75 x 4 mm flanged implant.

#### 3.2.2.1 Handpiece Distance from Abutment

As mentioned previously, the Periotest® instructions recommend that the handpiece be held between 0.5 to 2.0 mm from the object being measured. Figure 3.4 shows the results of the tests outlined in Section 2.4.2.1 in which the handpiece distance from the abutment was changed. Each column represents the average value of the five measurements at each distance with the standard deviation as the error bars. The mean value for measurements with the handpiece 0.5 mm from the abutment was 2098 ± 2 Hz while the reading at 2.5 mm was 2082 ± 6 Hz. It should be noted that for the 2.5 mm readings the Periotest® did not produce a PTV value, however a resonant frequency was obtained from the raw acceleration data. The tests indicate that the distance of the handpiece from the abutment has little influence on the resonant frequency. As long as the initial distance from the handpiece tip to the abutment tip was between 0.5 and 2.5 mm there were practically no differences in the measured fundamental frequencies.

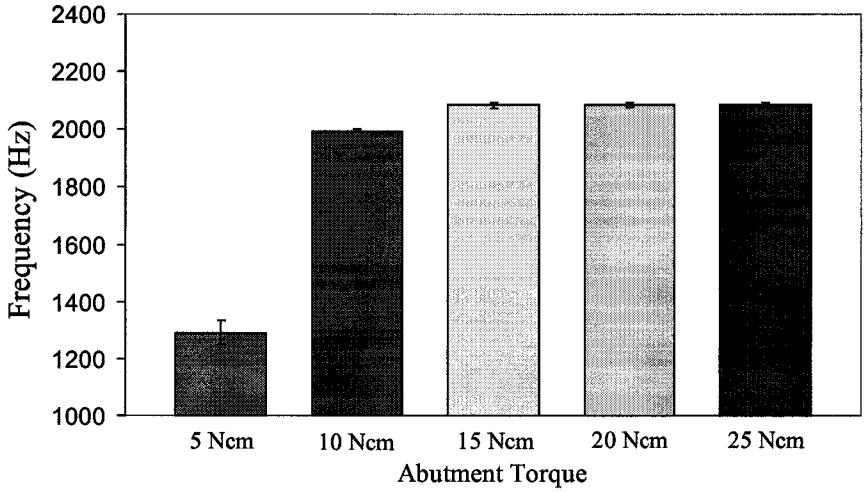


Figure 3.5: Effect of abutment torque on the fundamental frequency of a flanged Ø3.75 x 4 mm implant with a 5.5 mm abutment.

#### 3.2.2.2 Abutment Torque

The results of the abutment torque measurements discussed in Section 2.4.2.2 are shown in Figure 3.5. The tests utilized a flanged Ø3.75 x 4 mm implant with a 5.5 mm abutment which was connected at different torque values. From Figure 3.5, the measured frequencies are significantly lower for the abutments that were attached with 5 and 10 Ncm of torque than those that were attached with 15 Ncm and above. The 5 Ncm torque (which was noticeably loose) had the lowest frequency reading of 1293 Hz and the largest standard deviation of 43 Hz. The torque value at 10 Ncm was 1995 $\pm$ 7 Hz, while the torque values at 15, 20 and 25 Ncm were 2084 $\pm$ 9 Hz, 2085 $\pm$ 7 Hz and 2086 $\pm$ 7 Hz, respectively.

At torque values of 10 Ncm and below, the reduced stiffness of the joint caused a reduction in the fundamental frequency of the system. This effect has been reported previously (Faulkner, G. et al., 1999a) based on PTV values. For torques greater than 15 Ncm, the fundamental frequency remained essentially unchanged. It should be noted that these results are for a specific implant and abutment system. While it appears that torques above 15 Ncm produce consistent measured frequencies for the Brånemark system, this may not be

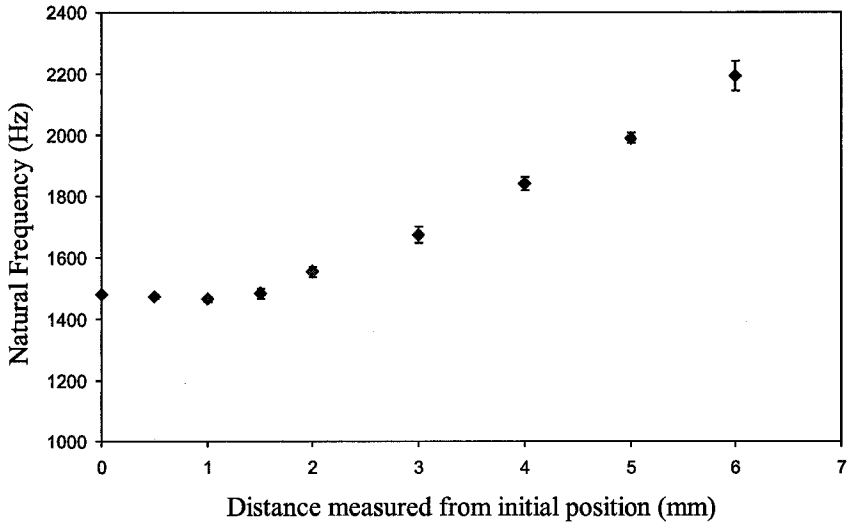


Figure 3.6: Effect of striking height on fundamental frequency of a flanged Ø3.75 x 4 mm implant with a 10 mm abutment.

the case for other implant-abutment systems.

#### 3.2.2.3 Striking Height

Figure 3.6 shows the results for the testing outlined in Section 2.4.2.3 in which a flanged Ø3.75 x 4 mm implant with a 10 mm abutment was struck at different locations along its length. Figure 3.6 illustrates the significant effect that striking height is known to have on the first mode resonant frequency. While there was very little change in the frequency when the handpiece was moved up to 1.5 mm from its initial position, there was a noticeable increase in the fundamental frequency between the 1.5 mm and 2 mm positions, and beyond.

The lack of change in the fundamental frequency until the handpiece was moved down 1.5-2.0 mm is due to the alignment of the impacting rod. Since the impacting rod is 2 mm in diameter, and the rod was aligned to hit the rim of the abutment in its original position there is a 2 mm "window" over which the flat tip of the Periotest® handpiece will strike the corner of the abutment. This effect is illustrated in Figure 3.7. As long as a portion of the Periotest® rod struck the rim of the abutment little variation in the first mode frequency results occurred.

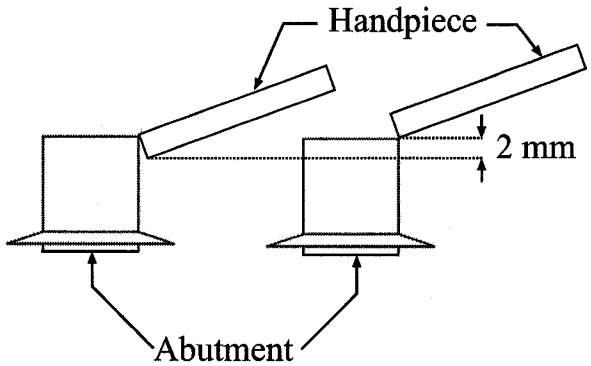


Figure 3.7: Schematic of handpiece when moved 2 mm vertically from the initial position.

#### 3.2.2.4 Angulation of the Handpiece

This section outlines the results from the measurements described in Section 2.4.2.4. As mentioned previously, the Periotest® instructions recommend an angulation of ±20° from the horizontal. Figure 3.8 demonstrates that as handpiece angulation increased from 0-20° the resonant frequency of the system increased from 2178 ± 19 Hz to 2236 ± 10 Hz. The results at 0° are noticeably different from the 1° readings, while the results appear more consistent between 1° and 5°.

When the angulation of the handpiece was kept within a 1-5° range no substantial differences were evident. The difference between the 0° and 1° measurements was likely caused from differences in the point of impact. When attempting to place the handpiece perpendicular to the striking surface it is not certain which part of the 2 mm diameter rod is striking the abutment. If the lower edge of the rod strikes the abutment (angle is slightly less than 0°) this results in a higher frequency reading than if the top part of the rod strikes the abutment (angle is slightly more than 0°). Effectively, there is a change in striking height as the rim of the abutment may not be the point of impact as demonstrated in Figure 3.9. Points A and B have different points of impact caused from a slightly different angulation. To eliminate this, a slight angulation of the handpiece is required. As angulation increased to 10° and higher there was a trend of increasing resonant frequency.

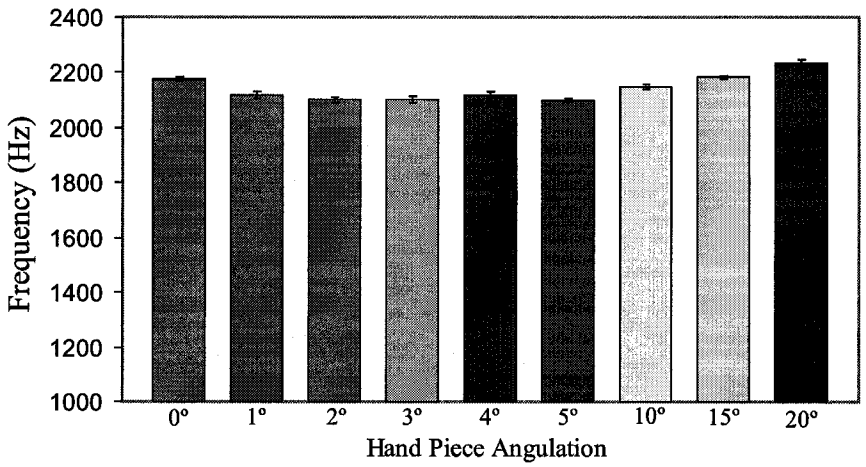


Figure 3.8: Effect of handpiece angulation on the fundamental frequency readings.

### 3.2.3 Impact Measurement Protocol

Based on the results obtained in the previous sections, certain conclusions concerning the precision possible with the proposed impact technique based on the raw accelerometer signal can be made. The frequency measurements determined from the raw accelerometer signal allow for a continuous variation in frequency instead of the limited resolution of the Periotest® value. It must be emphasized that these results are based on controlled testing in a laboratory setting.

- The repeatability and reproducibility measurements show that for 95% confidence (±2 standard deviations) the first mode resonant frequency can be determined to within ±24 Hz when using the raw accelerometer signal in *in vitro* tests.
- The distance of the impacting rod from the abutment prior to striking does not affect the results if kept within the 0.5-2.5 mm range.
- The torque applied when mounting a standard 5.5 mm abutment causes little variation in the resonant frequency for torques of 15-25 Ncm.

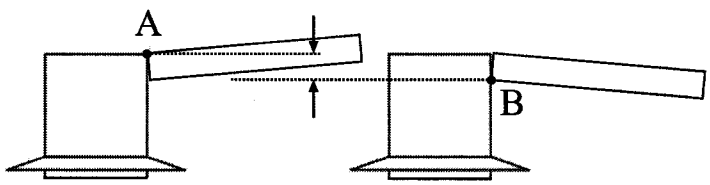


Figure 3.9: Schematic demonstrating difference in striking height caused from slight changes in handpiece angulation.

- As the effect of striking height on the resonant frequency is considerable, it is recommended that the impacting rod always strike the superior rim of the abutment, a point that is clinically easy to identify and a point that allows a ±1 mm variation when centered, without significantly changing the results.
- The ±20° handpiece angulation recommended by the Periotest® instructions is too large for implant-abutment systems. The angle of the impacting rod to the abutment should be kept in the range of 1-5° from the perpendicular to the abutment axis. If the handpiece is horizontal (0°), determining the exact point of contact becomes difficult and can affect the readings. For handpiece angulation values greater than 5° there is a trend of increasing frequency. Until these increases are understood, they should be avoided.

These recommendations will tend to maximize the precision and repeatability in implementing the presented impact test technique.

## 3.3 Intra/Inter Operator Variability Using Measurement Protocol

To test the reliability of the proposed measurement technique and protocol four experienced clinicians (experienced defined as having more than one year experience with the Periotest®) were asked to complete a series of measurements on an implant-abutment system. The implant used was a Ø3.75 x 4 mm flanged extraoral implant placed in an FRB-10 disk (as described in Section 2.1.2) with a 5.5 mm abutment which was affixed with 20 Ncm of torque. To ensure the implant disk did not move it was secured into the steel support stand described in Section 2.1.3. The measurement protocol outlined in Section 3.2.3 was explained to each clinician before the testing. Measurements were then

Table 3.1: Results of multiple clinicians using Periotest® handpiece to measure a Ø3.75 x 4 mm implant with a 5.5 mm abutment.

| | Operator 1 | Operator 2 | Operator 3 | Operator 4 |
|---|---|---|---|---|
| Trial 1 | 2221±20 Hz | 2294±39 Hz | 2350±14 Hz | 2193±15 Hz |
| Trial 2 | 2247±6 Hz | 2271±19 Hz | 2367±30 Hz | 2288±22 Hz |

conducted with each clinician completing five consecutive measurements on the implant-abutment. During the measurements the clinicians were isolated from each other and were given no feedback on the measurement results. Each clinician completed one trial of five consecutive measurements and upon completion would leave and the next clinician would enter the room and complete a set of five consecutive measurements. After all four clinicians had completed one trial, the entire process was repeated for an additional trial.

The average fundamental frequency and standard deviation for the five measurements for each clinician are shown in Table 3.1. The largest standard deviation for a set of five measurements when the handpiece was held was approximately twice the largest standard deviation value found when the handpiece was is fixed in the stand (39 Hz compared to 17 Hz). The difference between trials for Operators 1-3 was less than 30 Hz and was 95 Hz for Operator 4. The increased variation in the tests by one operator (intra-operator variation) indicates the need for multiple measurements when the handpiece is held (in later sections a minimum of three measurements were always performed). The difference between operators (inter-operator variation) was larger than the intra-operator variation with Operator 3 having the highest measured frequency values for both trials. The largest difference between two clinicians was 157 Hz (difference between Trial 1 for Operators 1 and 3). To reduce inter-operator variation it is recommended that only one clinician perform the measurements (if possible).

Based on the tests completed, the inconsistent and insensitive results reported when using the Periotest® for measuring implants may result from both the techniques used to analyze the accelerometer signal and from clinical variations which occur during measurements. The use of the raw accelerometer signal more closely represents the actual motion of the implant-abutment system during an impact and removes contact time distortion inherent in the Periotest® filtering, which could lead to erroneous measurements. Utilizing the raw accelerometer signal and the developed measurement protocol, it is believed that the impact measurements will provide reliable accelerometer data

for analysis of impact. Unless stated otherwise, the protocols outlined in this chapter are followed for all impact measurements taken in subsequent chapters.

# Chapter 4

# Analytical Model of the Periotest®/Implant System

In this chapter a mathematical model of the impact from the Periotest® rod striking an implant-abutment system is developed. With the appearance of at least one other frequency in the raw accelerometer signal, a multiple degree of freedom model could help explain the more complex signal. Previous authors (Giannitsios, D., 2001; Hurst, S., 2002) have detailed the development of a two degree of freedom analytical model. Attempts to use the two degree of freedom model by Hurst, S. (2002) to explain raw accelerometer results obtained *in vitro* met with limited success. This suggested that a more complex model needed to be considered. The development of this model is presented, followed by tests used to determine the values of model parameters. The model is then used to determine the stiffness and damping properties of the interface for the *in vitro* implant systems described in Chapter 2. Model predictions based on these interface properties are then compared to *in vitro* measurements outlined in Chapter 2. Finally, model results are used to analyze the vibrational response of the implant, abutment and striking rod during impact. It must be emphasized that the model and *in vitro* test results presented are for Brånemark system implants and abutments. Different implant-abutment designs may produce different results.

## 4.1 Analytical Model Development

The four degree of freedom analytical model presented is based on the two degree of freedom model first developed by Giannitsios, D. (2001) and then extended by Hurst, S. (2002). Hurst, S. (2002) used the model to determine the

horizontal and vertical interface stiffness values for a number of intraoral and extraoral implants based on the raw accelerometer signal from *in vitro* testing. Hurst, S. (2002) determined the horizontal and vertical stiffness values by using a least squares curve-fit to match model contact times over a range of abutment heights with measurements. While the implants tested were all installed in the same material with a similar procedure, the vertical stiffness values ranged from 9–46 times that of the horizontal. The variation in the stiffness values between the different implants in the same material and the large vertical to horizontal stiffness ratios indicated a need to modify the Giannitsios, D. (2001) model.

The four degree of freedom model developed is shown in Figure 4.1. The definitions of the variables shown in the figure are listed in Table 4.1. The presented model has some similarities to the model developed by Giannitsios, D. (2001). The striking rod is still considered as a particle, with mass $m_R$. The stiffness of the interface is still considered as a series of horizontal and vertical springs acting along the length of the implant, with a stiffness per unit length (shown as $k$). The differences in the presented model include:

- The vertical and horizontal springs acting along the length of the implant have the same stiffness, $k$.
- The implant and abutment are no longer considered as one rigid body, but are connected together with a pin and torsional spring at the implant-abutment joint.
- The local deformation of the impact rod and the abutment are included as stiffnesses $K_S$ and $K_D$.

These additions to the model result in two additional degrees of freedom in the model ($X_1$ and $\Theta_2$) that were not present in the Giannitsios, D. (2001) model. The complexity of the interface stiffness ($k$) was reduced in the model shown in Figure 4.1 by assuming that the stiffness along the interface was uniform and constant in both the vertical and horizontal directions. The interface stiffness $k$ is treated as a stiffness per unit length with units of GPa.

Jones, S. (2005) found during FEM simulations of a 20 mm solid aluminum post embedded 9 mm in FRB-10 that the aluminum post would bend during an impact initiated with the Periotest®. Based on the tests completed by Jones, S. (2005), the four degree of freedom model does not treat the implant-abutment as one solid cylinder. Instead, a torsional spring, $K_T$, is included and the implant and abutment are each considered as rigid bodies. The torsional spring simulates bending or flexibility about the implant-abutment joint. To

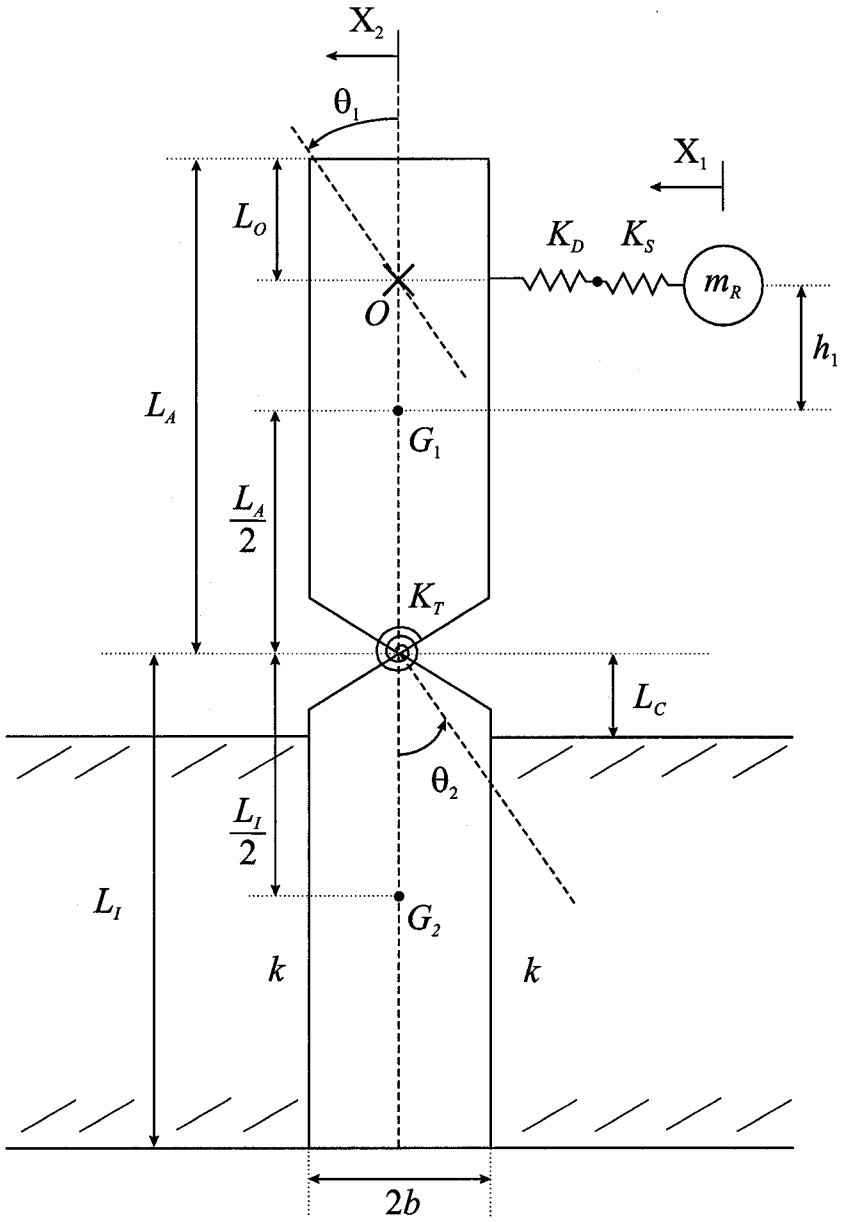


Figure 4.1: Four degree of freedom model.

Table 4.1: Variable definitions for Figure 4.1.

| Variable | Definition |
|---|---|
| $X_1$ | Coordinate describing horizontal position of impacting rod. |
| $X_2$ | Coordinate describing horizontal position of implant-abutment. |
| $\Theta_1$ | Coordinate describing angular rotation of the abutment. |
| $\Theta_2$ | Coordinate describing angular rotation of the implant. |
| $K_D$ | Stiffness of the abutment (local deformations). |
| $K_S$ | Stiffness of the Periotest® impact rod. |
| $K_T$ | Torsional spring at the implant-abutment joint. |
| $k$ | Stiffness of bone-implant interface (per unit length). |
| $O$ | Position along abutment longitudinal axis that crosses the line of impact. |
| $G_1$ | Location of abutment center of gravity. |
| $G_2$ | Location of implant center of gravity. |
| $L_A$ | Length of the abutment. |
| $L_I$ | Length of the implant. |
| $L_O$ | Vertical distance from the top of the abutment to point $O$. |
| $h_1$ | Vertical distance from $O$ to $G_1$. |
| $L_C$ | Distance joint is above the supporting material surface. |
| $b$ | Radius of implant-abutment system. |

account for rotation at the implant-abutment joint the model required an additional degree of freedom ($\Theta_2$). While simulating bending with two rigid bodies and a torsional spring is quite simplistic, it does provide an estimation of the bending while minimizing the added complexity to the mathematical model.

As the Periotest® measurement system is not infinitely stiff, when the Periotest® rod strikes the abutment some deformation occurs (represented as $K_S$). The abutment, although treated as a rigid body, also has some deformation at the point of contact (represented as $K_D$). To account for this, an additional degree of freedom ($X_1$) and the stiffness of the striking rod and the abutment at the point of contact are included in the model.

Studies done with the Periotest® often refer to the device as measuring the damping characteristics of the interface (Olivé, J. and Aparicio, C., 1990; van Steenberghe, D. et al., 1995). To determine the damping properties of the implant interface, damping was included in the model. While no damping is shown in the schematic diagram, it can be approximated by using proportional damping in which the damping matrix is assumed to be proportional (proportionality coefficient $\beta$) to the stiffness matrix so that the equations of motion become

$$[M]\{\ddot{x}\} + \beta[K]\{\dot{x}\} + [K]\{x\} = \{0\}. \tag{4.1}$$

Assuming proportional damping allows for normal mode analysis to be utilized and simplifies the analytical solution.

As the additional stiffness a flange provides implants is not well established, for the flanged extraoral implant an additional "flange" stiffness ($K_F$) was placed an effective distance $r$ from the center of the implant as shown in Figure 4.2. This stiffness simulates any additional support the flange provides. For implants without a flange, $K_F$ was set equal to zero. Determining the flange stiffness will quantify the effect a flange has on implant stability.

The developed mathematical solution to equation (4.1) utilizes a method based on the so-called normal mode approach. Once the [M] and [K] matrices are determined, the normal mode approach:

1. determines the normal modes of the system (natural frequencies and mode shapes)

2. calculates the response of the system to external forces by expressing the response as a linear combination of all the normal modes.

This combination of normal modes manifests itself as a summation of the contribution of each mode to the total solution. The analytical solution to equation (4.1) using the normal mode approach is developed in Appendix A.

### 4.1.1 Determination of Mass Matrix [M]

The analytical model is composed of two rigid bodies, the implant with mass $m_I$ and mass moment of inertia $J_I$, and an abutment with mass $m_A$ and mass moment of inertia $J_A$. A point mass with mass $m_R$ represents the striking rod. The abutments tested were cylindrical in shape with the top region of the abutment hollow and a screw passing through the length of the abutment. The implants were threaded along their length and had a threaded interior for connection with the abutment screw. The moments of inertia of these shapes were estimated by assuming the implants and abutments were uniform solid cylinders. The center of mass of the implant and abutment was also assumed to be located along the centerline half way along its length as shown in Figure 4.1 (points $G_1$ and $G_2$).

The mass matrix [M] was determined through the method of inertia influence coefficients as outlined in Rao, S.S. (1995). This method produced a symmetric 4x4 mass matrix which is shown in Appendix A.

### 4.1.2 Determination of Stiffness Matrix [K]

There are four main stiffness values shown in Figure 4.1, $K_D$, $K_S$, $K_T$ and $k$. For flanged implants, a flange stiffness ($K_F$) is included as shown in Figure 4.2. The flange is represented as a single spring on each side of the implant located an effective distance $r$ from the center of the implant. The flange is assumed to be coupled to the hard tissue.

The stiffness matrix [K] was determined from the method of stiffness influence coefficients as described in Rao, S.S. (1995). Similar to the mass matrix, this method produced a symmetric 4x4 stiffness matrix which is shown in Appendix A.

## 4.2 Estimation of Model Parameters

To calculate the interface stiffness and damping properties for the *in vitro* implants the appropriate stiffness values for the internal components in the system were first calculated. The internal stiffnesses of $K_D$, $K_S$, $K_T$ and $K_F$ were estimated through a combination of *in vitro* experimentation to directly determine stiffness values and comparison of model results to *in vitro* measurements. Once the internal stiffness components were determined the interface stiffness and damping values for extraoral and intraoral implants placed in FRB-10 could be estimated.

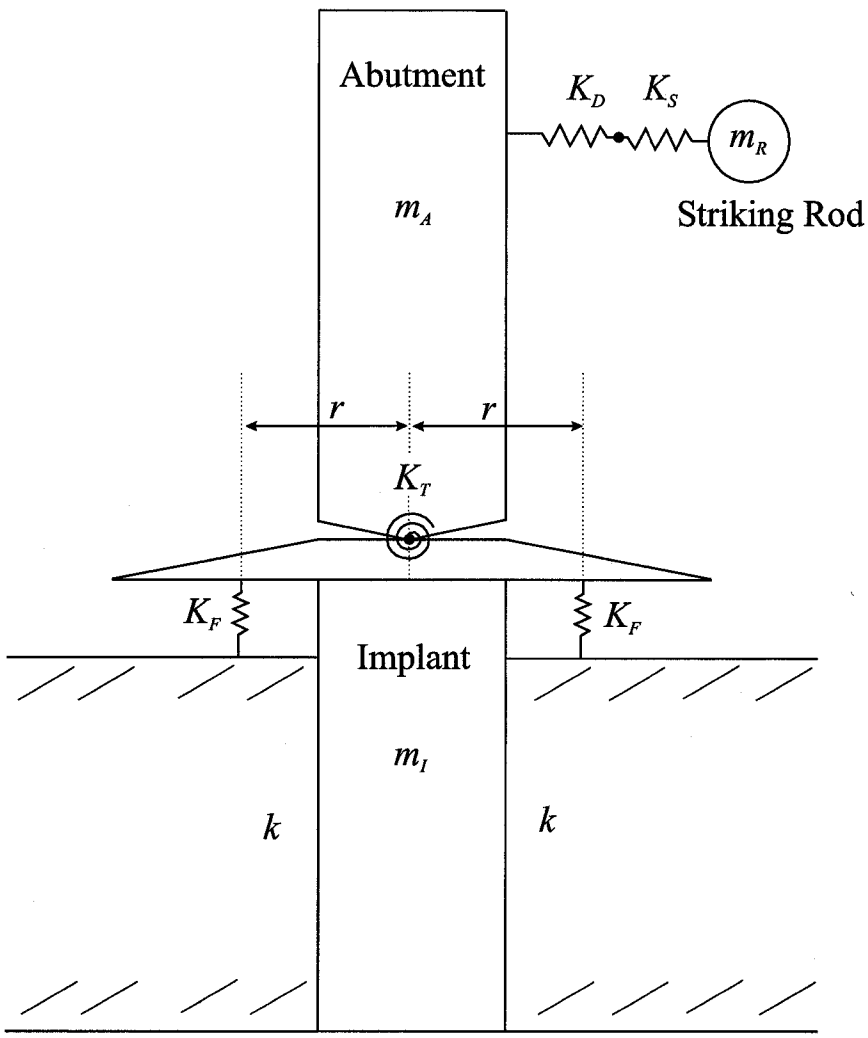


Figure 4.2: Four degree of freedom model with flange stiffness $K_F$.

Model results were obtained through the use of a custom made Matlab program that solved the equations outlined in Appendix A. To avoid confusion, resonant frequency values returned by the model are represented in the text as $p_r$ and measured frequency values are represented as $w_r$. The governing equations could be used in one of two ways.

1. The interface stiffness $k$ was assumed and the Matlab model would determine the natural frequencies ($p_r$) and the acceleration response of the impact in the time domain.

2. The measured first mode frequency ($\omega_1$) was given and the Matlab model would determine the interface stiffness $k$ and the acceleration response of the impact in the time domain.

As mentioned, the model could (given $k$) calculate the second mode frequency of the impact which could be compared to the measured higher frequency component found in the raw accelerometer signal. A number of methods were employed to compare the second mode frequencies between the model and the measurements. One method calculated the time between peaks to estimate the second mode frequency. This method was found to be imprecise. A second method employed an FFT analysis on the raw accelerometer signal to determine the second mode frequency. While the FFT analysis initially looked very promising, due to the short contact time of the impacts the frequency resolution was too large to be able to effectively compare the model and measurement results. The most direct and simple method to compare the model results with the measurements was found to be to directly compare the model acceleration response with the measured accelerometer response in the time domain. Although subjective, differences between the model results and the measurements were clearly visible using this method.

### 4.2.1 Determining the Internal Model Stiffness Values

#### 4.2.1.1 Impact Stiffness

When the Periotest® rod strikes an abutment it is assumed that both the striking rod and the abutment will both deform. The abutment stiffness is defined as $K_D$. The stiffness of the impacting rod was taken as $K_S$, which includes the stiffness of the Periotest® impacting rod, the accelerometer and the connection between the two. The impact stiffness, $K_I$, is the equivalent of $K_D$ and $K_S$ in series as demonstrated in Figure 4.3. The value of $K_I$ and $K_S$ were found through *in vitro* testing. The stiffness of $K_D$ could then be

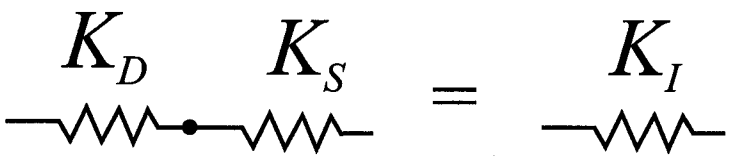


Figure 4.3: Series summation of $K_D$ and $K_S$ to give $K_I$.

determined, if desired, using

$$K_D = \frac{K_S K_I}{K_S - K_I}.$$

The stiffness of the Periotest® rod was determined by taking five resonant frequency readings on a large steel block (with a mass of approximately 14 kg) to simulate an immobile and rigid target. The Periotest® handpiece was placed in the holding stand as outlined Section 2.1.3 and the first mode frequency ($\omega_1$) was calculated from the measurements using the Matlab code outlined in Section 2.2.2. The stiffness of the striking rod ($K_S$) could be calculated as

$$K_S = (2\pi\omega_1)^2 m_R. \tag{4.2}$$

The average first mode frequency for the block was $\omega_1 = 4948$ Hz. The mass of the striking rod plus accelerometer $m_R$ was measured to be 9.4 g, so from equation (4.2) $K_S$ was found to be 9.09x$10^6$ N/m.

The impact stiffness, $K_I$, was estimated directly by clamping a steel block on one side of the abutment while impacting the opposite as shown in Figure 4.4. The purpose of this is to attempt to isolate the abutment from the support at the implant. The Periotest® handpiece was placed in the holding stand as outlined Section 2.1.3 and a series of five measurements were taken on 10, 7, 5.5 and 4 mm abutments which were connected to the flanged 4 mm extraoral disk with 20 Ncm of torque. By assuming the steel backing is rigid, the impact stiffness could be calculated from the measured first mode frequency using

$$K_I = (2\pi\omega_1)^2 m_R. \tag{4.3}$$

The results for the different abutment sizes are shown in Table 4.2. The $\omega_1$ values reported in the table are the average of the five readings for each abutment. Table 4.2 shows that for different size abutments, there is range of values for $K_I$. The $K_I$ value does not seem to be directly related to abutment length, with its value decreasing between the 10 and 7 mm abutments, then

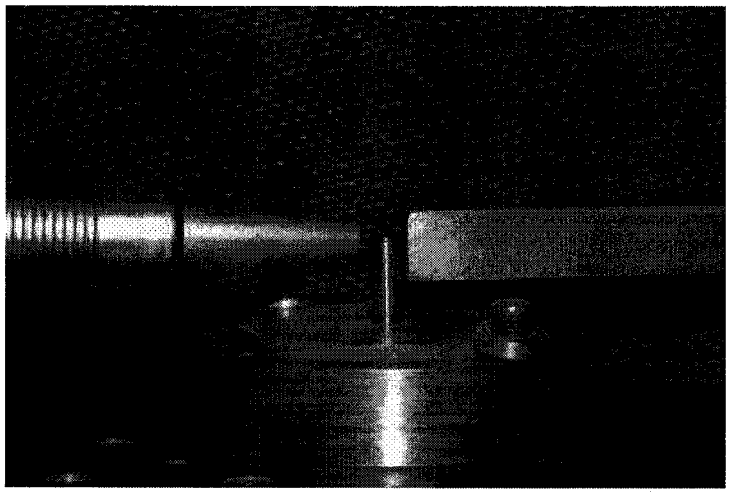

Figure 4.4: A 10 mm abutment with steel block backing.

Table 4.2: Calculated impact stiffness ($K_I$) for different length abutments.

| | $\omega_1$ (Hz) | Calculated $K_I$ (N/m) |
|---|---|---|
| 10.0 mm Abutment | 2624 | $2.56 \times 10^6$ |
| 7.0 mm Abutment | 2542 | $2.25 \times 10^6$ |
| 5.5 mm Abutment | 2690 | $2.68 \times 10^6$ |
| 4.0 mm Abutment | 2836 | $2.98 \times 10^6$ |

increasing with the 5.5 mm abutment and then increasing to the largest value $2.98 \times 10^6$ N/m with the 4 mm abutment. As the tests done were on a limited number of each of the abutments listed, it is presently not known how much variation of $K_I$ there is in the standard Nobel Biocare abutments. Similarly, it is not known how much $K_I$ may change if a different manufacturer's abutment were to be used.

#### 4.2.1.2 Torsional Stiffness

The torsional stiffness $K_T$ was estimated based on the assumption that the abutment behaves as a cantilever beam as shown in Figure 4.5a. The length of the cantilever, $L_T$, is the distance between the implant-abutment joint ($J$)

and the location of the applied load ($P$). The length, $L_T$, is determined by

$$L_T = L_A - L_O$$

where $L_A$ is the length of the abutment and $L_O$ is the distance from the top of the abutment the Periotest® rod strikes. For these calculations, it is assumed that the portion of the implant in the supporting material is fixed rigidly and that there is no flexibility in the implant-abutment joint (the flexibility in the joint will be accounted for in the following section).

The deflection, $\Delta$, of a cantilever loaded as shown in Figure 4.5a can be expressed as

$$\Delta = \frac{PL_T^3}{3EI}. \tag{4.4}$$

The cantilever bending system shown in Figure 4.5a was modeled with a torsional spring of stiffness $K_T$ as shown in Figure 4.5b. In this figure, the deflection $\Delta$ is

$$\Delta = \frac{PL_T^2}{K_T}. \tag{4.5}$$

Equating equations (4.4) and (4.5) the effective torsional stiffness, $K_T$, is

$$K_T = \frac{3EI}{L_T}, \tag{4.6}$$

Using $E = 110$ GPa for titanium, approximating the abutments as solid cylinders (as was done in Section 4.1.1) and using the nominal length for the size of abutment allows for the calculation of $K_T$.

#### 4.2.1.3 Verification of Determined Stiffness Values

As a test of the developed model, the simulated un-damped acceleration response ($\beta = 0$) was compared to one of the measured acceleration signals for the 10 mm implant with a 10 mm abutment (measurement procedure as outlined in Section 2.4.3). The 10 mm abutment was chosen as the amplitude of the second mode was found to be greater for the 10 mm abutment than for shorter abutments and this larger amplitude would better illustrate model and measurement results. The results of the comparison can be seen in Figure 4.6a which shows the acceleration response of 16 impact measurements and the predicted acceleration response from the model. With all the other stiffnesses now determined, the interface stiffness $k = 1.9$ GPa was found by matching the model first mode frequency to the measured frequency $\omega_1 = 1500$ Hz. To directly compare the model acceleration response to the measurements, the

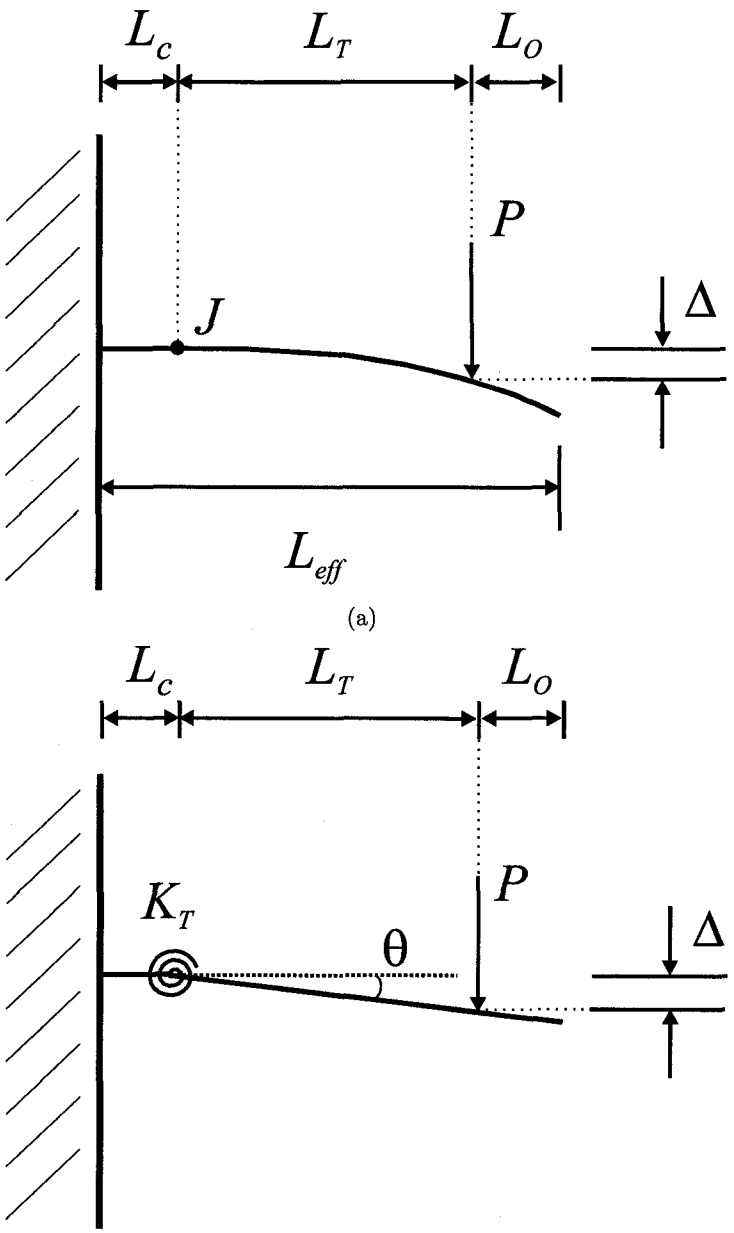


Figure 4.5: Modeling cantilever bending. a) Cantilever bending. b) Modeling cantilever bending with a torsional spring $K_T$.

model response was "normalized" by multiplying the response by a constant. This normalization was required because the model results have units of acceleration ($m/s^2$) while the measured accelerometer signal has units of voltage (V). The constant serves as the conversion between accelerometer voltage and acceleration. The constant was determined by approximately matching the model acceleration amplitude with the measured accelerometer signal amplitude.

While the relative amplitudes of the first and second mode frequencies are predicted well, there is a noticeable second mode frequency difference between the measured response and the model shown in Figure 4.6a. The model appears to over-predict the second mode frequency. To improve the predictions from the model, the value of $K_T$ estimated previously was reduced. Since $K_T$ was originally estimated based on an assumed rigid connection between the implant and the abutment, this overestimates the true stiffness in this joint due to the screw connection. To match the measured signal, $K_T$ is reduced to approximately $\frac{1}{4}$ of its original value to account for the flexibility in the implant-abutment joint. The stiffness $K_T$ is then given by

$$K_T = 0.26\left(\frac{3EI}{L_T}\right). \tag{4.7}$$

With this reduced $K_T$, a new interface stiffness $k = 7.5$ GPa was determined for the 10 mm implant and 10 mm abutment using the equations in Appendix A. While the geometry of the supporting material will affect the relationship between $k$ and the elastic modulus, the determined $k = 7.5$ GPa value compares well to the modulus of elasticity of FRB-10 which is 9.3 GPa. The resulting (un-damped) signal is shown in Figure 4.6b. From the figure, the model prediction has a much better agreement with the measured signal.

### 4.2.2 Model Damping Calculation

The normal mode solution presented requires a damping proportionality constant $\beta$, such that

$$\beta = \frac{2(\nu_r)}{p_r} \tag{4.8}$$

where $\nu_r$ = damping ratio for each mode and $p_r$ = resonant frequency for each mode. From this equation, for a given $\beta$ the damping ratio will be higher for those modes with higher frequencies so that the higher frequencies will damp out more rapidly than the lower ones.

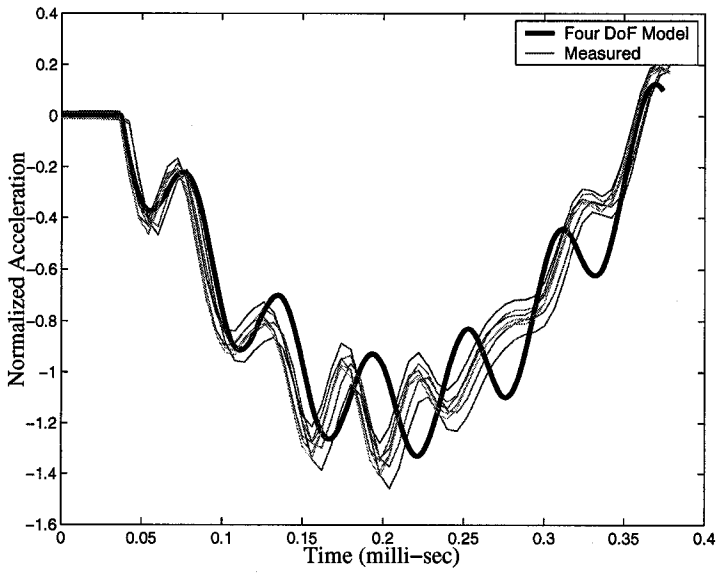


(a)

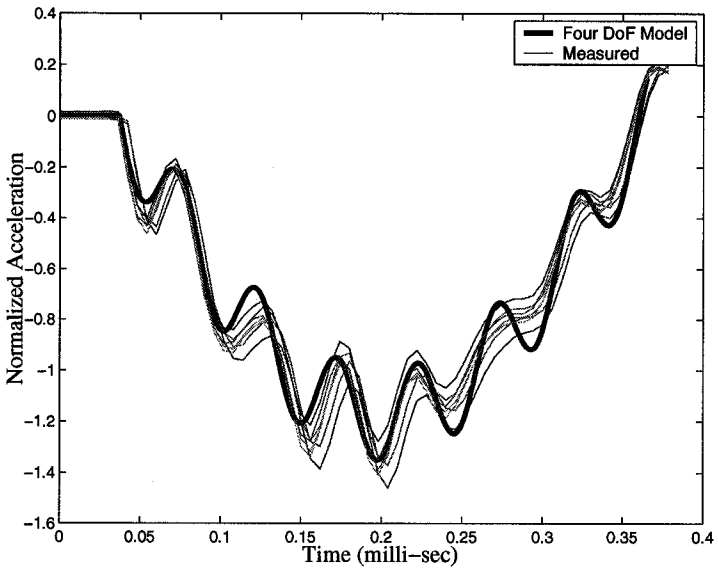


(b)

Figure 4.6: Impact test acceleration compared to model output for a 10 mm implant with a 10 mm abutment. a) Estimated $K_T$ from equation (4.6). b) $K_T$ modified to match 2nd mode frequency

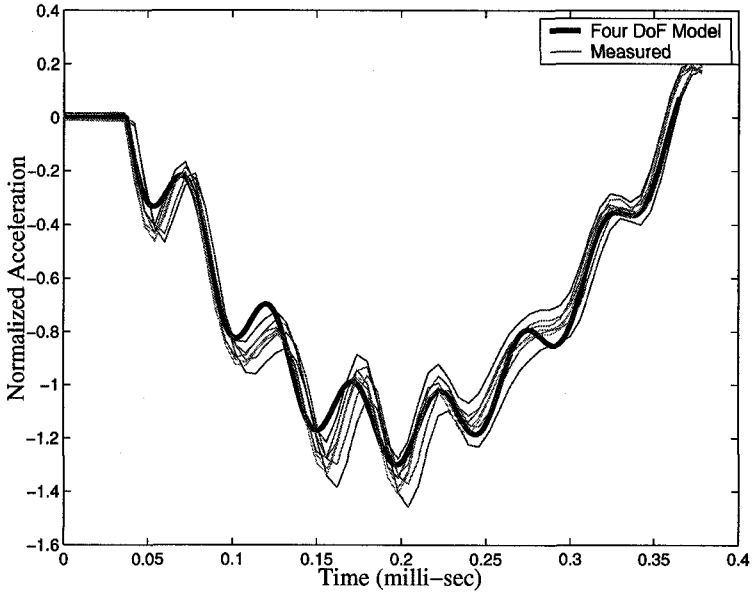


Figure 4.7: Damped model acceleration response compared to measurement for 10 mm implant with 10 mm abutment.

Table 4.3: Calculated damping ratio for each mode for implants placed in FRB-10.

| Mode | Damping Ratio (%) |
|---|---|
| 1 | 0.1 |
| 2 | 1.5 |
| 3 | 4.8 |
| 4 | 6.3 |

To estimate the damping coefficient $\beta$, the damping coefficient was increased in the model until the reduction in the second mode amplitude approximately matched the measured response as shown in Figure 4.7. From the figure, the damped model response agrees very well with the measurements. The value of the damping coefficient found was $\beta = 2.45\text{x}10^{-7}$ sec in this case. From equation (4.8) this damping proportionality constant results in a damping ratio for each mode as shown in Table 4.3. The determined value of the damping coefficient ($\beta = 2.45\text{x}10^{-7}$ sec) is used for all subsequent model simulations of implants placed in FRB-10. Based on these results, the FRB disks appear to have very little damping.

### 4.2.3 Effect of Flange

This section will make use of the 4 mm flanged implant readings with a 10 mm abutment as outlined in Section 2.4.3. Based on previous measurements, the 10 mm abutment provides a larger high frequency amplitude than other sized abutments. A very visible high frequency component in the measurement signal provides a better opportunity to evaluate how well the model results compare to the measurement for both frequencies.

When the 4 mm flanged implant with a 10 mm abutment was tested, the first mode measured frequency was found to be $\omega_1 = 1500$ Hz which was the same as when the 10 mm intraoral (unflanged) implant was used. As a result there is a larger $k$ determined for the 4 mm implant than for the 10 mm implant (12.0 GPa vs 7.5 GPa) even though the two implants were placed in the same material using a similar procedure. This difference was thought to be due to the flange on the 4 mm implant providing extra support compared to the flangeless 10 mm implant. To determine the effect of the flange, the flange was removed from the 4 mm implant so that *in vitro* resonant frequency measurements could be compared with and without a flange. When the flange

was removed, impact measurements were repeated. The measured resonant frequency decreased to $\omega_1 = 1300$ Hz, indicating that the flange was giving additional support to the implant. The resulting model $k$ for the flangeless 4 mm implant was 7.7 GPa which agrees well with the 7.5 GPa value found previously. The results of 16 impact measurements with a 4 mm flangeless implant with a 10 mm abutment compared to the model results with a model $k$ of 7.7 GPa are shown in Figure 4.8a. The model predicted acceleration response shows excellent agreement with the flangeless implant measurement.

For flanged implants the same internal model stiffness parameters previously described were used, however, the flanged implants also had a flange stiffness included. As previously discussed, to model the additional support provided by a flange, a spring of stiffness $K_F$ was placed at an effective distance $r$ from the center of the implant (for flangeless implants $K_F$ was set to zero) as shown in Figure 4.2. For the flanged implants the effective distance was taken as half the width of the 2 mm flange plus the radius of the implant (1.875 mm) to give $r = 2.875$ mm. To determine the value of $K_F$, the same internal model parameters $k$ was set to 7.7 GPa for the 4 mm flanged case and $K_F$ was increased until the model first mode frequency matched the measured first mode frequency of the flanged readings which occurred when $K_F = 3.65\text{x}10^7$ N/m. A comparison between the flanged measured results and model results is shown in Figure 4.8b.

In Figure 4.8b the model results do not match the measured signals as well as in previous tests. The predicted higher frequency component does not agree as well as for the flangeless implant. This may be due to the added complexity a flange adds to the system, which was modeled simplistically with the vertical springs $K_F$. Another difficulty with the flanged implant was caused when the implant was placed in the FRB-10. Some of the epoxy used to secure the implant ended up under the flange bonding the flange to the FRB-10 surface, which provided both vertical and horizontal support which was not modeled. It may be possible to reduce the difference between the model results and the measured signal for the flanged implants utilizing a more complex model of $K_F$. However, before this is attempted the present flange model will be used with the *in vivo* data to determine whether a refined flange model is required.

## 4.3 Model Validation

While the model simulations in previous sections indicated a very good comparison with the actual acceleration response, this was for a limited number of specific tests. In order for the model to be effective it should be able to

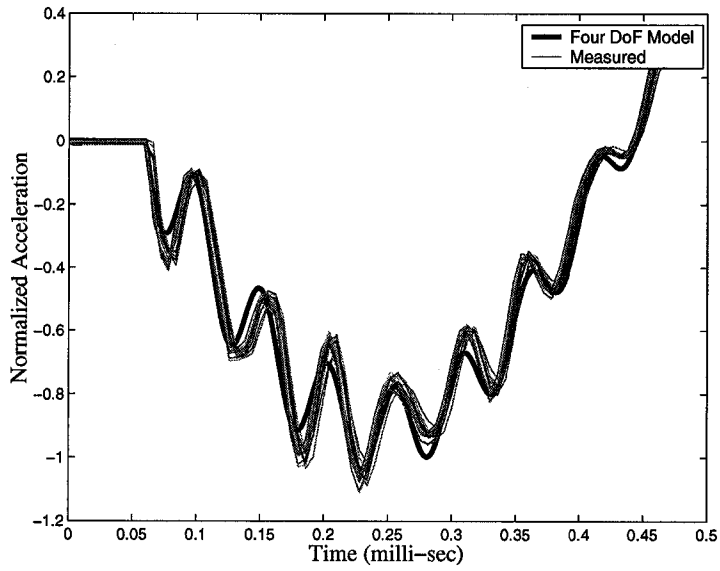


(a)

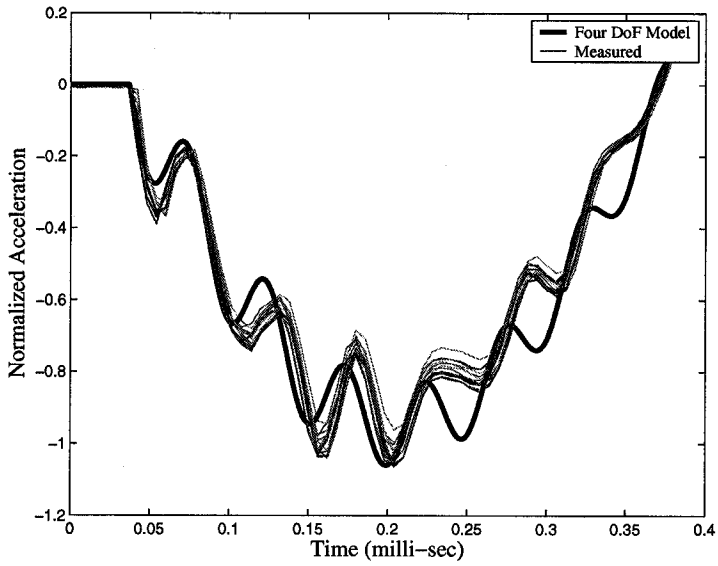


(b)

Figure 4.8: Damped model acceleration response compared to measurement for 4 mm implant with 10 mm abutment. a) 4 mm flangeless implant. b) 4 mm flanged implant.

accurately simulate a number of different clinical situations. To this end, the fundamental frequency measurement results from the measurements outlined in Section 2.4.3 were compared to the model results. Tests at different striking heights, different implant engagement lengths and with different abutment lengths allowed for testing of the model under different geometric conditions while holding $k$ constant.

The model results were compared to measurements utilizing both 4 and 10 mm implants. For the 4 mm implant $k$ was 7.7 GPa and for the 10 mm implant $k$ was 7.5 GPa as determined previously in Sections 4.2.1.3 and 4.2.3. These values were held constant for all the subsequent comparisons. Similarly, for all of the *in vitro* results, the $K_I$ for each length abutment was as listed in Table 4.2, $K_T$ values were as calculated from equation (4.7) and $K_F$, where appropriate, was 3.65x10$^7$ N/m.

### 4.3.1 Variations in Striking Height

One technique used to validate the model was to compare the model results with experimental results obtained from striking a 10 mm abutment at different heights above the disk surface. The measurement procedure for these tests are outlined in Section 2.4.3.1. The first mode frequency value for these measurements was obtained using the Matlab code outlined in Section 2.2.2.

The measured first mode frequencies ($\omega_1$) are compared to the predicted model first mode frequencies ($p_1$) in Figure 4.9. In the figure, the five measured frequency values are averaged and the error bars shown represent two standard deviations of the repeatability and reproducibility measurements in Section 3.2.1 ($\pm$24 Hz). From the figure, the model results agree very well with the measurements for both implants.

The results shown in Figure 4.9 differ from Figure 3.6 in Section 3.2.2.3. In Figure 4.9 the height the striking rod hit the abutment is reported as the distance above the implant-abutment joint (as opposed to the distance from the top of the implant). This change was made so that the variations in striking height could be more easily compared to variations in abutment lengths in the following section. Figure 4.9 also does not have the horizontal region caused when the handpiece is lowered with no corresponding change in the first mode frequency (as seen in Figure 3.6). This effect is avoided by taking measurements starting at the top corner of the abutments and then lowering the handpiece until the first mode frequency begins to change, this point is taken to be the top. The handpiece is then lowered distances of 1, 2, 3, and 4 mm.

To compare the second mode frequency to model results at different strik-

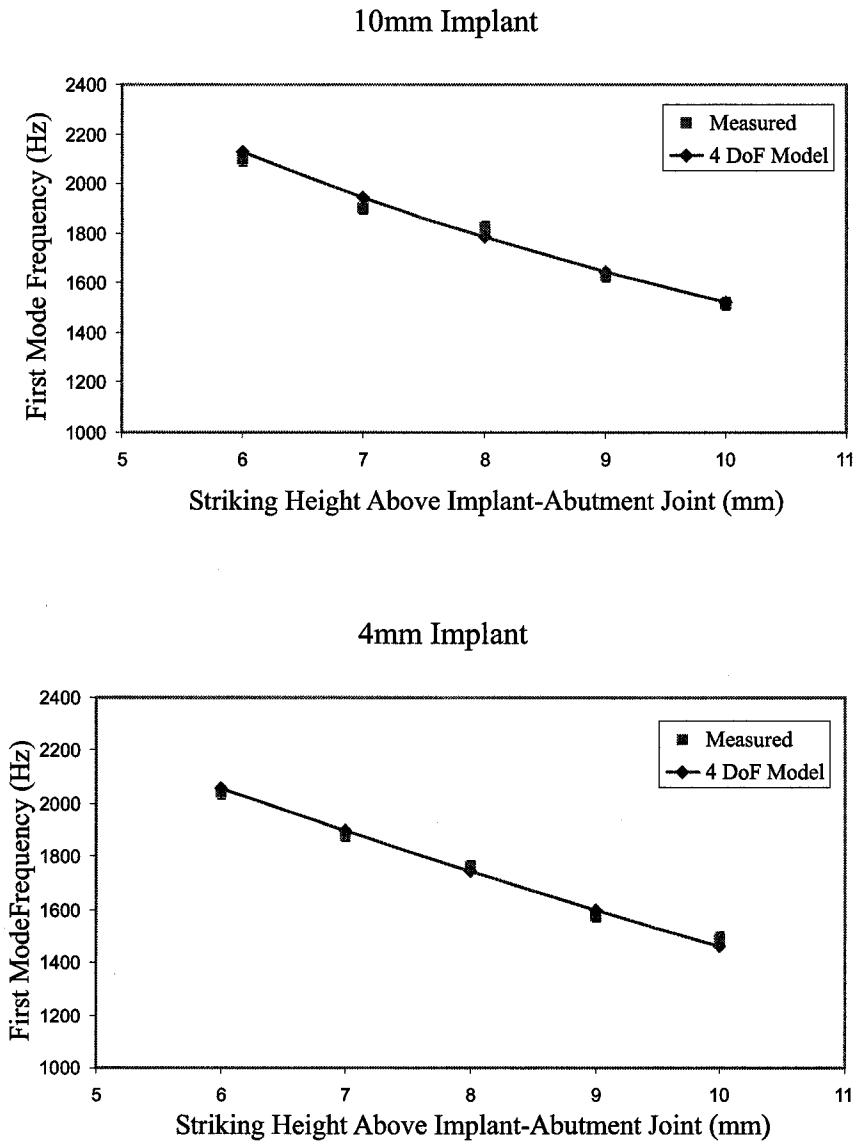


Figure 4.9: Comparison of model to measurement values for two implants at different heights along a 10 mm abutment.

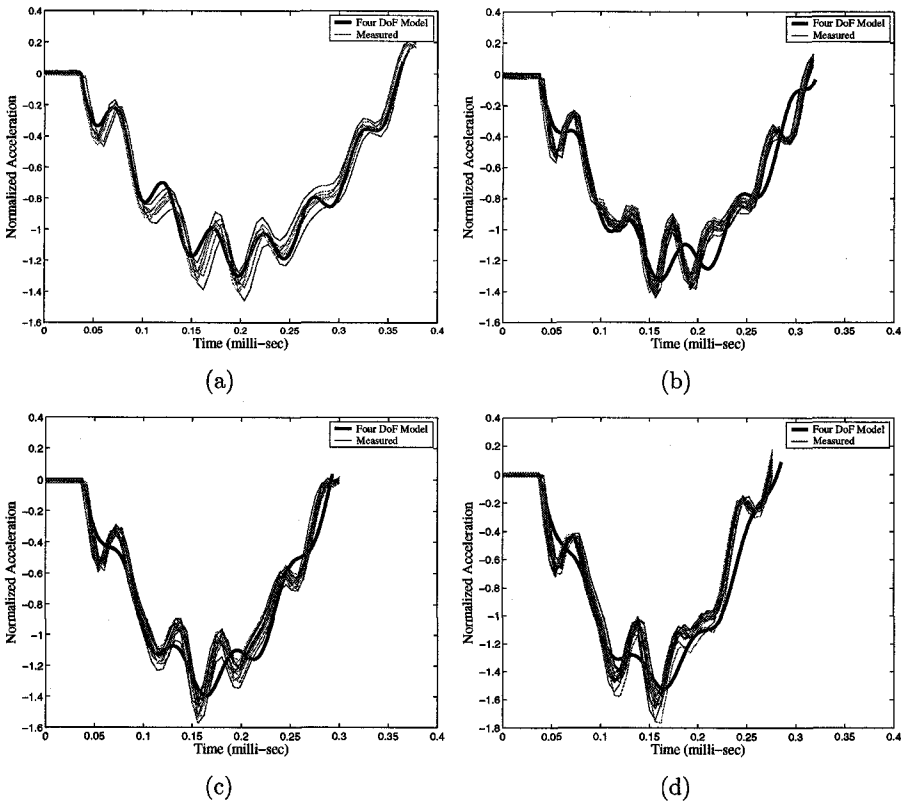


Figure 4.10: Model results compared to measurements for a 10 mm implant and 10 mm abutment struck at different points along the abutment. a) Abutment struck at the top. b) Abutment struck 2 mm from the top. c) Abutment struck 3 mm from the top. d) Abutment struck 4 mm from the top.

ing positions, the model predicted acceleration response for the 10 mm implant case was directly compared to measurements as shown in Figure 4.10. The measured second mode frequency appears to match the model frequency quite well for the different striking heights, with the exception of Figure 4.10b where the model under-predicts the second mode frequency. The model predicted amplitude of the second mode frequency appears to be smaller than the measurements in all but Figure 4.10a.

While the first mode frequency between the measurements and model match very well, there is some discrepancy between the model results and the measurements when comparing the second mode frequency and amplitude. These differences may be caused from assumptions made to take into account the deformation of the abutment. At different striking positions along the abutment, $K_D$ and therefore $K_I$ may have different values, as the rim of the abutment will likely be less stiff than the wall of the abutment. There may also be some errors introduced by the manner the model handles bending. Modeling bending with a torsional spring and single rigid body in equation (4.7) may be too simplistic to provide a higher level of agreement. Although the level of agreement in Figure 4.10 is not as good as in previous measurements, the level of agreement is still reasonable considering the simplifying assumptions made in the model. Clinically, only impacts at the top are relevant.

### 4.3.2 Effect of Using Different Abutment Lengths

Since different abutment sizes are commonly used with implants, it is important to compare the model results with different sized abutments. Section 2.4.3.2 outlined the procedure for measurements on 4, 5.5, 7 and 10 mm abutments. As in the previous section, model first mode frequencies ($p_1$) were compared to the measured fundamental frequencies ($\omega_1$) obtained from the measurements using the Matlab code in Section 2.2.2. The results of this comparison can be found in Figure 4.11. The measurement results in the figure are the average of the five readings and the error bars are two standard deviations of the repeatability and reproducibility results from Section 3.2.1 ($\pm$24 Hz). The results in Figure 4.11 show a good agreement between the model predicted fundamental frequency and the measured values for the abutments tested. The agreement between the predicted values and measurements provides evidence that the model correctly interprets the effects different length abutments have on the fundamental frequency.

The predicted model acceleration response for the different abutment sizes with a 10 mm implant are compared to the measured results in Figure 4.12. The second mode amplitude and frequencies match the measured values quite

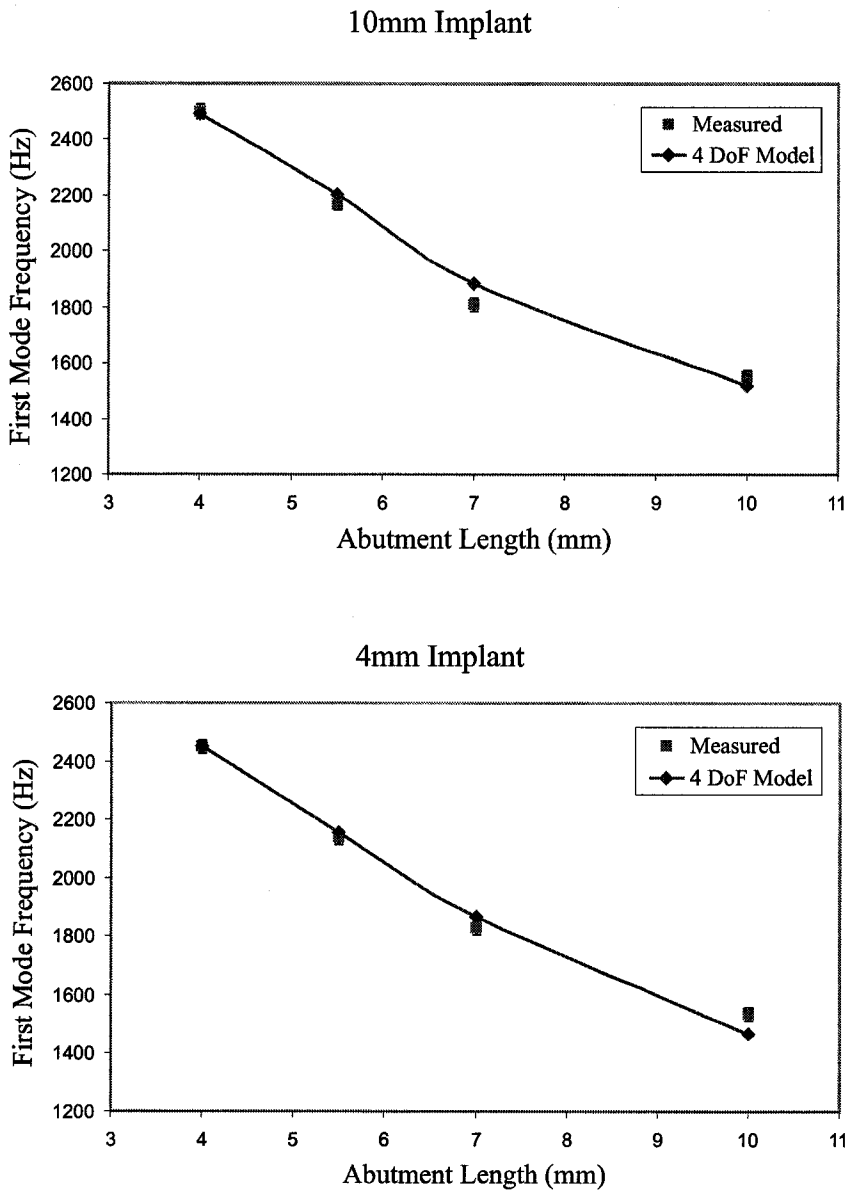


Figure 4.11: Comparison of model using changing $K_I$ values to measurements for two implants with different length abutments.

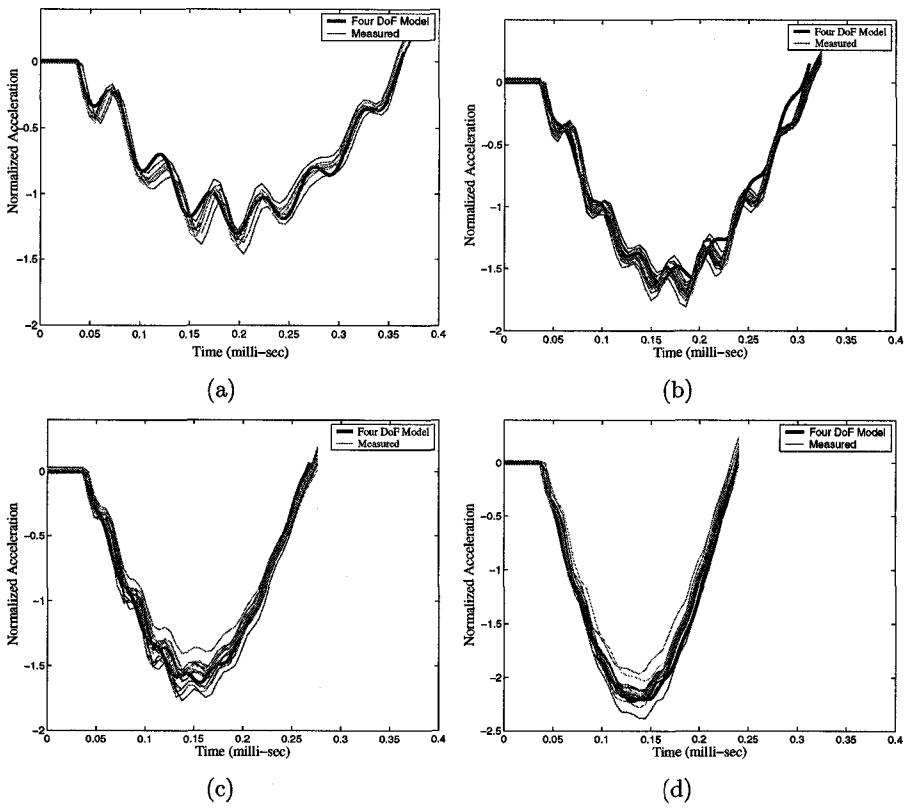


Figure 4.12: Model results compared to measurements for a 10 mm implant with different sized abutments. a) 10 mm abutment. b) 7 mm abutment. c) 5.5 mm abutment. d) 4 mm abutment.

well.

### 4.3.3 Simulation of Bone Loss

One of the potential uses for the analytical model is to predict the effects of bone loss around an implant. Brunski, J.B. (1999) discusses a number of failure mechanisms of implants, with one of the failure mechanisms based on bone loss starting at the top of the implant and progressing toward the base. As a test of how well the model predicts the effects of the loss of supporting material from the top of the implant down, model simulations were compared to measurements on a 10 mm implant which was placed 3 mm proud (the head of the implant was 3 mm above the FRB disk surface). The interface stiffness was assumed to be the same ($k$ of 7.5 GPa) as the 10 mm implant disk with the implant completely threaded. The first mode frequency model predictions were compared to the first mode frequency measurements (outlined in Section 2.4.3.3) on the proud implant with 4, 5.5, 7 and 10 mm length abutments as shown in Figure 4.13. The measurement results in the figure are the average of the five readings and the error bars are two standard deviations of the repeatability and reproducibility results from Section 3.2.1 ($\pm$24 Hz).

With an interface stiffness of 7.5 GPa the model over-predicted the measurement frequencies by over 100 Hz for each of the abutments. A much better agreement between the model results and measurements was obtained when the interface stiffness was lowered to 3.8 GPa. When the model acceleration response is compared to the measurements with a $k$ of 3.8 GPa, the second mode amplitude and frequency match the measurements quite well for all four abutments. Examples of the measured raw accelerometer response compared with the model results for 5.5 and 10 mm abutments is shown in Figure 4.14.

The $k$ of 3.8 GPa compared to 7.5-7.7 GPa for the other FRB-10 disks tested may be the result of errors in how the model handles the loss of material around the implant or due to actual differences between the FRB-10 disks. The consistency in the predicted results with the measurements at the lower interface stiffness indicates that a difference in the disks is a likely explanation. The FRB disks were constructed at different time intervals by Hurst, S. (2002). During fabrication of the disks Hurst, S. (2002) noted the existence of air pockets in the FRB material. Air pockets in close proximity to the implant could affect the interface stiffness. Inconsistencies in the method of installing the implant into the FRB disk may also influence the interface integrity. Variations in the diameter of the drilled hole or cut threads may cause differences in the interface integrity. It is also possible that Hurst, S. (2002) used FRB-20 for the construction of the implant disk tested. FRB-20

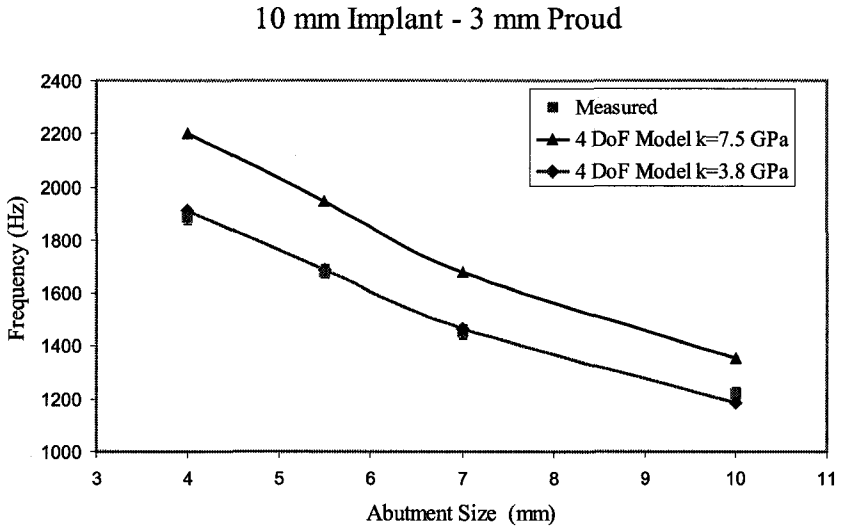


Figure 4.13: Comparison of model predicted results of material loss to measurements at different abutment heights.

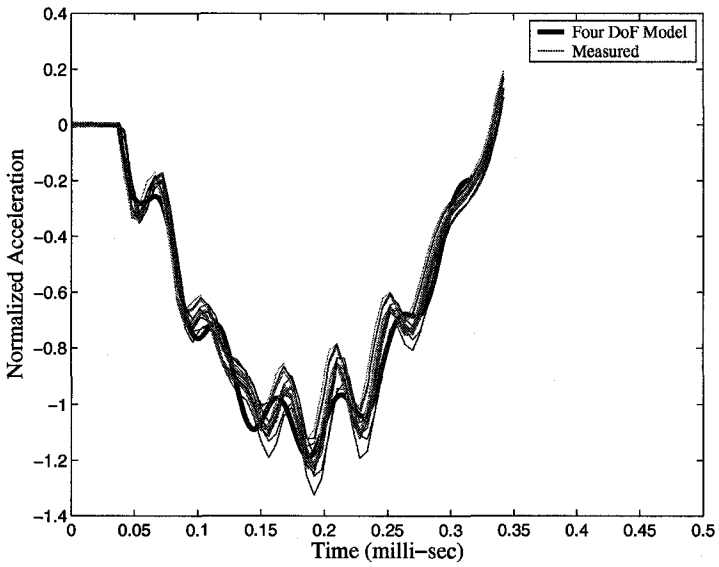


(a) 5.5 mm abutment

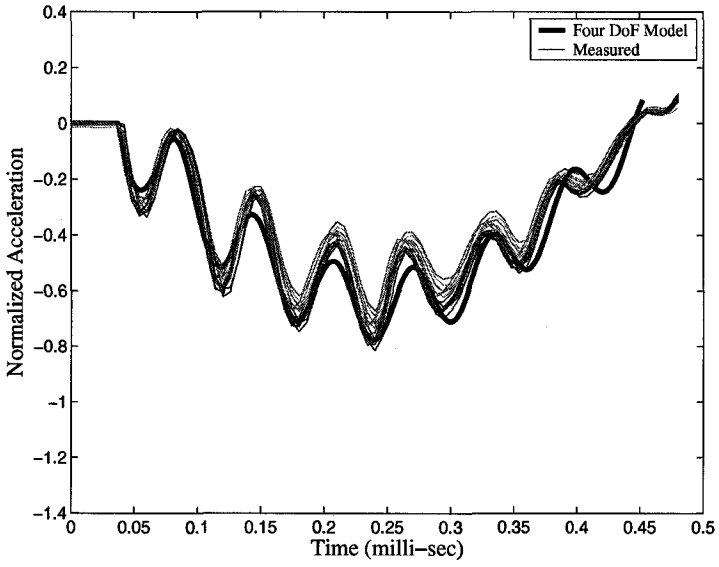


(b) 10 mm abutment

Figure 4.14: Comparison of model predicted results to measurements for a 10 mm implant left 3 mm proud with a 5.5 and 10 mm abutment.

has approximately one-third the modulus of FRB-10, which would result in a lower interface stiffness.

## 4.4 Analysis of the Vibrational Response of the Implant/Abutment/Striking Rod System During Impact

When analyzing a vibrating system two properties that are often discussed are the modal participation factor and the mode shape. The modal participation factor is a measure of the amplitude of vibration for each mode, while the mode shape describes the displacement configuration of the system for each normal mode.

The combination of normal modes manifests itself as a summation of the contribution of each mode to the total displacement solution (equation (A.19)) so that

$$\{x(t)\} = \sum_{r=1}^{4} e^{-\nu_r p_r t} \left[ \frac{1}{p_r} \{\mu\}_r^T [M] \{\dot{x}(0)\} \sin\left(\sqrt{1-\nu_r^2} p_r t\right) \right] \{\mu\}_r$$

where $p_r$ is the resonant frequency for each mode, $\{\mu\}_r$ is a column vector of the normalized modal matrix $[\mu]$, $\nu_r$ is the damping ratio for each mode, [M] is the mass matrix and $\{\dot{x}(0)\}$ is the initial velocity vector.

Thomson, W.T. and Dahleh, M.D. (1998) define the

$$\frac{1}{p_r} \{\mu\}_r^T [M] \{\dot{x}(0)\}$$

term found in the above equation as the "coefficients indicating how much of each mode is present". This term will be referred to as the displacement modal participation factor.

Since the impact measurements utilize accelerations, the model responses can be expressed using $\{\ddot{x}(t)\}$ instead of $\{x(t)\}$. The acceleration modal participation factor can be defined in an analogous manner to the displacement case. From equation (A.20) in Appendix A, the acceleration response can be written

$$\{\ddot{x}(t)\} = \sum_{r=1}^{4} e^{-\nu_r p_r t} \left[ (3\nu_r^2 - \nu_r^4 - 1) p_r \{\mu\}_r^T [M] \{\dot{x}(0)\} \sin(\sqrt{1-\nu_r^2} p_r t) \right] \{\mu\}_r.$$

If the acceleration solution is considered to be composed of the sum of an acceleration term $\{A\}_r$, multiplied by a function of time term, $T_r$, $\{\ddot{x}(t)\}$ can be expressed as

$$\{\ddot{x}(t)\} = \sum_{r=1}^{4} \{A\}_r T_r.$$

Based on this, the acceleration modal participation factor for each mode ($\{A\}_r$) becomes

$$\{A\}_r = (3\nu_r^2 - \nu_r^4 - 1) p_r \{\mu\}_r^T [M] \{\dot{x}(0)\} \{\mu\}_r. \tag{4.9}$$

The acceleration modal participation factor for specific implant-abutment geometries will be used to indicate the amount each mode present in the model acceleration response. The mode shapes for each mode are then used to determine the configuration of the system for each mode during impact.

### 4.4.1 Acceleration Modal Participation Factor

The model acceleration response for a 10 mm implant with a 10 mm abutment and a $k$ of 7.5 GPa is shown in Figure 4.15. The 10 mm abutment case was selected to emphasize the high frequency component in the measured accelerometer signal. The damping constant was set to the value determined for FRB-10 in Section 4.2.2. This is the same response that was shown to agree with the *in vitro* measurements in Section 4.2.1.3. The acceleration response shown is in actuality a sum of four different acceleration responses superimposed (as demonstrated in equation (A.20)).

The four individual modal acceleration responses that are combined to get the final acceleration response are shown in Figure 4.16. From the figure, the maximum amplitude of the second mode acceleration response is about an order of magnitude smaller than the maximum amplitude of the first mode frequency. The maximum amplitude of the third mode is about three orders of magnitude smaller than the first mode and the fourth mode maximum amplitude is four orders of magnitude smaller than the first mode. When the four responses are added together, the only two modes that visibly contribute are the first and second modes. Table 4.4 shows the acceleration modal participation factors for the 10 mm implant along with the normalized acceleration participation factor and the damping ratio for each mode. The amplitudes of the acceleration response were normalized in Figures 4.15 and 4.16 so that the amplitudes could be compared to measurements (as described in Section 4.2.1.3). The normalized acceleration participation factors for each mode represent the magnitude of the acceleration responses for each mode shown in Figure 4.16. This figure also demonstrates the effects of damping in the model. The higher

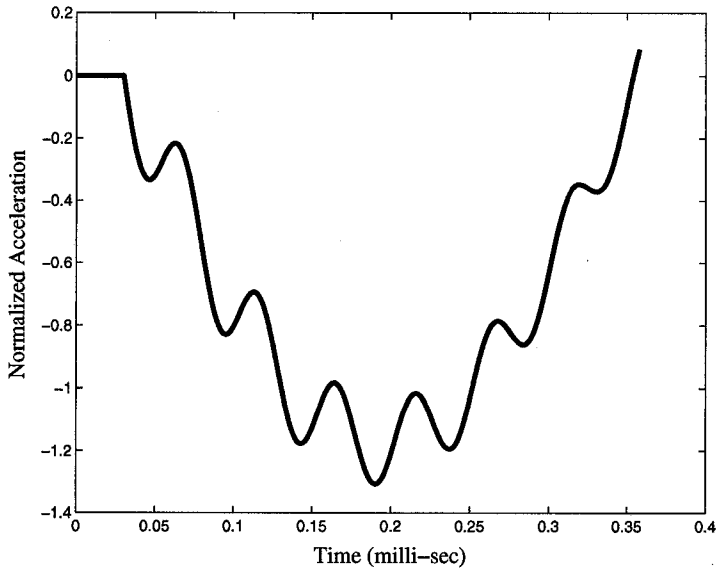


Figure 4.15: Model acceleration response for a 10 mm implant with a 10 mm abutment.

modes are damped out more quickly than the lower ones, as the damping ratio is higher for these modes. The damping ratio is proportional to the resonant frequency, the higher the resonant frequency the higher the damping ratio (as described in Section 4.2.2).

The acceleration modal participation factors shown in Table 4.4 are for a specific implant-abutment geometry with a specific supporting $k$. From equation (4.9), the modal participation factors are essentially determined by system properties such as mass and resonant frequency. Changes to striking location, implant-abutment geometry, mass, initial conditions or supporting material stiffness will result in different participation factors.

Figure 4.17 shows the comparison of model results to the measurements of a 10 mm implant with a 10 mm abutment (as in Section 4.3.2). The measurements show that for the 10 mm abutment there are two visible frequencies present. The model results match the measurements for this case very well, demonstrating that the third and fourth acceleration participation factors should be comparatively small to the first mode (as was shown to be the case).

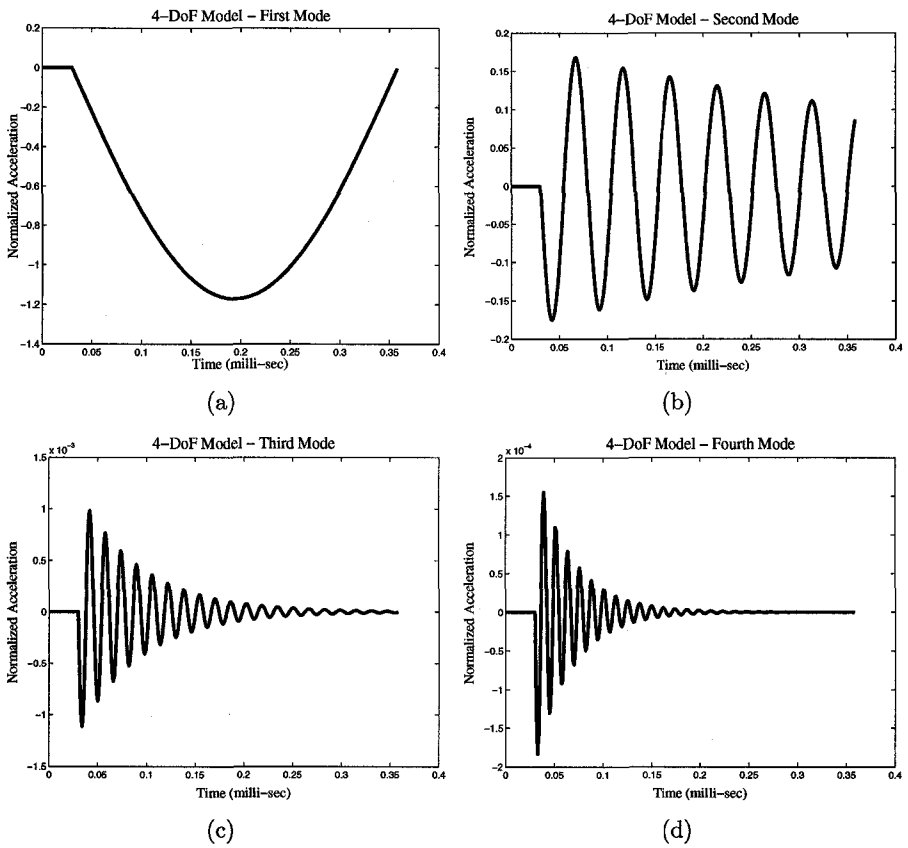


Figure 4.16: Modal acceleration components for a 10 mm implant with a 10 mm abutment and $k$ of 7.5 GPa

Table 4.4: Acceleration modal participation factors and damping ratios for a 10 mm implant with a 10 mm abutment placed into FRB-10.

| Mode | 10 mm Abutment | | |
|---|---|---|---|
| | $A$ (m/s$^2$) | Normalized $A$ | Damping Ratio (%) |
| 1 | -1.89x10$^3$ | -1.2 | 0.1 |
| 2 | -288.0 | -0.2 | 1.5 |
| 3 | -1.9 | -1.2x10$^{-3}$ | 4.8 |
| 4 | -0.3 | -1.9x10$^{-4}$ | 6.3 |

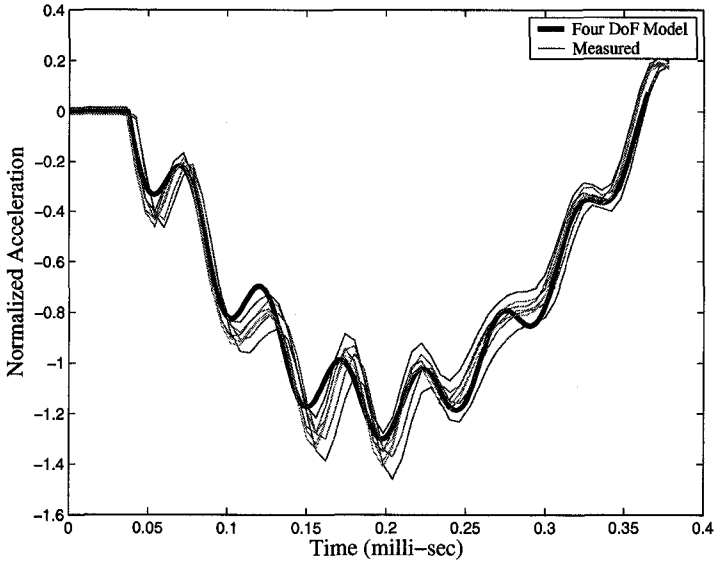


Figure 4.17: Model acceleration response for a 10 mm implant and 10 mm abutment compared to measurements.

### 4.4.2 Mode Shapes

Equation (A.5) in Appendix A is a standard eigenvalue/eigenvector problem in which the undamped resonant frequencies (eigenvalues) and the mode shapes (eigenvectors) can be determined for the four degree of freedom model. The mode shapes can be used to construct a physical representation of the motion of the implant, abutment and impacting rod for a given input initial condition. As an example, a 4 mm flanged implant, with a 10 mm abutment and $k$ of 1 GPa has a first mode frequency modal vector

$$\{u\}_1 = \begin{Bmatrix} 0.32 \\ 0.24 \\ 0.02 \\ 0.01 \end{Bmatrix}.$$

This modal vector $\{u\}_1$ is illustrated in Figure 4.18 where the initial position is shown as a dotted line. The center of mass of the striking rod is represented as a square along the striking rod. The implant-abutment joint is represented by the circled "x". The y-direction on the plot measures distance from the bottom of the implant (point 0) to the top of the abutment (14 mm for a

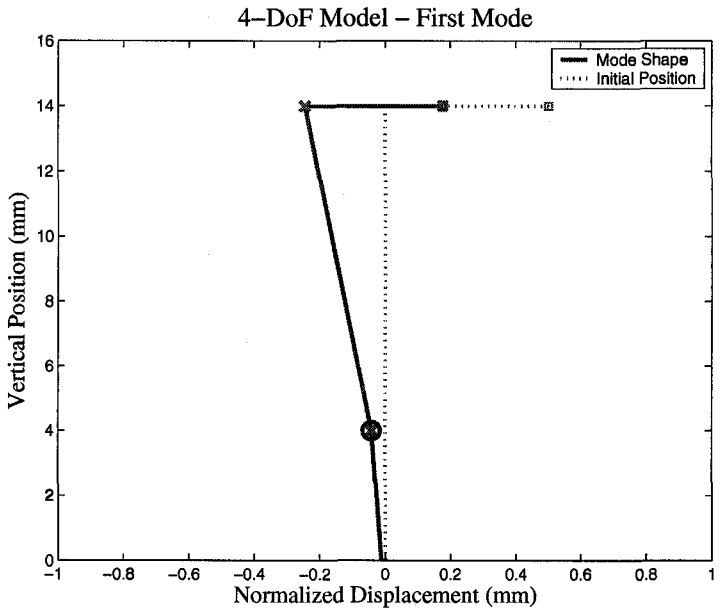


Figure 4.18: First mode resonant frequency mode plot for a 4 mm flanged implant with a 10 mm abutment and $k = 1$ GPa.

10 mm abutment on a 4 mm implant). In the figure, positive motion is from right to left. Places in which the solid line for the implant and abutment cross the dotted line are points that remain stationary for the impact. Such a point is often referred to as a *node*. The *nodal* point for this mode occurs slightly below the bottom of the implant.

Table 4.5 details the *nodal* point locations for two different implant systems with two different $k$ values. A 4 mm flanged extraoral implant (4 mm engagement length) with a 10 mm abutment and a 10 mm intraoral implant (10 mm engagement length) with a 10 mm abutment were simulated with $k$ either 1 or 7.5 GPa. Two different implants were used to show the variations between an intraoral implant and a shorter, flanged extraoral implant. The flange stiffness used for the extraoral implant was $K_F = 3.65\text{x}10^7$ N/m as determined in Section 4.2.3. The $K_F$ value used is larger than what would be found clinically, as the $K_F$ value was determined with an epoxy layer under the flange. This simulation does, however, provide an example of a case where the flange is osseointegrated to the bone surface and provides maximum support to the implant. A $k$ value of 1 GPa represents a system in which the implant-

Table 4.5: *Nodal* point locations for both 4 mm and 10 mm implants at $k$ of 1 and 7.5 GPa

| Mode | $k = 1$ GPa | | $k = 7.5$ GPa | |
|---|---|---|---|---|
| | 4 mm Implant | 10 mm Implant | 4 mm Implant | 10 mm Implant |
| 1 | -1.6 mm | 4.2 mm | 1.2 mm | 4.2 mm |
| 2 | -13.9 mm | 2.3 mm | 0.1 mm | 3.6 mm |
| 3 | 20.6 mm | 18.2 mm | -19.2 mm | -1.3 mm |
| 4 | 3.0 mm | 5.4 mm | 3.2 mm | 7.7 mm |

bone interface is relatively low compared to the interface stiffness determined for the 10 mm implant FRB disk in Section 4.2.1.3 (7.5 GPa).

The different mode shapes for each frequency for the 4 mm implant with a 10 mm abutment and $k$ of 1 GPa are shown in Figure 4.19. The first mode shape has the center of mass of the striking rod moving to the left with the top of the abutment. Both the implant and abutment rotate counter-clockwise, with little bending occurring about the joint. The horizontal displacement of the center of mass of the striking rod is slightly more than that of the top of the abutment, which would put the spring $K_I$ in slight compression. The second mode has the implant and abutment moving to the right, back into the striking rod, with the striking rod center of mass staying in approximately the same position (very little movement). The implant and abutment both rotate clockwise almost the same amount, producing little bending about the joint. The *nodes* for both the first and second modes are located below the implant.

The mode shapes for the 4 mm implant with a 10 mm abutment and a $k$ of 7.5 GPa are shown in Figure 4.20. The mode shapes are similar to those in Figure 4.19, however, there appears to be less displacement (less motion to the left or right of the dotted line) of the implant and more bending about the joint in the 7.5 GPa case. The *nodes* for the first and second modes increased from -1.6 and -13.9 mm to 1.2 and 0.1 mm, respectively.

The 10 mm implant mode shapes for the two different $k$ values are shown in Figures 4.21 and 4.22. The mode shapes for the 10 mm implant are similar to those of the 4 mm implant. For the first and second modes, the increase in $k$ reduced both the horizontal and rotational displacements of the implant. There was also an increase in the amount of bending about the joint. The location of the *node* in the first mode did not change when $k$ was increased, however, the second mode *node* moved from 2.3 to 3.6 mm along the length

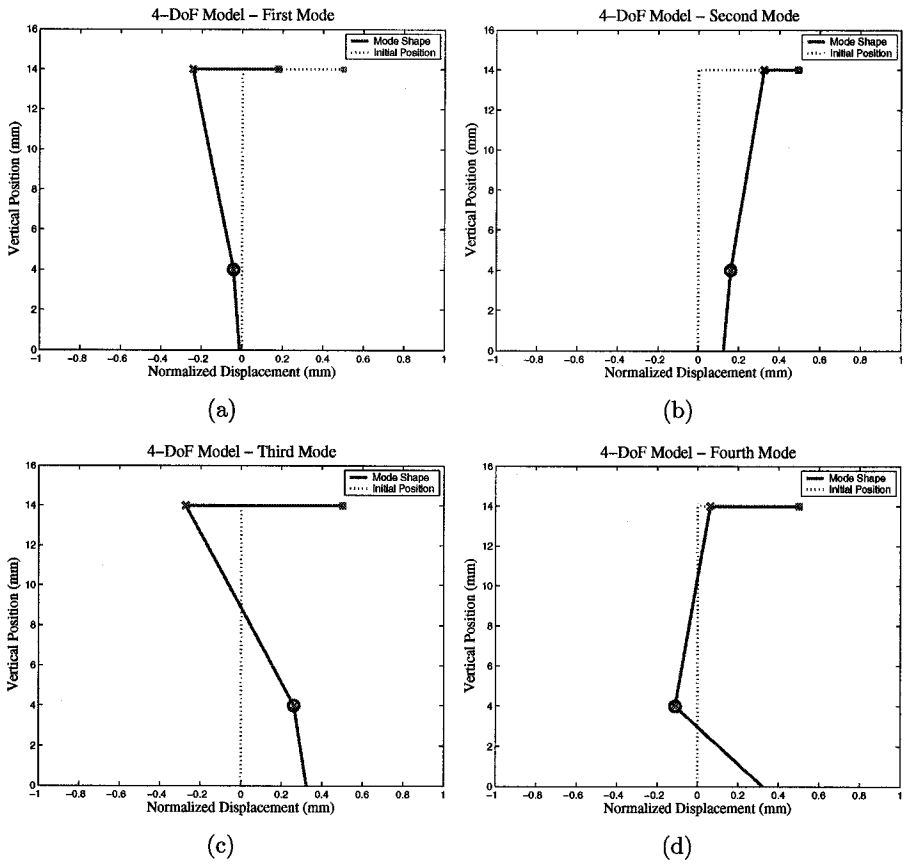


Figure 4.19: Mode shapes for a 4 mm implant with a 10 mm abutment and $k$ of 1 GPa

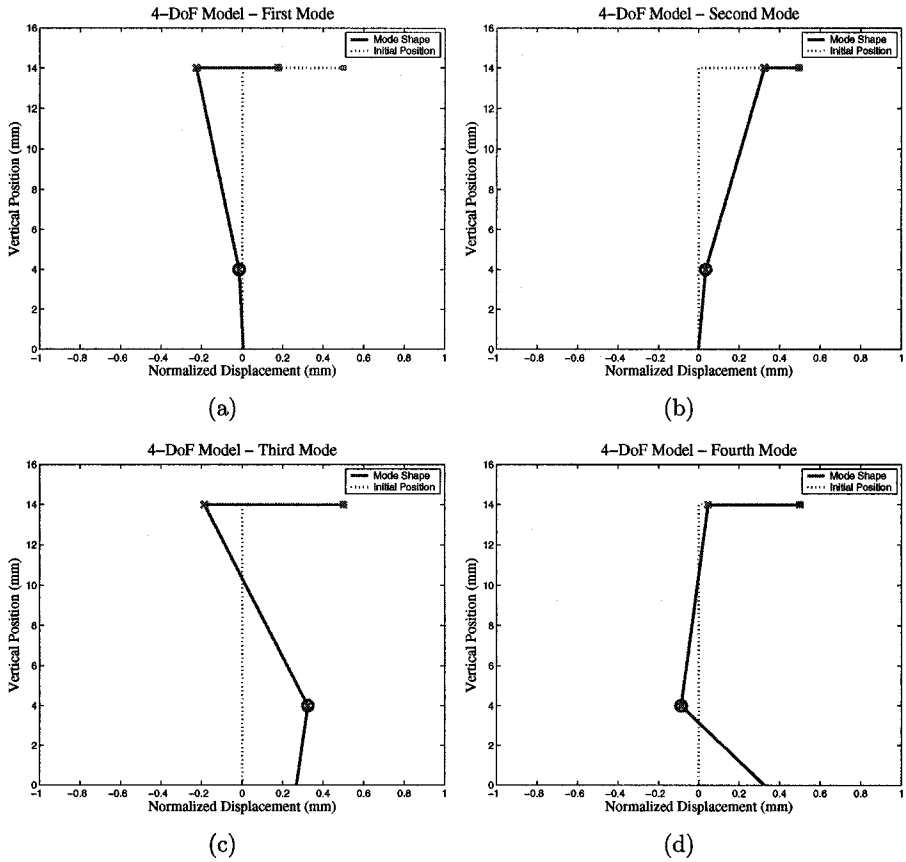


Figure 4.20: Mode shapes for a 4 mm implant with a 10 mm abutment and $k$ of 7.5 GPa

of the implant.

Overall, the mode shapes for the two different length implants are similar. It appears that increasing the stiffness of the interface $k$ has the effect of increasing the bending about the joint and decreasing the displacement of the implant (both the angular and horizontal). For the first and second mode shapes, increasing $k$ also had the effect of moving the *node* locations upward along the length of the implant in all but one case (the first mode for the 10 mm implant).

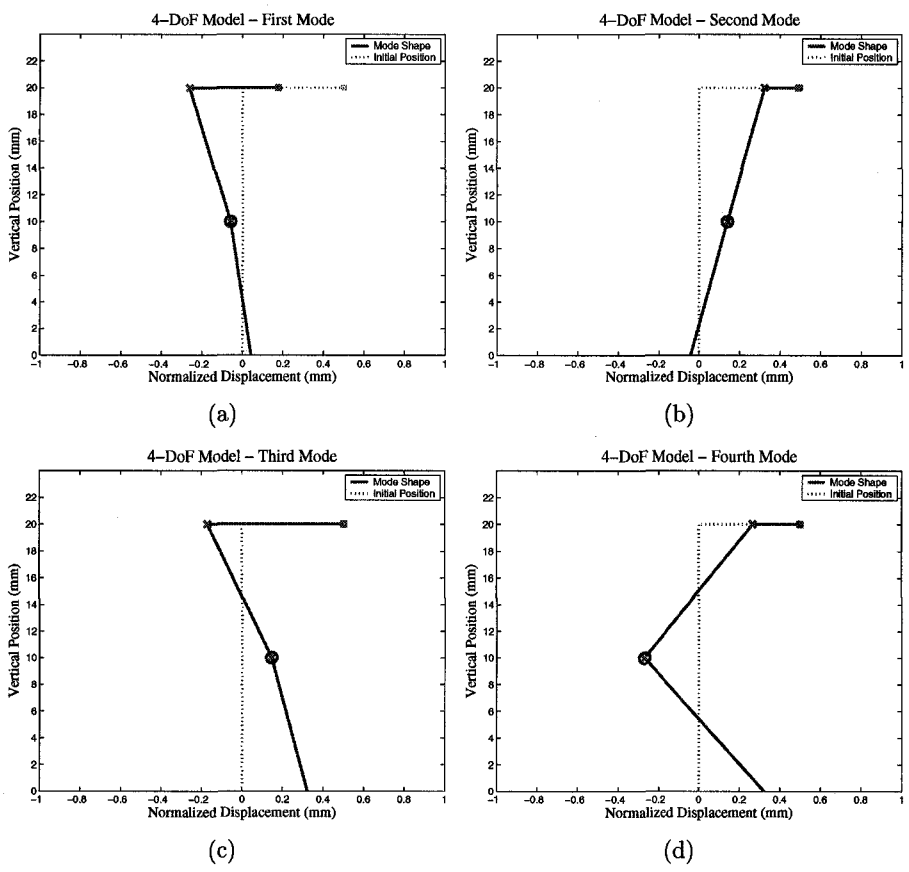


Figure 4.21: Mode shapes for a 10 mm implant with a 10 mm abutment and $k$ of 1 GPa

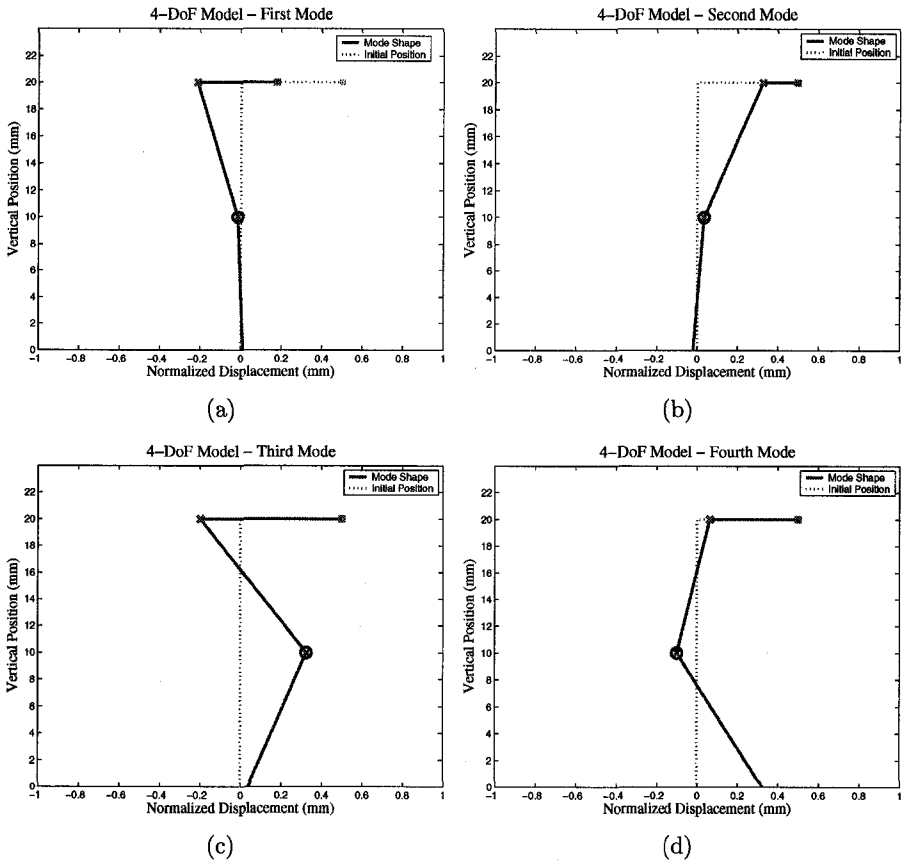


Figure 4.22: Mode shapes for a 10 mm implant with a 10 mm abutment and $k$ of 7.5 GPa

# Chapter 5

# Analytical Model Simulations

In this chapter the previously developed model is used to investigate expected changes in the resonant frequencies of Brånemark implant-abutment systems due to simulated changes in the health of the bone-implant interface. Two changes in bone structure were investigated with the analytical model; changes in the supporting bone stiffness and marginal bone height losses around the neck of the implant. The model was then used to determine if it would be possible to predict the effect a flange has on implant stability *in vivo*. The flange stiffness determined from Chapter 4 represents a flange bonded to the support surface (such as would occur of the flange was osseointegrated with the bone surface). Simulations with this flange stiffness will provide simulations for cases in which the flange is providing a maximum amount of support.

## 5.1 Sensitivity of Determined Model Parameters

This section evaluates the sensitivity of the first and second mode frequencies to some of the estimated parameters determined in earlier sections. These simulations will determine how any uncertainties in the estimation of the parameters will affect the results.

The model simulations are for a 10 mm intraoral implant with a 10 mm abutment impacted at the upper rim. A 10 mm abutment was chosen to ensure some bending of the abutment was represented in the simulations. The interface stiffness, $k$, was set to 7.5 GPa. Only one variable in the analytical model was changed (the variable being tested) at a time.

### 5.1.1 Sensitivity to Changes in Impact Stiffness

From Table 4.2 in Section 4.2.1.1, the $K_I$ for a 10 mm abutment was found to be 2.56x10$^6$ N/m (which is shown on Figure 5.1). To determine how sensitive the model is to the impact stiffness, $K_I$ was varied from 1x10$^6$ to 5x10$^6$ N/m (roughly from one half to twice the 2.56x10$^6$ N/m value determined for a 10 mm abutment). The $K_I$ value determined for a 10 mm abutment in Chapter 4 is indicated on the figure. The effects on the first and second mode frequencies due to changing $K_I$ are shown in Figure 5.1. From the figure, the first mode frequency changes from 1230 Hz to 1655 Hz and the second mode frequency changes from 15.6 kHz to 25.6 kHz. The changes in $K_I$ result in a 35% increase in the first mode frequency and a 64% increase in the second mode frequency, overall. Compared to the first mode frequency, the second mode frequency had a larger overall increase (10 kHz) and a larger percent increase (64%), which suggests that the second mode frequency is more sensitive to changes in $K_I$. In Figure 5.1a as $K_I$ increases the slope of the curve decreases, indicating that as $K_I$ increases the first mode frequency becomes less sensitive to these changes. In Figure 5.1b the second mode frequency changes over the range of $K_I$ is essentially linear.

From the plots, $K_I$ has the potential to significantly affect both first and second mode frequencies. The $K_I$ value for the different length abutments shown in Table 4.2 ranged from 2.25x10$^6$ N/m to 2.98x10$^6$ N/m, a 28% difference that would result in a 69 Hz difference in first mode frequency and 1870 Hz difference in the second mode frequency. As there is currently no data available on how much $K_I$ may vary with different abutment designs by different manufacturers, the effect of $K_I$ cannot be ignored. As such, $K_I$ needs to be determined for each abutment being tested.

### 5.1.2 Sensitivity to Changes in the Torsional Stiffness

Figure 5.2 shows the effect of changing $K_T$ on the first and second mode resonant frequencies. The value of $K_T$ for a 10 mm abutment was found to be 164.7 Nm/rad from equation (4.7) in Section 4.2.1.3 (indicated on the figure). The value of $K_T$ was varied between 80 and 350 Nm/rad (from roughly one half to twice its estimated value), which resulted in the first mode frequency changing from 1220 Hz to 1800 Hz and the second mode frequency changing from 19.1 kHz to 21.9 kHz. The changes in $K_T$ result in a 48% increase in the first mode frequency and a 15% increase in the second mode frequency. If the change in second mode frequency is compared to the first mode frequency, the overall change of 2.8 kHz for the second mode is larger than the 580 Hz change

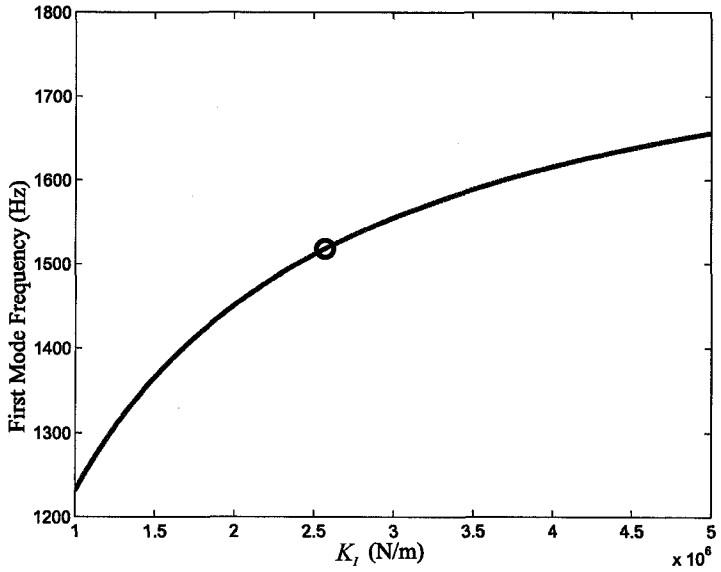


(a)

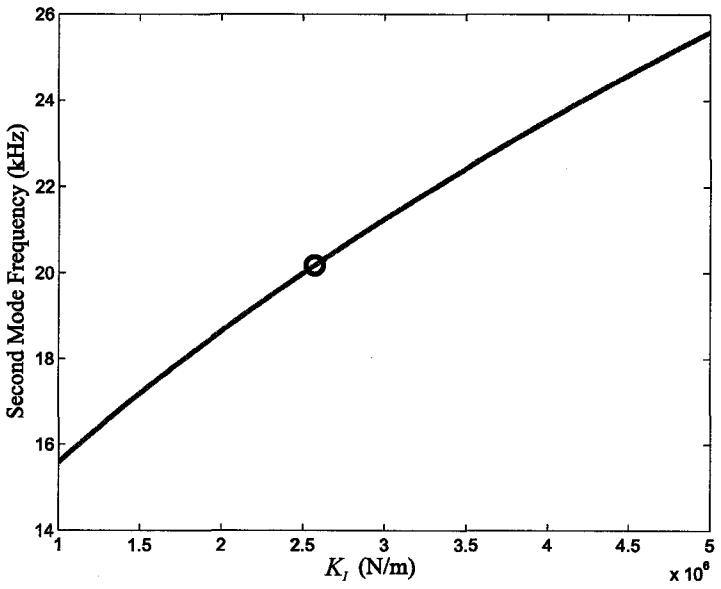


(b)

Figure 5.1: Effects of varying $K_I$ on the resonant frequencies for a 10 mm implant with a 10 mm abutment. (a) First mode frequency. (b) Second mode frequency.

in the first mode frequency. However, proportionally the first mode frequency changes much more than the second mode (48% increase versus 15% increase). This indicates that, at least proportionally, the first mode frequency is more sensitive to changes in $K_T$ than the second mode. From Figure 5.2a as $K_T$ increases the slope of the curve decreases, indicating that similar to $K_I$, as the stiffness of $K_T$ increases the first mode frequency become less sensitive to the change. The second mode frequency response as shown in Figure 5.2b is nearly linear, and appears relatively insensitive to the change in $K_T$ (the line is much more horizontal than was found in the $K_I$ case). The simulation shown for the 10 mm abutment has a lower $K_T$ value than shorter implants. This "least stiff" case has the largest sensitivity to $K_T$. As the stiffness of $K_T$ increases the system becomes less sensitive to variations in the value of $K_T$.

## 5.2 Simulation of Changes to Interface Stiffness

Changes in the supporting interface can be modeled by changing the stiffness of the horizontal and vertical springs ($k$) in the analytical model. The simulations of changes in $k$ were done over a range of implant-abutment geometries, a 4 mm extraoral implant with 5.5 mm and 7 mm standard abutments and a 10 mm intraoral implant with 5.5 mm and 7 mm standard abutments. While a 10 mm abutment has been used in many of the previous simulations, the 10 mm abutment is not used clinically as often as the shorter abutments simulated in these tests.

For the simulations, all impacts occur at the top rim of the abutments. The stiffness $k$ was then varied from 0.75 to 15.0 GPa for each implant with each different abutment.

### 5.2.1 First Mode Frequency

The effects of varying $k$ on the first mode frequency are shown in Figure 5.3. As expected for both implants, the effect of increasing the abutment length from 5.5 to 7 mm lowered the resonant frequency. For the flanged 4 mm implant two separate simulations were done for each abutment, one simulation without a flange and one with the flange value determined from the *in vitro* simulations in Section 4.2.3. The $K_F$ value determined in Section 4.2.3 was for a flange with a thin epoxy layer bonding it to the FRB disk surface, and was taken as a maximum possible flange contribution. In Figure 5.3b the upper curve for each abutment represents the maximum flange effect and the lower curve shows

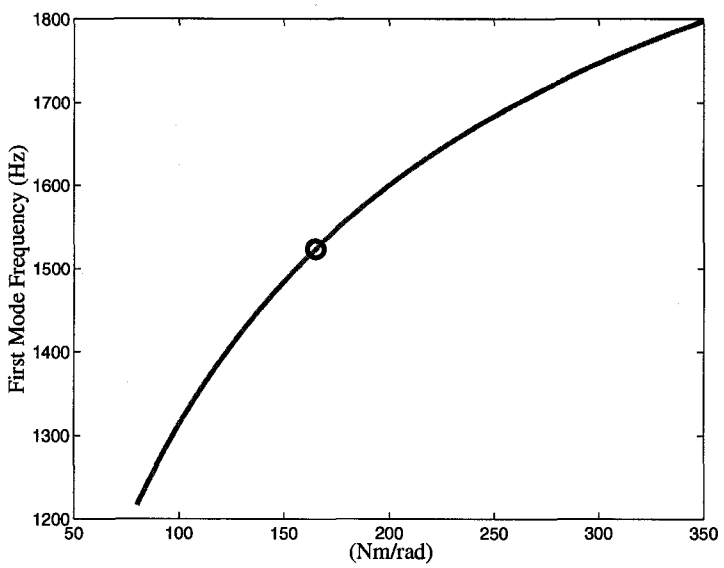


(a)

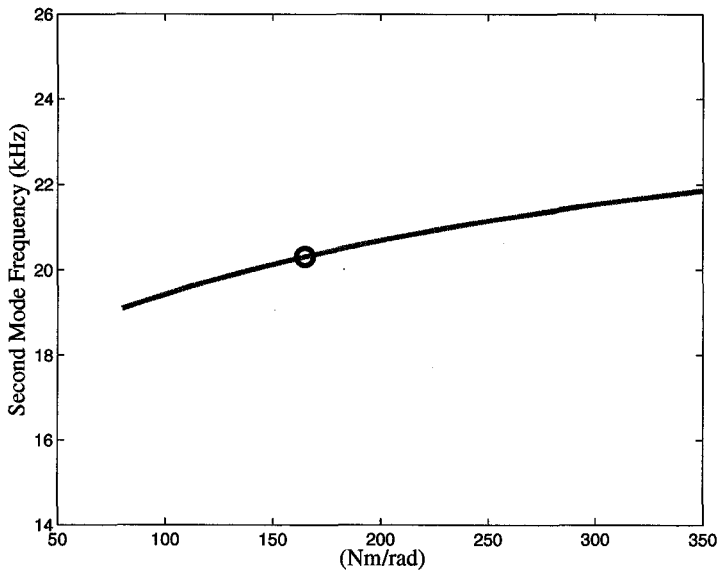


(b)

Figure 5.2: Effects of varying $K_T$ on the resonant frequencies for a 10 mm implant with a 10 mm abutment. (a) First mode frequency. (b) Second mode frequency.

the effect without a flange. In a clinical situation the flange stiffness would produce an effect between the maximum and minimum curves shown. From Figure 5.3, the 5.5 mm abutment has a slightly greater change in frequency over the range of $k$ than the 7 mm abutment for both implants.

Figure 5.3b also shows that the curves without a flange have a greater frequency range than with a flange. The inclusion of a flange has the effect of reducing the sensitivity of the resonant frequency to changes in the interface stiffness $k$.

In Figure 5.3, a steeper slope indicates a greater frequency sensitivity to changes in $k$. For both implants the curves start to plateau after approximately 5 GPa. This indicates that as the stiffness of the interface ($k$) continues to increase the resonant frequency becomes less sensitive to the changes. For stiff interfaces the measurement system may be unable to determine changes occurring at the implant interface. However, for values of $k$ in this upper range, the implant is generally considered well integrated and not in immediate danger of failing, so the changes which may occur in $k$ are of less importance.

### 5.2.2 Second Mode Frequency

The effects of varying $k$ on the second mode frequency are shown in Figure 5.4. The flanged 4 mm implant was treated in the same manner as in the previous section with $K_F$ varying between zero and a maximum value. Similar to the first mode results, the longer abutment lowers the resonant frequencies. The second mode frequency difference between the 5.5 and 7 mm abutment curves is much greater for both implants than was found for the first mode frequency. This indicates that in the second mode, the 5.5 mm abutment is significantly more sensitive to changes in $k$ than the 7 mm abutment. There also appears to be less difference between the maximum flange and no flange curves than was found in the first mode, indicating the flange has less of an effect on the second mode frequency. Both the 5.5 and 7 mm abutments have a greater overall change in frequency for the 10 mm implant case, compared to the 4 mm implant case. The second mode curves do not appear to plateau as significantly as was found in the first mode.

Increasing the length of the abutment had the effect of lowering both the first and second mode frequencies for both implants. An explanation for this is that as abutment length increases, $K_T$ decreases (as can be seen in equation (4.7), in Section 4.2.1.3). A lower $K_T$ stiffness will result in more bending about the implant-abutment joint and a lower resonant frequency for both first and second mode.

For both first and second mode frequencies, the 5.5 mm abutment had a

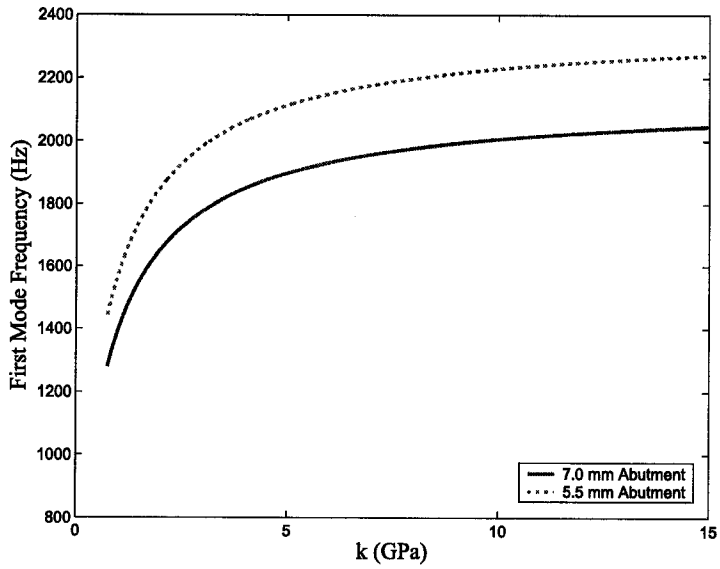


(a)

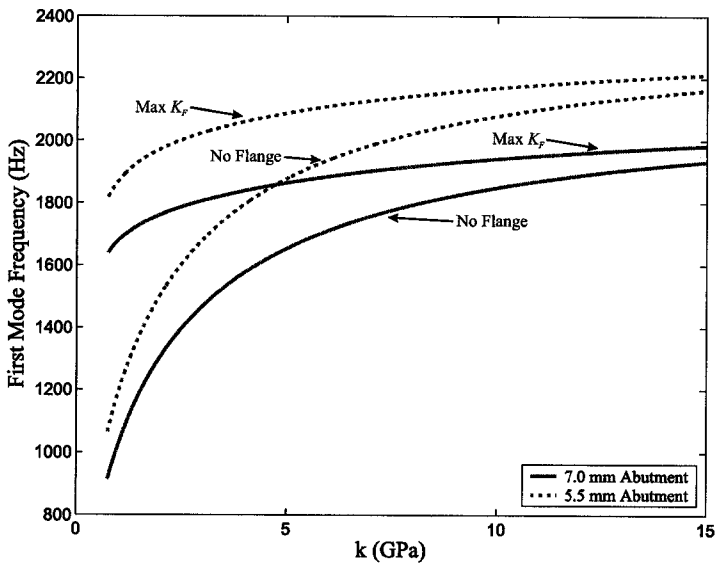


(b)

Figure 5.3: Effects of varying $k$ on the first mode frequency for two abutment lengths. (a) 10 mm implant. (b) 4 mm implant.

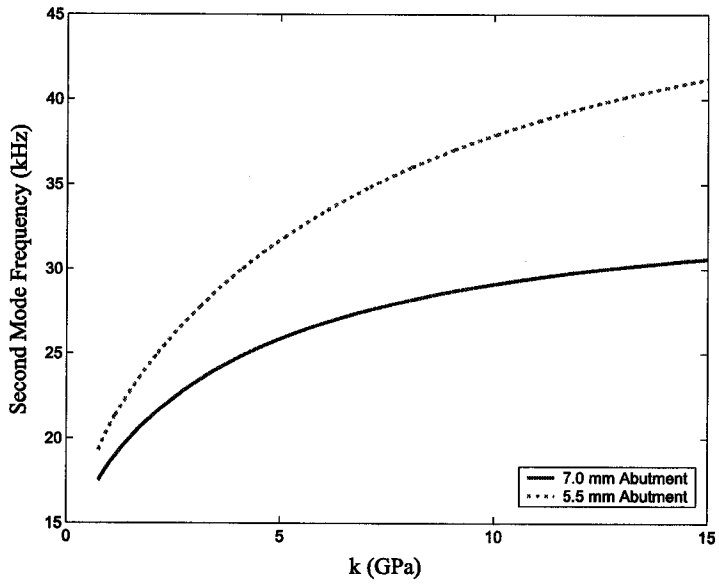


(a)

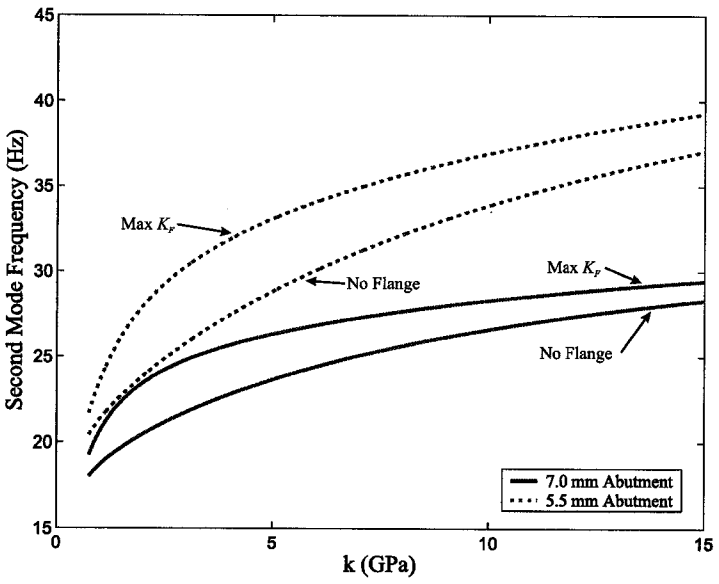


(b)

Figure 5.4: Effects of varying $k$ on the second mode frequency for two abutment lengths. (a) 10 mm implant. (b) 4 mm implant.

greater change in frequency over the range of $k$ than the 7 mm abutment (which could be seen for both implants). As abutment length decreases, $K_T$ increases which causes the first mode resonant frequency to be more sensitive to $k$. Essentially, as $K_T$ increases the system becomes more rigid so the first mode frequency is more directly related to the underlying bone-implant stiffness $k$.

The first mode frequency values begin to plateau at higher $k$ values for both abutments on both implants. Physically, as the bone-implant interface increases in stiffness, what is essentially being measured is the flexibility of the attached components ($K_T$ and $K_I$). These flat areas indicate an upper level of $k$ that the measurement system can effectively determine.

The second mode frequencies did not plateau to the same degree as was found in the first mode, and overall the second mode appears more sensitive to $k$. For example, the 5.5 mm abutment with the 10 mm implant the second mode frequency changes from 19 kHz to 41 kHz (approximately 2 times) over the range of $k$, while the first mode frequency changes from 1.4 kHz to 2.3 kHz (about 1.6 times).

## 5.3 Simulation of Bone Loss

One of the mechanisms with which an implant can fail is from crestal bone loss around the head of the implant. Brunski, J.B. (1999) suggests that in some cases, implant failure may be the result of a "positive feedback" loop in which bone loss at the top of the implant leads to more bone loss and this continues until implant failure. If implants can be identified as having bone loss early enough, preventative measures may save the implant. As such, the ability to measure implant bone loss would be of clinical value. To this end, the model was used in a number of simulations to help determine how bone loss may manifest itself in the impact measurements.

For the simulations, bone loss starts at the top of the implant and progresses down the length of the implant toward the base. For the bone loss calculations, two implant-abutment geometries were used, a 4 mm extraoral implant with a 5.5 mm abutment and a 10 mm intraoral implant with a 5.5 mm abutment. In the simulations the engagement length was lowered 5 mm in 0.5 mm increments for the 10 mm implant, and 2 mm in 0.5 mm increments for the 4 mm implant. This was done for $k$ values of 1, 5, and 10 GPa.

### 5.3.1 Intraoral Implants

The simulations of the changes in first and second mode frequencies due to bone loss around a 10 mm intraoral implant is shown in Figure 5.5. The $k$ of 1 GPa curve in Figure 5.5a shows a linear relationship between bone loss and first mode frequency. At higher interface stiffness values the first mode frequency curves become less linear and there is a smaller overall change in frequency corresponding to the bone loss. At a $k$ of 1 GPa the first mode frequency changes by approximately 800 Hz (amounting to a change of about 80 Hz per half-millimeter of bone loss) while the $k$ of 10 GPa curve changes by approximately 500 Hz. The second mode frequency curves shown in Figure 5.5b are all quite linear, with the higher interface stiffness curves showing a greater amount of frequency change as bone resorbs around the implant. For the second mode frequency the $k$ of 1 GPa curve changes 600 Hz per half-millimeter of bone loss while the 10 GPa curve changes approximately 1600 Hz per half-millimeter of bone loss.

Clinically, the results of these tests indicate that for less stiff interfaces the first mode frequency is more sensitive to bone loss while the second mode frequency is less sensitive than at higher interface stiffnesses.

### 5.3.2 ExtraOral Flanged Implants

The 4 mm implant curves shown in Figure 5.6 are all essentially linear for both first and second mode frequencies, however, there is an initial rapid decrease in stability during the first 0.5 mm of bone loss. This decrease in the first 0.5 mm was caused by the removal of the flange stiffness $K_F$ as material is removed from under it. This is more extreme than what likely occurs in practice, as the $K_F$ value used was larger than would be expected clinically. The removal of the flange was less significant to the 10 GPa case than for the 1 GPa case. This is due to the underlying stiffness $k$ being higher in the 10 GPa case, thus $K_F$ provides proportionally less stability than it does for the 1 GPa case. This indicates that as the bone-implant interface becomes stiffer, the effect of $K_F$ becomes less significant.

After the initial loss of $K_F$, the curves for both the first and second mode frequencies appear linear. Similar to the intraoral implant case, the first mode sensitivity to bone loss shown in Figure 5.6a decreases as the interface stiffness increases. There is a change of about 100 Hz per half-millimeter of bone loss for the $k$ of 1 GPa and 75 Hz per half-millimeter of bone loss for a $k$ of 10 GPa. The second mode frequency curves shown in Figure 5.6b also show similar results to the intraoral case, with the second mode frequency becoming

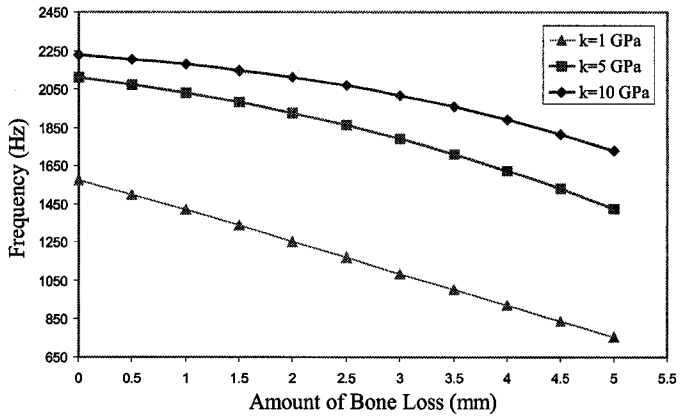


(a)

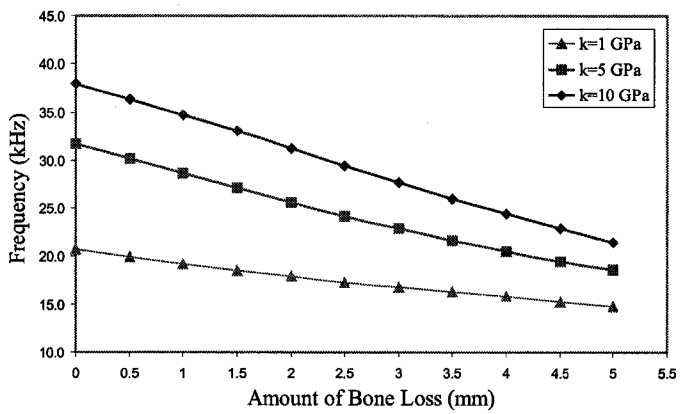


(b)

Figure 5.5: Effects on resonant frequency of bone loss from top of a 10 mm intraoral implant towards base. (a) First mode frequency. (b) Second mode frequency.

less sensitive to bone loss at the lower interface stiffness. The 4 mm extraoral implants have a greater change in frequency per half-millimeter of bone lost as compared to the longer intraoral implants (100 Hz compared to 80 Hz in the first mode, 700 Hz compared to 590 Hz in the second mode for a $k$ of 1 GPa). This is not entirely unexpected, as it indicates that shorter implants are more sensitive to the loss of bone along their lengths than a longer implant.

## 5.4 Simulation of Flange Loss

In the previous Section 5.3.2, it was shown that the loss of the flange reduces the stability of the 4 mm extraoral flanged implant. It would be useful if the model could predict the effect of a flange *in vivo* based on the measured impact accelerometer response. The flange value used was a $K_F$ of $3.65\text{x}10^7$ N/m determined in Section 4.2.3. As discussed previously, this $K_F$ value represents a maximum flange contribution case with the flange bonded to the supporting surface. Clinically, the value of $K_F$ would fall between either no flange support or the maximum $K_F$ value that was determined in Section 4.2.3. To this end, the model acceleration response for a 4 mm extraoral implant with a 10 mm abutment was compared with and without a flange at two different first mode frequencies as shown in Figure 5.7. The two frequencies were chosen to represent a stable implant measurement (1500 Hz) and a less stable implant measurement (1300 Hz). Figure 5.7a shows the model predictions for stable implants which have higher measured first mode frequencies (1500 Hz). There is no difference between the results with and without a flange, indicating that for more stable implants, the inclusion of a flange has a negligible effect on the model output response. However, for less stable implants (1300 Hz) there is a noticeable difference between the higher frequency component in the response for the flange and no-flange signals. This suggests that by comparing the measured results to the model predictions, the model may be able to determine whether the flange is contributing to the overall stiffness of the system for less stable implants.

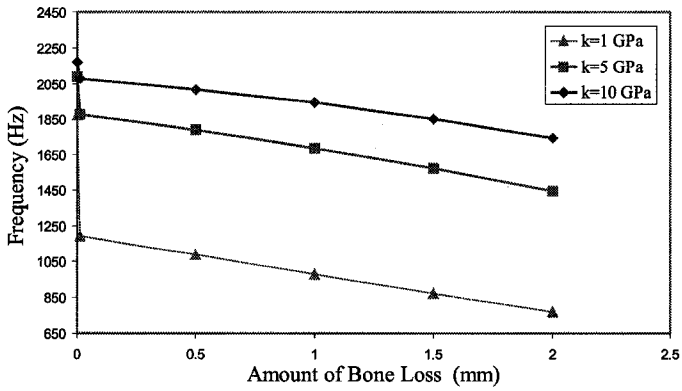


(a)

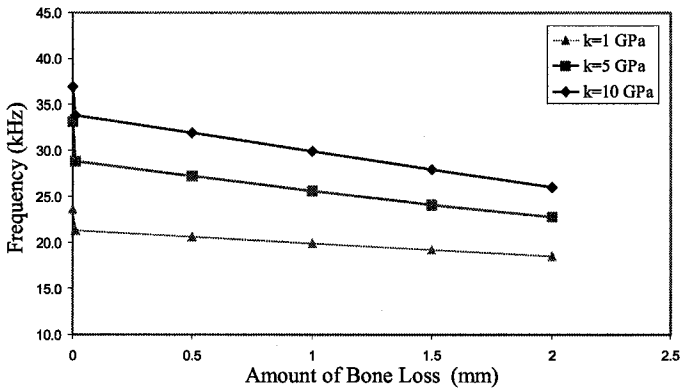


(b)

Figure 5.6: Effects on resonant frequency of bone loss from top of a 4 mm extraoral flanged implant towards base. (a) First mode frequency. (b) Second mode frequency.

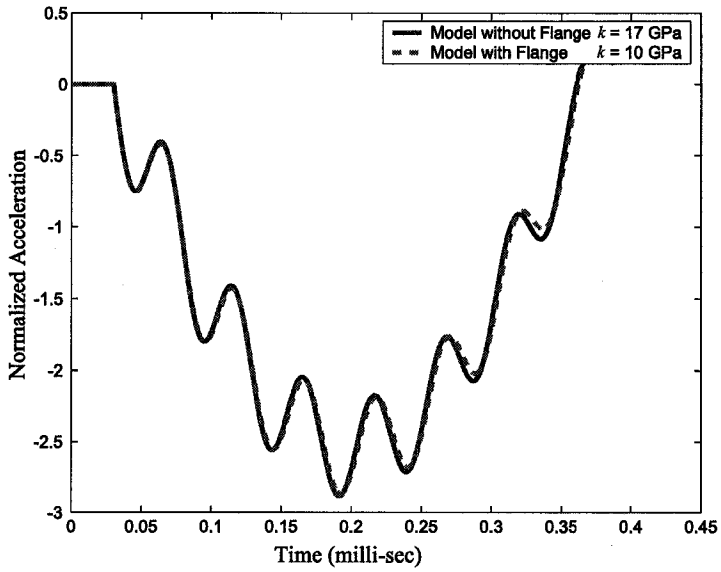


(a)

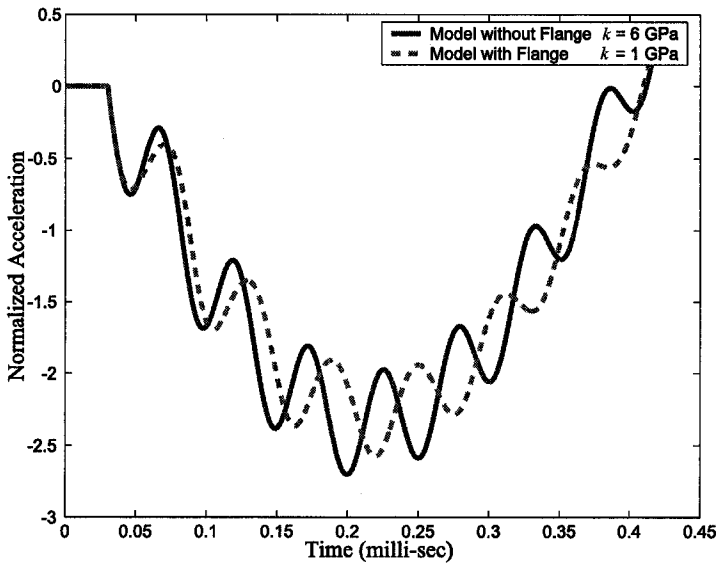


(b)

Figure 5.7: Model results with and without a flange at two different first mode frequencies. (a) $p_1 = 1500$ Hz. (b) $p_1 = 1300$

# Chapter 6

# *In Vivo* Results

This chapter details the use of the previously described impact technique utilizing the Periotest® handpiece in an *in vivo* clinical setting. The testing was done in conjunction with the Craniofacial Osseointegration and Maxillofacial Prosthetic Rehabilitation Unit (C.O.M.P.R.U.), located at the Misericordia Community Hospital, Edmonton, Alberta, Canada. All testing was approved by the University of Alberta Health Research Ethics Board and patients signed an informed consent prior to taking part in the study. Twelve patients treated with Bone Anchored Hearing Aid (BAHA®) implants enrolled into a longitudinal study in which impact tests were conducted at installation as well as at the 1, 2, 3, 6 and 12 month patient visits. The goal of this testing is to collect and use the raw accelerometer signal with the mathematical model to estimate the corresponding changes in the bone-implant interface properties.

## 6.1 Testing Methods and Materials

The patient study group consisted of 12 patients, 8 males and 4 females. The mean patient age at time of implant placement was 53 years (range 27-75 years). Patients enrolled in the study were treated with Bone Anchored Hearing Aid (BAHA®) implants which were left to heal for 3 months before the patients received their hearing processors. To have been considered for the study the patients:

- had to be 18 years of age or older,
- meet audiological criteria for selection into the BAHA® program,
- had to be able to maintain a skin penetrating abutment,

- did not have any condition that could jeopardize osseointegration e.g. malignancy in the temporal region, radiation therapy of the temporal region, undergoing chemotherapy,
- had to be able to understand and read English well.

Following a one-stage procedure, 12 flanged extraoral implants (Ø 3.75 mm, SEC 002-0, Entific Medical Systems, Toronto, Ontario, Canada) were placed (one per patient). The implants for 11 of the patients were 4 mm in length while one patient had a 3 mm implant. Implants were installed on either the right or left side, based on the audiological recommendation.

### 6.1.1 Measurement System

The *in vivo* measurements made use of similar measuring equipment as previously described in detail in Chapter 2. Impact readings utilized the Periotest® handpiece to initiate the impact. The Periotest® used was modified as described in Section 2.1.1 so that the raw accelerometer signal could be collected. The accelerometer signals were collected from the handpiece with the Instrunet analog/digital model 100 sampling system with a sampling rate of 167 kHz which was connected to a Toshiba Satellite A10 laptop computer.

### 6.1.2 Clinical Periotest® Handpiece Protocol

An *in vivo* protocol was developed prior to patient measurements for the use of the Periotest® handpiece. The protocol was based on measurement recommendations outlined in Section 3.2.3. Prior to the *in vivo* measurements, the clinicians were instructed as follows:

1. The handpiece would be aligned so that the impacting rod would strike the superior rim of the abutment.
2. The handpiece should be held with a slight angulation (1 to 5°) from a line perpendicular to the longitudinal abutment axis.
3. To ensure the measurements were taken in a consistent azimuthal direction, the handpiece was oriented parallel to the longitudinal axis of the patient (ie. handpiece pointed towards the patient's feet when lying flat).

### 6.1.3 Use of Calibration Block

To ensure the *in vivo* measurement values were as precise as possible, a measurement calibration block was used. The calibration block was previously developed and used by Hurst, S. (2002). The block consists of four aluminum posts with lengths of 4, 6, 8 and 10 mm threaded 4 mm into a rectangular piece of FRB-10. Epoxy was applied to the post threads during installation, to provide a uniform interface and to prevent any loosening of the posts over time. The FRB-10 block was then mounted to a stainless steel base. After the block was constructed five measurements were taken on each post by aligning the impacting rod so that it would strike the superior rim of the post and the handpiece held with a slight angulation (as outlined in Section 6.1.2). The PTV values were recorded and engraved on the calibration block for each post.

Measurements were taken by the clinician on each of the four block posts prior to the patient measurements, as shown in Figure 6.1. The clinician was instructed to align the impacting rod so that it would strike the superior rim of the post and with an angulation between 1 to 5°. The calibration measurements consisted of at least one impact measurement per post, with the measurement PTV values being compared to the values engraved on the calibration block. The calibration block serves two important purposes, it provides a method for evaluating any longitudinal changes in the Periotest® output, and it focused the operator on the proper measuring technique before the patient measurements.

### 6.1.4 *In Vivo* Measurements

The *in vivo* study consisted of taking measurements with different abutment geometries at one patient visit as well as longitudinal patient readings over the course of one year. Measurements on different abutment geometries provided another opportunity to verify the analytical model, as the different readings on different abutments could be analyzed and the model results compared (the model $k$ for the different abutments should be the same, as the interface remains constant in the tests).

The longitudinal study was done to evaluate how the raw accelerometer signal changes from the time the implant is installed to one year after installation. The raw accelerometer signal could then be related to the bone-implant interface stiffness with the use of the mathematical model.

To reduce inter-operator variability (as discussed in Section 3.3) only one clinician conducted the measurements at all but implant installation. Due to the scheduling of the surgeries it was not always possible for the same clinician

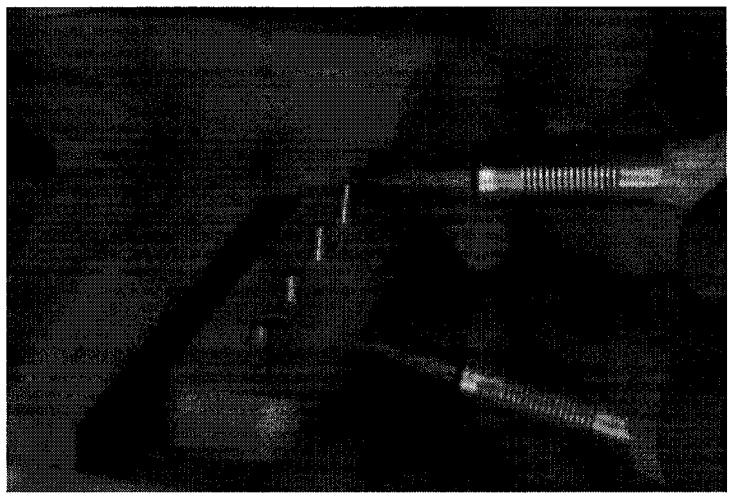

Figure 6.1: Calibration block used during *in vivo* measurements.

to be present during implant installation. In these cases, either another experienced clinician or the surgeon performed the calibration and measurements.

Occasionally during the course of testing the clinician would request to re-take a measurement or the Periotest® would indicate a reading that was significantly different than other readings (greater than a 1 PTV difference in the display). An example of a measurement that was found to be significantly different than the other measurements is shown in Figure 6.2a with a prior measurement result shown in Figure 6.2b. These "bad" measurements could be the result of improper handpiece alignment, or the Periotest® rod not making solid contact with the abutment during the test. For these cases the bad measurement was discarded and an additional measurement was completed.

#### 6.1.4.1 *In Vivo* Measurements on Different Length Abutments

Measurements were completed utilizing standard 7 and 5.5 mm abutments for eleven of the twelve patients (the multiple abutment measurement was missed for one of the patients). The additional 7 mm abutment measurement was done at the 6-month visit for one of the patients and at the 12-month patient visit for ten of the patients. The additional measurement was moved from the 6-month to 12-month visit to limit any negative effects the repeated torquing would have on the interface during healing. Having one patient with 6-month data did not cause any difficulties, as the different length abutment data was

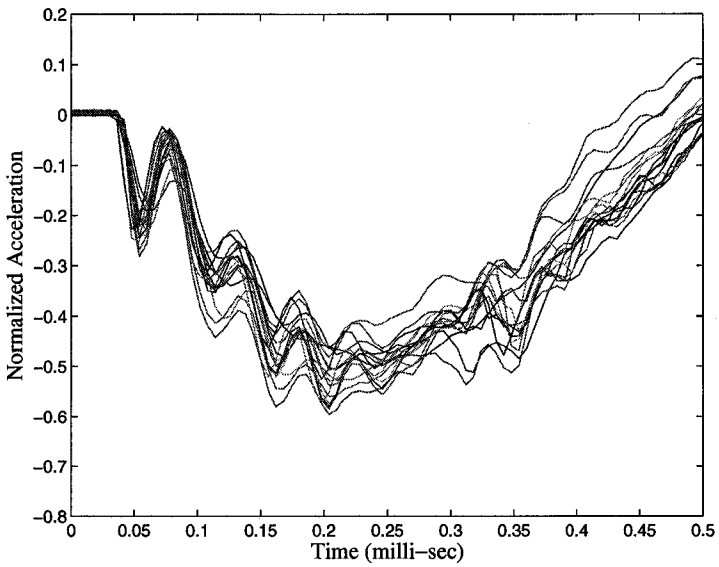


(a)

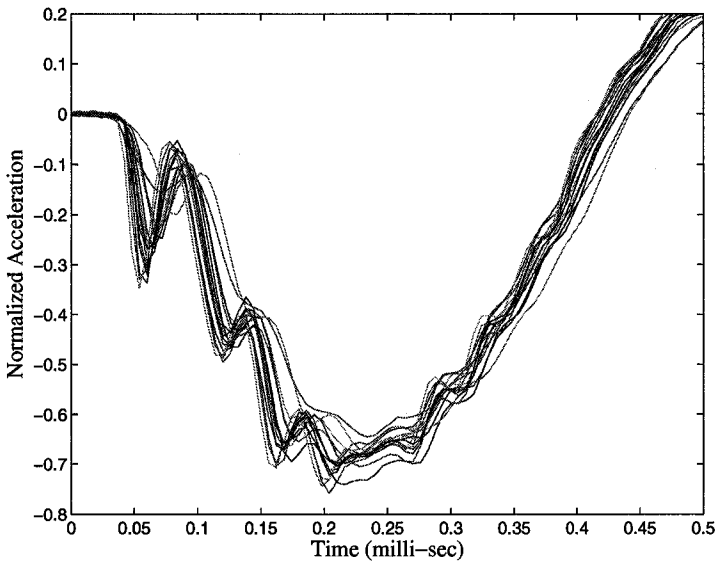


(b)

Figure 6.2: a) Example of a measurement that was re-taken. b) Example of a previous more consistent measurement.

not averaged or compared across the patients. The purpose of the additional measurement was to provide impact data for two abutment geometries (5.5 and 7 mm abutments) on the same patient with the same underlying interface properties. Based on the measured impact signals the estimated interface stiffnesses from the model could be compared for the two different abutment geometries.

The multiple abutment *in vivo* protocol was as outlined in Section 6.1.2. After three impact measurements on the 5.5 mm abutment the 7 mm was connected to the implant with 20 Ncm of torque and three additional measurements were completed.

#### 6.1.4.2 Longitudinal Impact Measurements

The *in vivo* longitudinal study consisted of three impact measurements for each patient at implant installation and then at 1, 2, 3, 6 and 12 month scheduled patient visits. The measurements were completed during the patient's regular scheduled visits, to minimize any additional time commitments to the study for the patients.

The impact measurements were taken on a 5.5 mm standard abutment (Nobel Biocare, Toronto, Ontario, Canada) coupled to the implants with a torque of 20 Ncm. A previous *in vivo* study by Hurst, S. (2002) utilized a 4 mm abutment for the testing. The length of the abutment was increased from 4 mm to 5.5 mm in the present work based on model simulations, which suggested that a 5.5 mm abutment would result in a greater amplitude of the second mode in the accelerometer signal which could then be more easily investigated.

## 6.2 Measurement Results and Discussion

It was shown in Chapter 4 that the raw accelerometer response *in vitro* had two frequency components in the signal which corresponded to the four degree of freedom model's first and second mode responses. This section presents the raw accelerometer results collected *in vivo* and the analysis of the impact signals. The four degree of freedom model is also used to aid in the interpretation of the raw accelerometer signal.

To gain as much information from the impact data as possible, multiple aspects of the accelerometer response were investigated. An accelerometer impact response collected from a patient at implant installation is shown in Figure 6.3. The accelerometer response shown has four signal characteristics

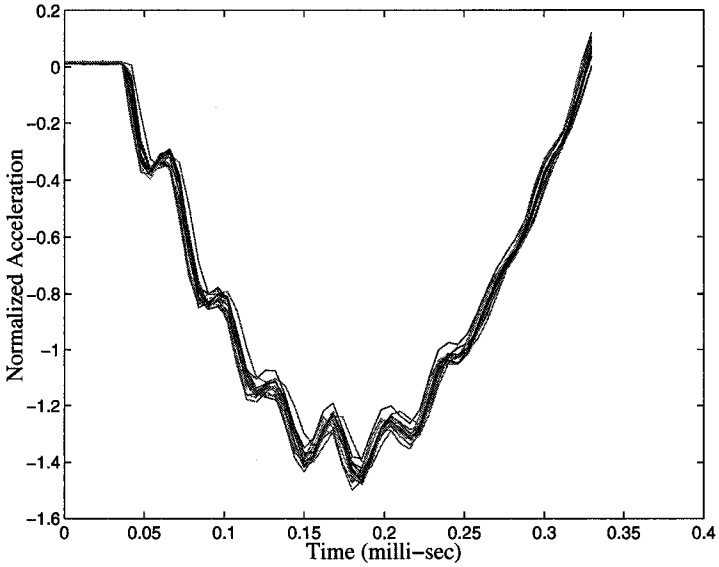


Figure 6.3: Sample of an impact accelerometer signal taken at implant installation *in vivo*.

that were examined

1. first mode frequency,
2. second mode frequency,
3. first and second modal participation factors,
4. damping of the second mode frequency.

The first mode frequency was determined from the contact time of the accelerometer response as described in Section 2.2.2. The second mode frequency, modal participation factors and damping were examined with the help of the four degree of freedom model by comparing the model impact response to the measured impact response. Damping was determined "subjectively" from matching the model acceleration response to the measured raw accelerometer response in an effort to evaluate if it changed substantially.

### 6.2.1 *In vivo* Longitudinal First Mode Frequency Measurements

The first mode resonant frequency was determined for each *in vivo* impact measurement using the procedure outlined in Section 2.2.2. The results of these measurements are shown for four patients in Figures 6.4 and 6.5. These patient results were chosen to show the variability in the first mode frequency during the initial healing period. Of the four results shown, the first mode frequency decreases for two of the patients and increases for two of the patients in the first month. All the patient plots are shown in Appendix B. On the plots, the multiple readings at each patient visit were averaged. The error bars on the plots correspond to the standard deviations of the multiple readings.

The size of the error bars (standard deviation) of the measurements vary from 118 Hz at the six months to 11 Hz at twelve months for Patient 1 in Figure 6.4a. The variation in the *in vivo* measured values were larger than those found *in vitro*. The largest *in vitro* variation for repeated measurements on a 5.5 mm abutment in Section 3.2.1 was found to be 12 Hz. One explanation for the increased variation *in vivo* is that in the *in vivo* measurements an operator holds the Periotest® handpiece by hand. The *in vitro* measurements were done in a stand, where variables such as striking angulation and height can be tightly controlled. Another potential cause for the variation in some of the measured values comes from how the impact data is collected. The only feedback to the operators on the repeatability of the measurements is in the form of a Periotest® value (PTV). As discussed in Chapter 3, the Periotest® is not the most reliable value to be using. An example of this is the twelve month measurement for Patient 5. The PTV for the readings taken were all -6, however, once the data was analyzed and the first mode frequency determined, there was a 128 Hz standard deviation. The internal Periotest® filtering used to determine the -6 PTV value may have been masking differences in the raw accelerometer signal between the different trials shown in Figure 6.6. To eliminate these feedback errors, future measurements should have raw accelerometer signal data available so that operators can be aware of any variation in the measurements at the time of testing. The observed measurement variation emphasizes the need to take multiple measurements *in vivo*, as a single measurement may not properly represent the system.

The plots in Figure 6.4 show two patients with similar measurement trends. The plots show a significant decrease in the measured first mode resonant frequency between installation and the first month measurement. There was an increase in the second month and then little change in the measurements at the third month visit. The patient shown in Figure 6.4a had an increase in the

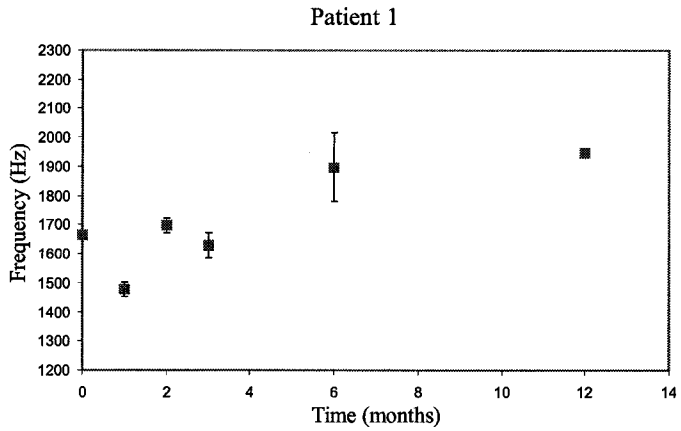


(a)

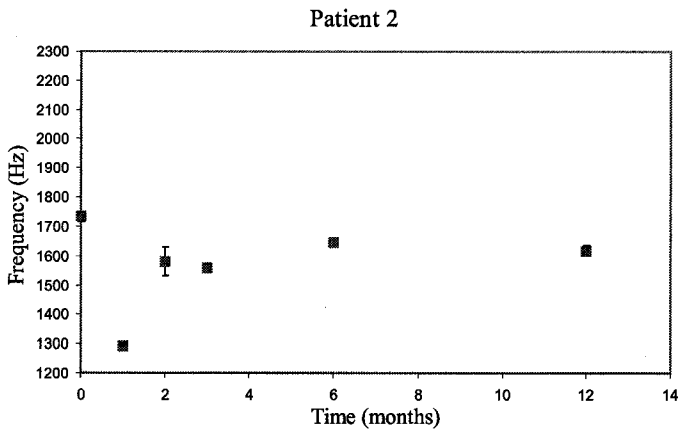


(b)

Figure 6.4: *In vivo* longitudinal patient first mode frequency measurements.

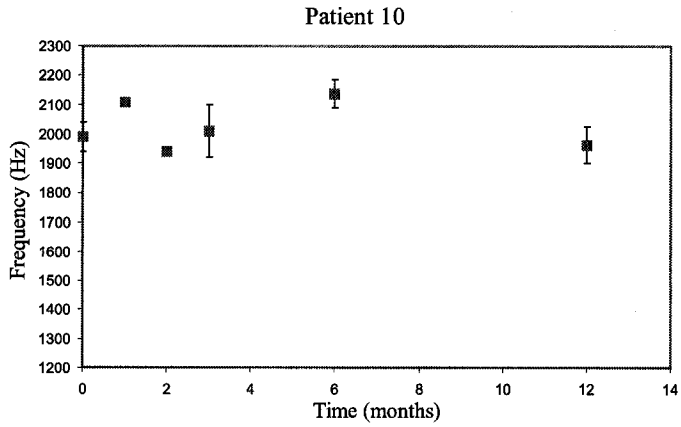


(a)

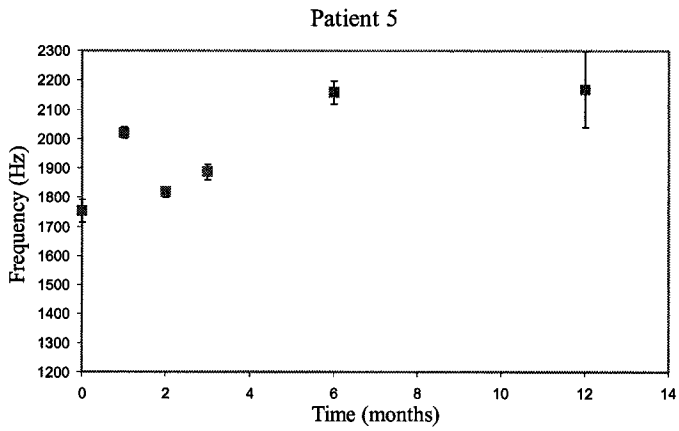


(b)

Figure 6.5: *In vivo* longitudinal patient first mode frequency measurements.

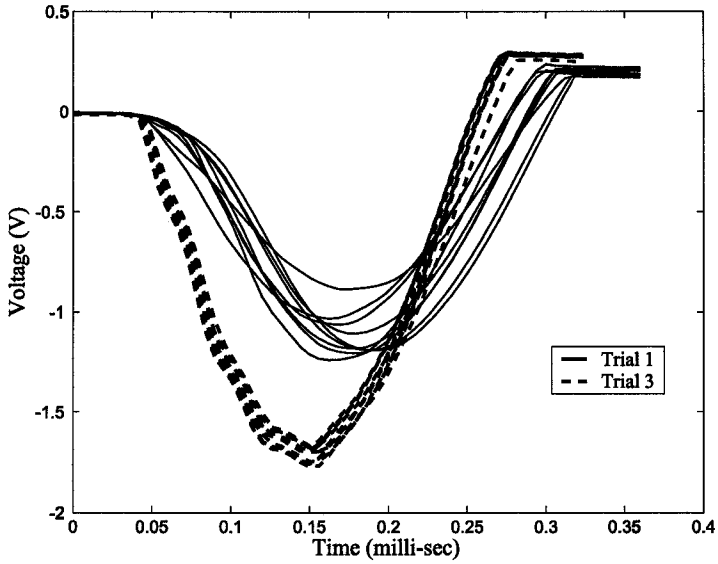


Figure 6.6: Difference in raw accelerometer signals for two trials in which the Periotest® provided the same -6 PTV.

average measured frequency at the six month visit, then a similar measurement at the twelve month patient visit. The patient shown in Figure 6.4b had little change in the measurements after the three month mark.

The plots in Figure 6.5 also show two patients with similar measurement trends. However, in this case the plots show an increase in the measured first mode frequency between installation and the first month. There is then a decrease in the measurements at the second month patient visits. The patient shown in Figure 6.5a shows an increase in the average measurement at the three and sixth month measurements, but then shows a decrease in the measured frequency at the twelve month measurement. The patient in Figure 6.5b also shows an increase at the third and sixth month measurements, however, for this case the twelve month measurement remains similar to the sixth month measurement, although with a larger standard deviation.

When Figure 6.4 and Figure 6.5 are compared, a number of observations can be made. In Figure 6.4a the initial frequency is approximately 300 Hz lower than Figure 6.5a, it then decreases (as Patient 10 increases), however, the two patients end with very similar final measurements at twelve months. Figures 6.4b and 6.5b each have similar starting frequencies (approximately

1750 Hz). The measured frequency for Patient 2 in Figure 6.4b then decreases (as the frequency increases for Patient 5 in Figure 6.5b) after installation, and the twelve month measurement ends significantly lower than for Patient 5 (1600 Hz compared to 2170 Hz). This data demonstrates that although some patients had decreases in the measured frequency in the first month, the final frequency could be at a similar value as patients who had an increase in the measured frequency in the first month. Furthermore, patients with similar initial stability readings can have significantly different final stability measurements, and patients with significantly different initial readings can have similar final measurement values. Both patients in Figure 6.4 showing a lower fundamental frequency reading after one month are female, while both patients showing an increase in the fundamental frequency in the first month shown in Figure 6.5 are male. Of the seven patients shown in Appendix B to have an increase in the fundamental frequency in the first month, six were male. However, it should be emphasized that the sample size of patients was not large enough to draw conclusions based on gender differences.

### 6.2.2 Determination of Role of Implant Flange in Implant Stability *In Vivo*

Before the model can be used, the flange stiffness ($K_F$) needs to be determined *in vivo*. The model interface stiffness ($k$) and subsequent acceleration response is dependant on the value of $K_F$.

*In vitro* testing of the model in Section 5.4 found that for flanged implants the model has the potential to predict the effect the flange has on implant stability. To determine how much support the flange provides *in vivo* the measurement results were compared to model results with a large flange stiffness and without a flange for each patient at implant installation. For the comparison with a flange, the flange stiffness used was $K_F = 3.65\text{x}10^7$ N/m as determined *in vitro* in Section 4.2.3 (this flange value would represent a maximum flange contribution). $K_F$ was set to zero for the comparison without a flange. The measurements used a 5.5 mm abutment, therefore $K_I$ was set to $2.68\text{x}10^6$ N/m and $K_T$ was calculated from equation (4.7). Two representative results for these comparisons are shown in Figures 6.7 and 6.8.

The model $k$ values were determined by matching the model first mode frequency to the measurements. Figures 6.7a and 6.8a show the model results compared to the measurements with a flange. While the contact times of the model compared to the measurements are the same (as they should be, since $k$ was determined by this matching) the higher frequency component of

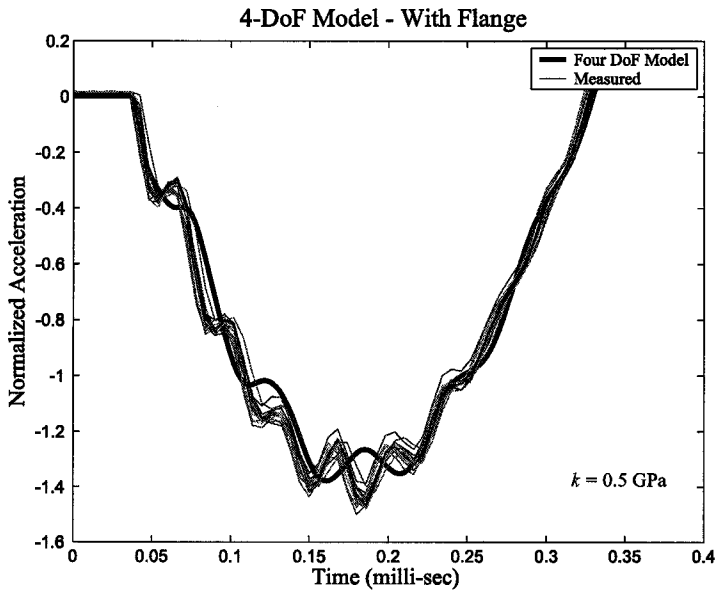


(a)

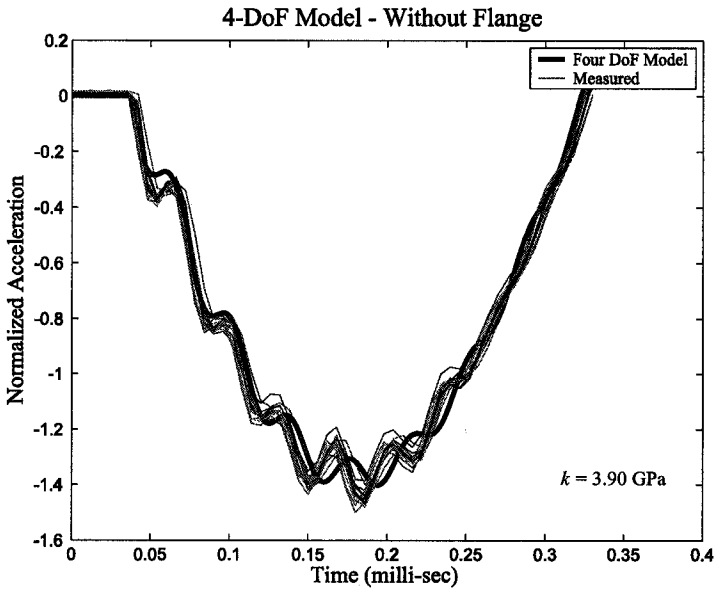


(b)

Figure 6.7: Patient 4 acceleration measurement compared to predicted model response at implant installation ($\omega_1 = 1739$ Hz). a) Model with flange. b) Model without flange

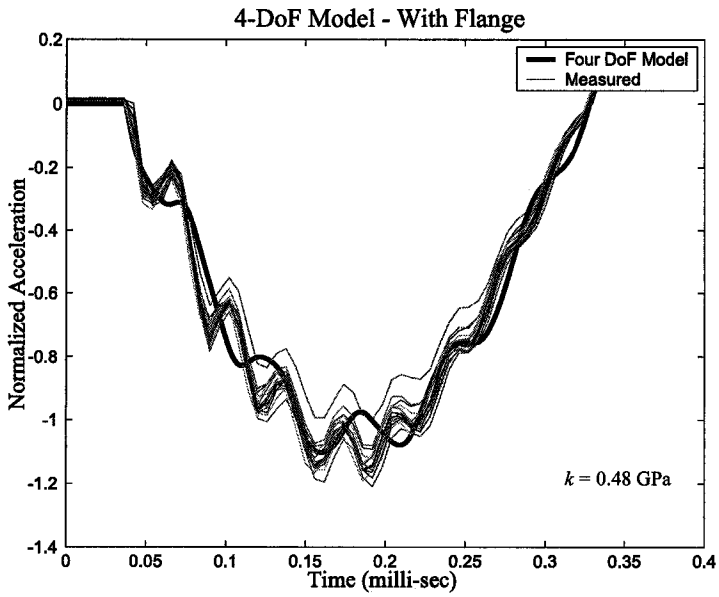


(a)

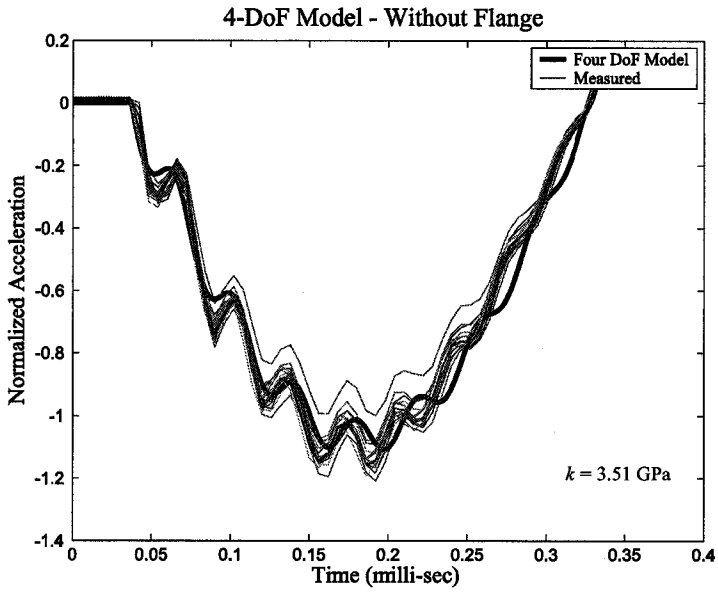


(b)

Figure 6.8: Patient 12 acceleration measurement compared to predicted model response at implant installation ($\omega_1 = 1715$ Hz). a) Model with flange. b) Model without flange

the model does not match up well with the measurements. From the figures, the model second mode frequency appears lower than the measurements (the model prediction appears to have fewer peaks than the measurement values). The results without a flange shown in Figures 6.7b and 6.8b appear to match the measurements somewhat better. This suggests that for these patients the flange may not be contributing to the implants stiffness.

The model results in Section 5.4 showed that for higher first mode frequencies, the model results with and without a flange were so similar that the model would not be able to predict what may be occurring *in vivo*. This was indeed found to be the case, as shown in Figure 6.9. While there are some differences between the model results shown in Figure 6.9a and 6.9b, there is not enough of a difference to indicate that the flange is or is not contributing to the overall stiffness.

A summary of the $k$ values determined for the results shown in Figures 6.7-6.9 are displayed in Table 6.1. From the table, the $k$ values without a flange are significantly larger than with a flange. This demonstrates the effect $K_F$ has on the estimated $k$ value. If the flange stiffness is included in measurements where the flange is not actually in contact with the bone, the model can significantly underestimate the interface stiffness.

For the patient measurements in which a clear difference in model results with and without a flange exist (Figures 6.7 and 6.8) the results without the flange tend to be in much better agreement with the measured second mode frequencies. Based on this, in the following sections it is assumed that the flange does not provide additional support for the implant in the patient measurements ($K_F = 0$). This includes those cases where the model does not give any indication whether the flange is contributing or not (Figure 6.9).

Table 6.1: *In vivo* model $k$ values for patients with and without a flange.

| | $k$ (GPa) | |
|---|---|---|
| | Flange | No Flange |
| Patient 4 | 0.50 | 3.90 |
| Patient 7 | 3.90 | 9.55 |
| Patient 12 | 0.48 | 3.51 |

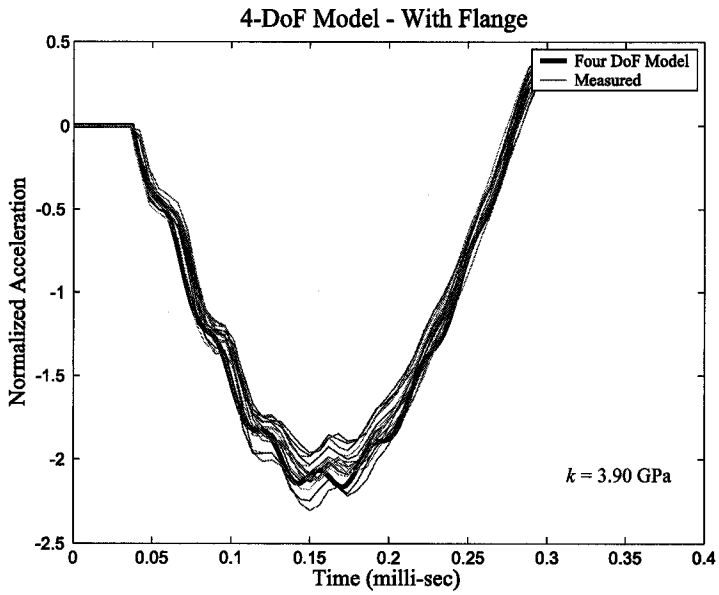


(a)

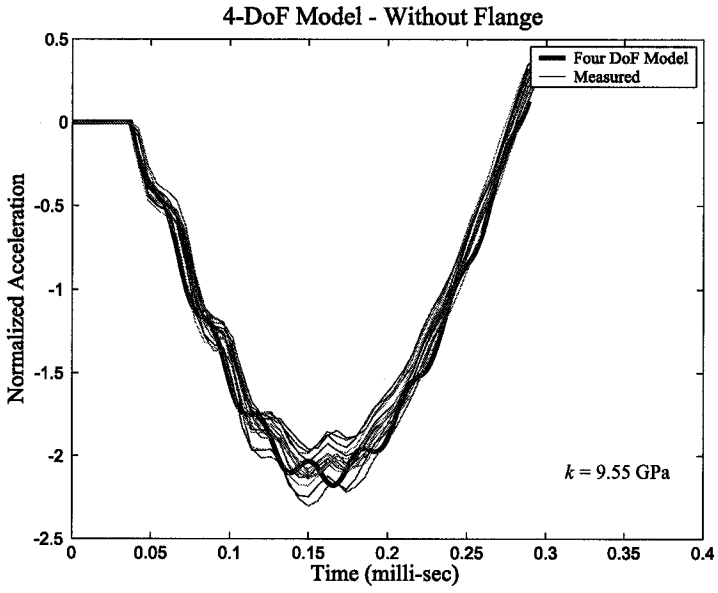


(b)

Figure 6.9: Patient 7 acceleration measurement compared to predicted model response at installation for a higher measured first mode frequency ($\omega_1 = 2020$ Hz). a) Model with flange. b) Model without flange

### 6.2.3 Calculation of Bone-Implant Interface Properties *In Vivo*

The implant interface stiffness, $k$, was calculated for the *in vivo* measurements from the mathematical model by matching the model first mode frequency to the measured average first mode resonant frequency value for each set of measurements. From the results in Section 6.2.2 is was assumed that the flange was not contributing to the implant stability in the patient measurements (ie. $K_F = 0$). The model also assumes uniform interface parameters along the length of the implant. The stiffnesses $K_I$ and $K_T$ were set for a 5.5 mm abutment and the implants were assumed to be completely threaded into the supporting bone (ie. not left proud).

To account for the variation in the measured first mode frequencies *in vivo*, $k$ values are reported as a range. The lower $k$ value of the range corresponds to the average measurement minus the standard deviation, and the upper $k$ range value corresponds to the average frequency measurement plus the standard deviation. For example, Patient 5 (shown in Figure 6.5b in Section 6.2.1) had a measured first mode frequency at implant installation of 1753±38 Hz which corresponds to a $k$ range of 3.61–4.35 GPa. The $k$ value corresponding to the average measured frequency value is also reported, and for the Patient 5 installation it corresponds to a $k$ of 3.96 GPa.

In Section 5.2 it was shown that as the frequency continues to increase $k$ becomes more sensitive to changes in first mode frequency. Figure 6.10 illustrates the relationship between the first mode frequency and $k$ for a 4 mm implant (without flange) and a 5.5 mm abutment. From the figure, after a $k$ value of about 5 GPa (corresponding to a measured first mode frequency of 1878 Hz) the slope of the curve decreases with the result that relatively small changes in frequency can correspond to significant changes in $k$. For those implants with a measured frequency greater than approximately 1900 Hz, the range of $k$ (due to the standard deviation of the measurements) can be large. As an example, Patient 5 at the 12 month patient visit had a measured first mode frequency of 2169±128 Hz which corresponds to a $k$ range of 9.21–56.8 GPa. As a result of this nonlinear relationship between $k$ and the first mode frequency the average $k$ value is not midway in the range of $k$ reported. The $k$ range for a measured frequency of 1985±25 Hz is shown in Figure 6.11. The $k$ range is from 6.45–7.68 Hz with the average measured value of 1985 Hz corresponding to 7.00 GPa.

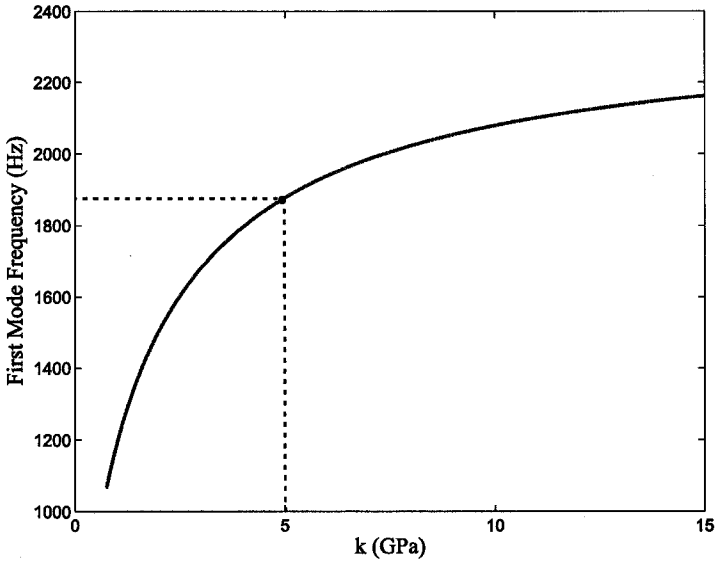


Figure 6.10: Effects of varying $k$ for a 4 mm implant without a flange and a 5.5 mm abutment.

#### 6.2.3.1 *In Vivo* Interface Stiffness Calculations for Different Length Abutments

The $k$ values calculated for two different length abutments for each patient are in Table 6.2. The patient number and gender is included in the first column. The average measured first mode frequencies ($\omega_1$) for each abutment are shown along with the standard deviation. The $k$ values are shown in the table as a range, with the $k$ value corresponding to the average measured frequency shown in parenthesis after the range. The percent difference between the average $k$ for the two abutments is shown in the last column.

Ideally, the model would give the same average $k$ value for the two different abutment geometries for the same patient. The largest percent difference was 33% and the smallest was 4%. One explanation for some of the variation between the two abutment readings can be explained by the measurement variation (standard deviation). In the table, the only $k$ ranges that do not overlap for the two abutments are for Patients 2 and 9. Another explanation for the variation is that for seven of the twelve patients the average $k$ was greater than 5 GPa for both abutments. As previously discussed in Section 6.2.3, as $k$ increases past 5 GPa the variability in the predicted $k$ increases reducing the

Table 6.2: *In Vivo* $k$ values for a 5.5 mm and 7 mm abutment on the same patient.

| Patient | 5.5 mm Abutment | | 7.0 mm Abutment | | % Difference |
|---|---|---|---|---|---|
| | $\omega_1$ (Hz) | $k$ (GPa) | $\omega_1$ (Hz) | $k$ (GPa) | |
| 1 (F) | - | - | - | - | - |
| 2 (F) | $1619 \pm 17$ | 3.66–3.95 (3.80) | $1422 \pm 19$ | 4.09–4.52 (4.30) | -13% |
| 3 (M) | $1521 \pm 34$ | 2.14–2.49 (2.31) | $1314 \pm 39$ | 2.18–2.66 (2.41) | -4% |
| 4 (M) | $1823 \pm 17$ | 4.53–4.95 (4.73) | $1537 \pm 83$ | 3.47–5.61 (4.37) | 8% |
| 5 (M) | $2169 \pm 128$ | 9.21–56.77 (16.10) | $1857 \pm 30$ | 12.37–17.14 (14.42) | 11% |
| 6 (M) | $1551 \pm 81$ | 2.07–2.97 (2.47) | $1390 \pm 63$ | 2.49–3.46 (2.93) | -19% |
| 7 (M) | $2077 \pm 50$ | 8.76–13.10 (10.60) | $1734 \pm 128$ | 5.37–14.83 (8.31) | 21% |
| 8 (F) | $1944 \pm 18$ | 6.31–7.05 (6.66) | $1647 \pm 20$ | 5.73–6.53 (6.11) | 8% |
| 9* (M) | $1962 \pm 19$ | 6.64–7.49 (7.05) | $1765 \pm 31$ | 8.31–10.71 (9.39) | -33% |
| 10 (M) | $1969 \pm 62$ | 5.97–8.89 (7.21) | $1671 \pm 19$ | 6.22–7.07 (6.62) | 8% |
| 11 (F) | $1898 \pm 17$ | 5.54–6.11 (5.81) | $1613 \pm 24$ | 5.09–5.92 (5.48) | 6% |
| 12 (M) | $1961 \pm 71$ | 5.68–8.92 (7.03) | $1715 \pm 12$ | 7.41–8.09 (7.74) | -10% |

* Measurement done at the six month patient visit

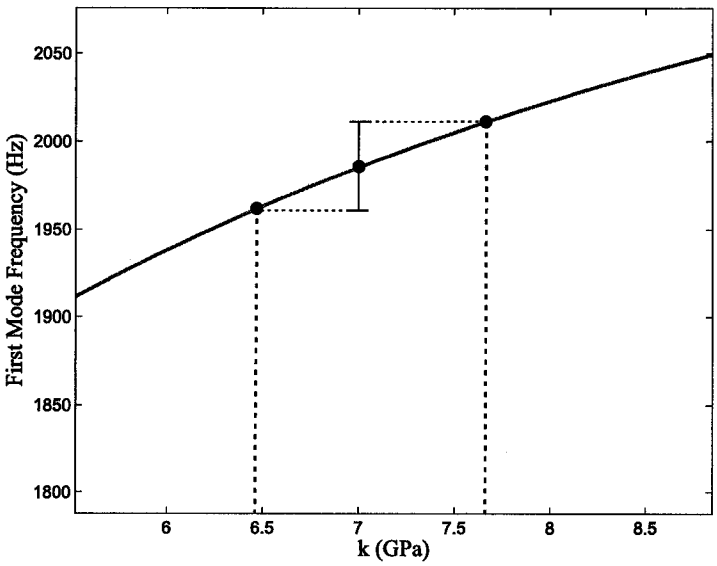


Figure 6.11: The $k$ range for a measured first mode frequency of 1985±25 Hz for a 5.5 mm abutment on a 4 mm implant without flange.

accuracy of the predicted results.

An example of the model acceleration response based on the calculated $k$ for two abutment lengths is shown in Figure 6.12 along with the measured accelerometer signal. The modal participation factors (relative amplitude of the signals) and second mode frequency appear to be predicted quite well by the model. This agreement provides further evidence that the model is predicting the effects of different sized abutments properly.

#### 6.2.3.2 Longitudinal Changes in Patient Interface Stiffness

This section discusses the use of the four degree of freedom model to estimate the interface properties for the longitudinal *in vivo* measurements. The model impact response is compared to the measurement impact response on the Ø 3.75 mm BAHA® implants with a 5.5 mm abutment. The model parameters used were,

- the interface stiffness, $k$, was assumed to be uniform,
- the implant flange was assumed to have no effect on the implant stability (ie. was set to zero),

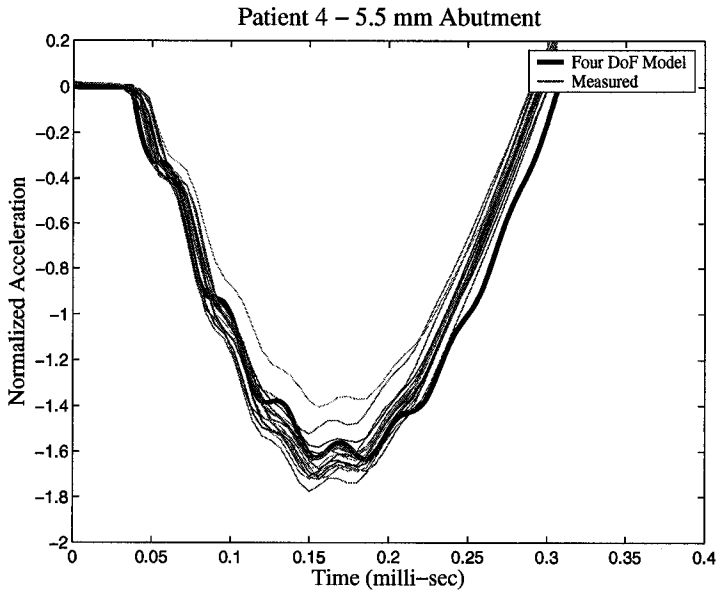


(a)

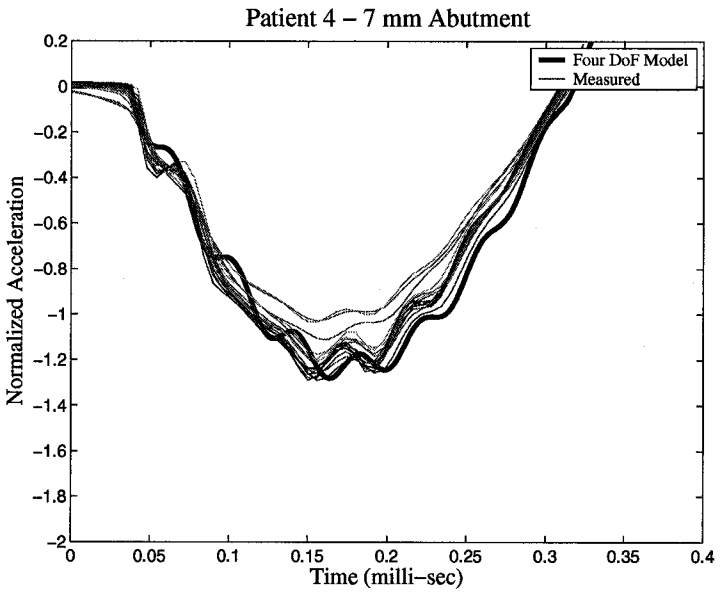


(b)

Figure 6.12: Patient 4 acceleration measurement compared to predicted model response at the 12 month measurement for two different abutment lengths a) 5.5 mm abutment. b) 7 mm abutment.

- $K_T$ and $K_I$ were as calculated for a 5.5 mm abutment,
- the implants were assumed to be completely threaded into the supporting bone.

The longitudinal interface stiffnesses estimated by the model for all 12 patients along with the measured first mode frequencies are shown in Tables 6.3a and 6.3b. The discussion will concentrate on the results for two of the patients, Patient 1 and Patient 5. These two patients were selected to demonstrate the range of interface stiffnesses that occurred across the study group. For ease of comparison, the longitudinal results for Patients 1 and 5 are listed in Table 6.4. Both patients in Table 6.4 start with similar interface stiffnesses. However, after one month the average interface stiffness for Patient 1 decreased 34% and the average interface stiffness increased for Patient 5 by 118%. This difference between the one month response for the two patients may be caused from differences in the healing rates and the corresponding rate of bone modelling/remodelling at the implant interface. Another possibility is that the measurement at patient installation is sensitive to the implant installation procedure. If the drilled hole for Patient 5 is slightly over sized, then the measured frequency and corresponding interface stiffness could be lower than if the hole was slightly undersized.

The largest percent change between consecutive visits in the interface stiffness occurred between the three and six month measurements for both patients. Patients 1 and 5 had 97% and 169% increases in this time interval. Prior to the three month visit, measurements were done monthly therefore the larger change in the interface properties over this time period may be due to the increased time between measurements. The magnitude of the interface stiffness change indicates that the bone-implant interface may still be undergoing significant physiological changes between the three and six month time interval. Increases in stability may be the result of increased mineralization of new bone and increased direct bone contact at the interface (Roberts, W.E., 1993). Changes occurring at the interface during this time period are further complicated by implant loading. Patients received their processors at the three month visit. In addition to any changes already in progress, the stresses caused from the load applied to the implant may have triggered an adaptive response in the bone around the implant as suggested by Wolff's Law (Cowin, S., 2001). As a note of caution, the difference between the interface stiffnesses at some of the patient visits may also be exaggerated by the model. As previously discussed in Section 6.2.3, as the fundamental frequency values become larger than $\simeq$1900 Hz the model becomes less sensitive to $k$, reducing the accuracy of the predicted interface stiffness.

Table 6.3a: Estimated $k$ values based on impact measurements at installation, 1 month and 2 months for 12 patients fitted with BAHA® implants.

| Patient | Installation | | 1 Month | | 2 Month | |
|---|---|---|---|---|---|---|
| | $\omega_1$ (Hz) | $k$ (GPa) | $\omega_1$ (Hz) | $k$ (GPa) | $\omega_1$ (Hz) | $k$ (GPa) |
| 1 (F) | $1662 \pm 15$ | 3.07–3.29 (3.18) | $1476 \pm 25$ | 1.98–2.21 (2.09) | $1699 \pm 25$ | 3.27–3.69 (3.47) |
| 2*(F) | $1733 \pm 18$ | 4.76–5.20 (4.98) | $1291 \pm 15$ | 1.79–1.91 (1.85) | $1581 \pm 48$ | 3.13–3.89 (3.49) |
| 3 (M) | $1409 \pm 95$ | 1.47–2.23 (1.81) | $1480 \pm 17$ | 2.03–2.19 (2.11) | $1628 \pm 38$ | 2.70–3.21 (2.94) |
| 4 (M) | $1770 \pm 121$ | 3.09–5.70 (4.13) | $1831 \pm 30$ | 4.47–5.24 (4.83) | $1863 \pm 24$ | 4.94–5.63 (5.27) |
| 5 (M) | $1753 \pm 38$ | 3.61–4.35 (3.96) | $2023 \pm 17$ | 8.14–9.18 (8.64) | $1819 \pm 17$ | 4.48–4.90 (4.68) |
| 6 (M) | $2038 \pm 52$ | 7.61–11.1 (9.11) | $1373 \pm 21$ | 1.60–1.75 (1.67) | $1505 \pm 32$ | 2.08–2.39 (2.23) |
| 7 (M) | $2020 \pm 84$ | 6.50–11.8 (8.55) | $2113 \pm 30$ | 10.8–14.1 (12.3) | $2100 \pm 37$ | 10.0–13.7 (11.6) |
| 8 (F) | $1605 \pm 55$ | 2.46–3.17 (2.79) | $1555 \pm 36$ | 2.30–2.70 (2.49) | $1640 \pm 17$ | 2.91–3.14 (3.02) |
| 9 (M) | $2059 \pm 33$ | 8.73–11.2 (9.86) | $1969 \pm 158$ | 4.59–13.1 (7.21) | $2275 \pm 12$ | 30.6–38.9 (34.3) |
| 10 (M) | $1994 \pm 51$ | 6.64–9.35 (7.82) | $2109 \pm 6$ | 11.8–12.4 (12.1) | $1942 \pm 5$ | 6.52–6.73 (6.62) |
| 11 (F) | $1661 \pm 94$ | 2.56–3.98 (3.17) | $1764 \pm 45$ | 3.64–4.56 (4.07) | $1688 \pm 13$ | 3.28–3.49 (3.38) |
| 12 (M) | $1704 \pm 9$ | 3.44–3.59 (3.51) | $1936 \pm 49$ | 5.63–7.59 (6.50) | $1936 \pm 20$ | 6.13–6.92 (6.50) |

* Patient with a 3 mm implant (all other patients have 4 mm implants)

Table 6.3b: Estimated $k$ values based on impact measurements at 3, 6 and 12 months for 12 patients fitted with BAHA® implants.

| Patient | 3 Month | | 6 Month | | 12 Month | |
|---|---|---|---|---|---|---|
| | $\omega_1$ (Hz) | $k$ (GPa) | $\omega_1$ (Hz) | $k$ (GPa) | $\omega_1$ (Hz) | $k$ (GPa) |
| 1 (F) | $1629 \pm 44$ | 2.67–3.26 (2.95) | $1897 \pm 118$ | 4.22–8.40 (5.80) | $1946 \pm 11$ | 6.48–6.94 (6.71) |
| 2*(F) | $1557 \pm 11$ | 3.23–3.39 (3.31) | $1646 \pm 7$ | 3.98–4.11 (4.05) | $1619 \pm 17$ | 3.66–3.95 (3.80) |
| 3 (M) | $1772 \pm 41$ | 3.75–4.61 (4.15) | $1736 \pm 10$ | 3.70–3.89 (3.80) | $1521 \pm 34$ | 2.14–2.49 (2.31) |
| 4 (M) | $1680 \pm 42$ | 3.01–3.67 (3.32) | $1937 \pm 2$ | 6.48–6.56 (6.52) | $1823 \pm 17$ | 4.53–4.95 (4.73) |
| 5 (M) | $1888 \pm 27$ | 5.24–6.11 (5.65) | $2158 \pm 38$ | 12.7–18.8 (15.2) | $2169 \pm 128$ | 9.21–56.8 (16.1) |
| 6 (M) | $1332 \pm 6$ | 1.51–1.55 (1.53) | $1674 \pm 17$ | 3.14–3.41 (3.27) | $1551 \pm 81$ | 2.07–2.97 (2.47) |
| 7 (M) | $2256 \pm 1$ | 28.6–29.1 (28.8) | $2163 \pm 43$ | 12.7–20.0 (15.6) | $2077 \pm 50$ | 8.76–13.1 (10.6) |
| 8 (F) | $1721 \pm 3$ | 3.63–3.69 (3.66) | $1785 \pm 9$ | 4.19–4.39 (4.29) | $1944 \pm 18$ | 6.31–7.05 (6.66) |
| 9 (M) | $2145 \pm 62$ | 10.8–20.1 (14.3) | $1962 \pm 19$ | 6.64–7.49 (7.05) | $2218 \pm 25$ | 18.5–25.9 (21.6) |
| 10 (M) | $2014 \pm 89$ | 6.29–11.8 (8.37) | $2138 \pm 49$ | 11.1–17.8 (13.8) | $1969 \pm 62$ | 5.97–8.89 (7.21) |
| 11 (F) | $1783 \pm 4$ | 4.22–4.31 (4.27) | $1990 \pm 17$ | 7.30–8.17 (7.72) | $1898 \pm 17$ | 5.54–6.11 (5.81) |
| 12 (M) | $1963 \pm 6$ | 6.94–7.21 (7.07) | $1965 \pm 55$ | 6.02–8.55 (7.12) | $1961 \pm 71$ | 5.68–8.92 (7.03) |

* Patient with a 3 mm implant (all other patients have 4 mm implants)

Table 6.4: *In Vivo* $k$ values for Patient 1 and Patient 5.

| Time | Patient 1 (F) | | Patient 5 (M) | |
|---|---|---|---|---|
| (Months) | $\omega_1$ (Hz) | $k$ (GPa) | $\omega_1$ (Hz) | $k$ (GPa) |
| 0 | $1662 \pm 15$ | 3.07–3.29 (3.18) | $1753 \pm 38$ | 3.61–4.35 (3.96) |
| 1 | $1476 \pm 25$ | 1.98–2.21 (2.09) | $2023 \pm 17$ | 8.14–9.18 (8.64) |
| 2 | $1699 \pm 25$ | 3.27–3.69 (3.47) | $1819 \pm 17$ | 4.48–4.90 (4.68) |
| 3 | $1629 \pm 44$ | 2.67–3.26 (2.95) | $1888 \pm 27$ | 5.24–6.11 (5.65) |
| 6 | $1897 \pm 118$ | 4.22–8.40 (5.80) | $2158 \pm 38$ | 12.7–18.8 (15.2) |
| 12 | $1946 \pm 11$ | 6.48–6.94 (6.71) | $2169 \pm 128$ | 9.21–56.8 (16.1) |

Between the six and twelve month patient measurements there was a 16% and 6% increase in the bone-implant interface stiffness for Patients 1 and 5. The difference between six and twelve month stiffnesses for these two patients is considerably less than that found between the three and six month values. This may indicate that for these patients the majority of the stiffness changes to the bone-implant interface were complete by six months. This falls in the 4-12 month interval cited by Roberts, W.E. (1993) in which secondary mineralization of new bone and increased direct bone contact at the interface occurs and the remodelling of the non-vital interface and supporting bone is completed. The average interface stiffness determined at the twelve month visit were found to be 6.71 and 16.1 GPa for Patients 1 and 5, respectively. While the relationship between $k$ and modulus will depend on the supporting bone geometry, these $k$ values are of the magnitude of Young's modulus values of 13.4 GPa for cortical bone and 7.7 GPa for trabecular bone used in finite element simulations of the human skull (Jafari, A. et al., 2003).

While the number of total patients included in the study is not large, there are some trends in the interface stiffness data that prove interesting. The average stiffness at the twelve month measurement for the men was 9.01 GPa and 5.75 GPa for the women, with the top five twelve month stiffness values belonging to men. These values are comparable to modulus values reported for the human skull which are between 7.7–13.4 GPa (Jafari, A. et al., 2003). Overall, 67% of the patients had the lowest interface stiffness within the first month. Five of the patients had the lowest $k$ value at implant installation, with another three at the one month mark. By the third month, all but one patient had recorded its lowest $k$ value. From the stiffness values determined, the initial three month healing period appears to be when the implants are least stable. Roberts, W.E. (1993) states that the woven bone lattice that

forms at the implant interface occurs within the first 0.5 months and that the woven bone cavities then fill with high quality lamellae gaining strength for load bearing within the first 0.5–1.5 months. The lower interface stiffness values during this time frame may correspond to the less stiff woven bone lattice and increases in stiffness after this point indicating the placement of the high quality lamellae.

Based on the tests completed, the current practice of processor connection and implant loading after three months appears reasonable. Loading implants during the period of initial instability may have negative consequences. In a review of the healing around endosseous implants, Raghavendra, S. et al. (2005) discusses the transition from primary mechanical stability (stability of old bone) to biologic stability (stability of newly formed bone). During this transition, there is a period of healing in which the initial mechanical stability has decreased but the formation of new bone has not yet occurred to the level required to maintain implant stability. At this point, Raghavendra, S. et al. (2005) claims that a loaded implant would be at greatest risk of relative motion and would be (at least theoretically) most susceptible to failure of osseointegration.

#### 6.2.3.3 Comparison of Analytical Model Acceleration Response to Longitudinal Patient Raw Accelerometer Measurements

The model predicted impact response compared to the measured impacts over the one year time period for the two patients previously discussed (Patients 1 and 5) are shown in Figures 6.13 and 6.14. The $k$ values used with the model to obtain the impact response are the average values shown in Table 6.4. The figures for all patients are shown in Appendix C.

Overall the model predicted impact response and the measurements are similar. For both patients there is less agreement in the second mode frequency at installation and the one month measurement than the other stages. The discrepancies between the model predicted second mode frequencies and the measurements at the early stages may be due to the assumption that the interface stiffness is uniform along its length. At implant placement the interface may differ along the length of the implant depending on the gaps between the implant threads and the surrounding bone. The initial healing of the implant may also not be uniform along its length. The agreement between the second mode frequency and the measurements at later stages may indicate that the interface becomes more uniform over time.

The measured amplitude of the higher frequency term matches the model response for both patients. For Patient 5 as the stiffness of the interface

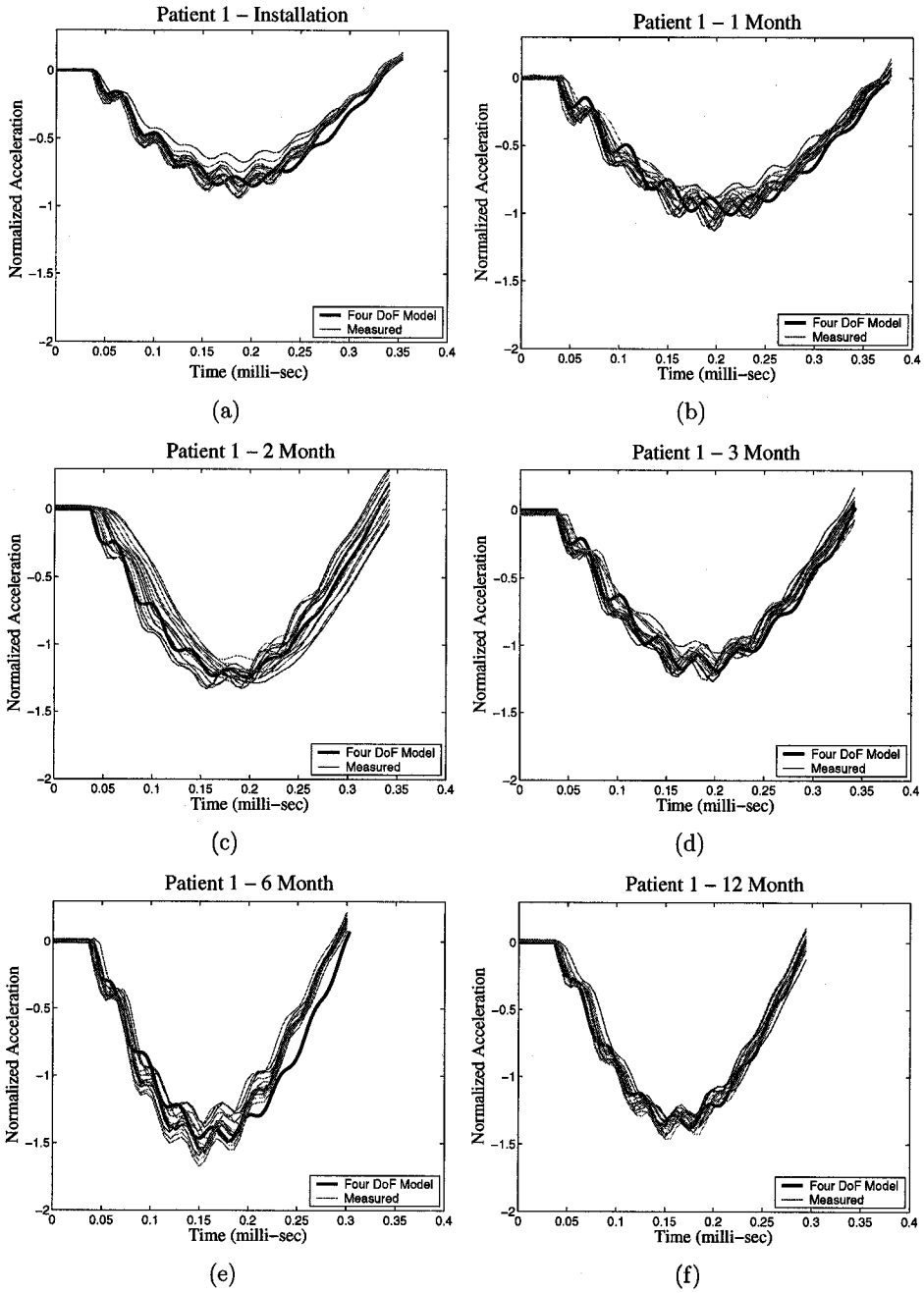


Figure 6.13: Patient 1 acceleration measurement compared to predicted model response at different patient visits.

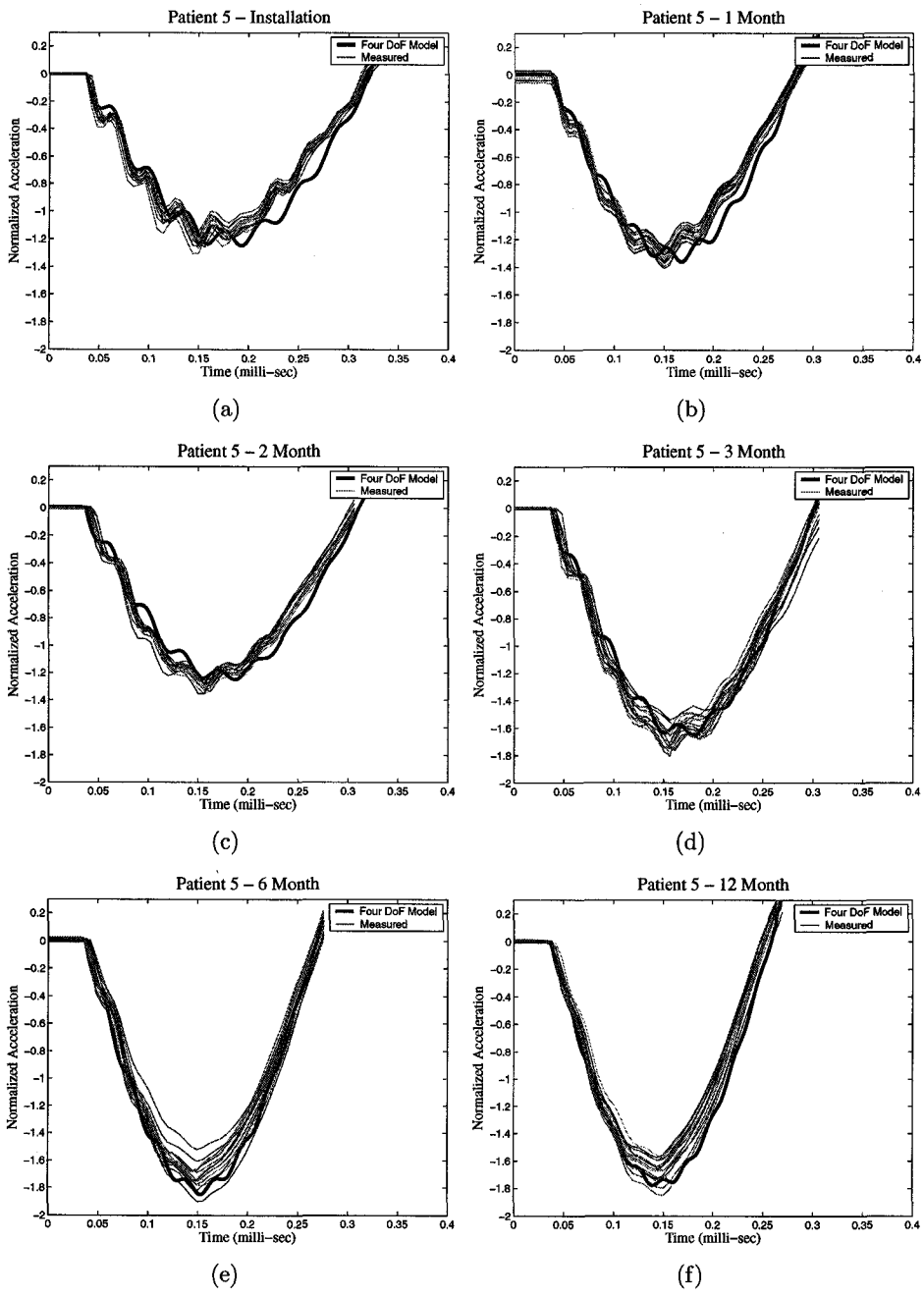


Figure 6.14: Patient 5 acceleration measurement compared to predicted model response at different patient visits.

increases the amplitude of higher frequency term decreases. The model acceleration modal participation factors also predict this decrease, as can be seen in Figure 6.14e and Figure 6.14f.

#### 6.2.3.4 Longitudinal Changes in Patient Interface Damping Properties

Along with changes in the stiffness, it is believed that the damping properties of the bone changes as the implant osseointegrates (Roberts, W.E., 1993). Some studies completed with the Periotest® refer to the device as measuring the damping characteristics of the interface (Olivé, J. and Aparicio, C., 1990; van Steenberghe, D. et al., 1995). To estimate the damping for the patient data the measurements were matched to model results by manually increasing or decreasing the damping ratio within the model until the model acceleration response approximately matched the measured raw accelerometer signal (this was the same procedure used to determine the damping properties of *in vitro* measurements as discussed in Section 4.2.2). This method is subjective and was used to obtain a preliminary approximation of the amount of damping present at the interface.

The second mode damping ratios, $\nu_2$, for Patients 1 and 5 at the different patient visits are shown in Table 6.5. The damping ratios were determined by matching the damped model response to the measurements as shown in Figures 6.13 and 6.14.

While damping appears to be present in the measurements, the largest damping ratio calculated for the two patients was 4.7%. Although the data was obtained in a somewhat subjective manner, there does not appear to be a large change in the damping properties of the implant interface over time. The low damping ratios shown in Table 6.5 emphasize that the longitudinal changes in the resonant frequency of the *in vivo* implants tested are caused primarily from changes in the interface stiffness and not from changes in the damping properties of the bone at the implant interface. It should be emphasized that the damping ratios shown are for healthy implants. A failing implant may have considerably different damping ratios than those shown. For this reason, further measurements of the damping ratio on a failing implant may be worthwhile. However, due to the small magnitudes of the damping ratios determined for healthy implants, a more precise method of calculation the damping ratios will be required before longitudinal trends can be evaluated.

Table 6.5: *In vivo* model second mode damping ratio for Patients 1 and 5.

| Time (Months) | $\nu_2$ | |
|---|---|---|
| | Patient 1 | Patient 5 |
| 0 | 3.0% | 2.1% |
| 1 | 2.9% | 2.1% |
| 2 | 4.7% | 3.2% |
| 3 | 2.7% | 3.0% |
| 6 | 1.9% | 1.5% |
| 12 | 1.5% | 1.0% |

# Chapter 7

# Summary and Conclusions

## 7.1 Summary

In this work an impact testing technique based on the Periotest® raw accelerometer signal has been developed. The inconsistent and insensitive results previously reported when using the Periotest® for implant measurements are believed to be caused from a lack of understanding of how the instrument processes the measured signal and how the signal is obtained. The filtered accelerometer signal used in determining the Periotest® value (PTV) removes valuable higher frequency information from the signal that can be related to the properties of the bone-implant interface. Further, when compared to strain gauge measurements the filtering appears to increase the contact time. This increase in contact time due to filtering becomes significant for stiffer systems such as implants.

The developed impact technique uses the un-filtered raw accelerometer signal from the Periotest® handpiece which more closely matched the results of the strain gauge measurements. In addition, the effect on the fundamental frequency of clinical variables such as handpiece distance from the abutment, abutment torque, striking height along the length of the abutment and handpiece angulation were evaluated. The distance the impacting rod is held from the abutment prior to striking did not affect the results if kept between 0.5–2.5 mm. The abutment torque caused little variation in the fundamental frequency for torque values between 15–25 Ncm. Striking height along the abutment was found to significantly affect the fundamental frequency, however, if the striking rod was set to strike the superior rim of the abutment the height could be changed ±1 mm without significantly changing the results. The handpiece angulation was also found to significantly affect the fundamen-

tal frequency. To avoid this affect it was recommended that the handpiece be held with a slight angulation, between 1-5°.

The impact technique presented has a number of advantages and drawbacks. The main disadvantage of the technique is its sensitivity to clinical variables such as striking height and handpiece angulation. While *in vitro* these variables can be controlled with the use of a handpiece stand, in the *in vivo* testing the handpiece is held by the operator. The use of the developed measurement protocol and calibration block will help to reduce this variability. Although holding the handpiece adds variability to the measurements, it also has several advantages for clinical use. These include the ability to access areas which would be too difficult for other instruments and that it can be used on non-retrievable implant systems.

To aid in the understanding of the impact technique an analytical four-degree of freedom model was developed. The model was used to relate the acceleration response of the system to the bone-implant interface properties. Model predicted impact accelerations were compared to measured raw accelerometer signals obtained in *in vitro* tests. When the fundamental frequency of the model was matched to the measured fundamental frequency for the *in vitro* tests, the interface stiffness ($k$) for the FRB-10 material was found to be 7.5 GPa for the 10 mm implant disk and 7.7 GPa for the 4 mm implant disk. When the fundamental frequency between the model and measurements were matched, the second mode frequency from the model closely resembled the higher frequency term found in the raw accelerometer signal. This indicated that the higher frequency term was, in fact, the second mode of vibration of the system. Model results utilizing these $k$ values where then compared to *in vitro* tests over a range of implant-abutment geometries. Due to the similarities in first and second mode frequencies as well as modal participation factors between the model and measurements this technique has been shown to be effective for modeling the impact response of percutaneous implant and abutment systems *in vitro*.

The analytical model was then used to predict the effect on resonant frequency measurements of changes in the stiffness $k$. The system is very sensitive to changes in $k$ up to approximately 5 GPa (steep slope) before starting to lose sensitivity as $k$ continues to increase beyond this point. This establishes an upper limit to the stiffness the impact measurement can effectively distinguish. The model results show that as the interface becomes less stiff, the changes in resonant frequency become more pronounced and are easier to detect which is fortunate from a clinical perspective. The simulations also show that the second mode frequency appears more sensitive to changes in $k$ than the fundamental frequency. However, the second mode frequency is also more sensitive

to internal model parameters such as $K_I$.

Model simulations were also used to determine the effects bone loss and an implant flange have on the accelerometer response. The fundamental frequency for both the 4 mm extraoral, and 10 mm intraoral implants was found to be sensitive to bone loss, with the 10 mm implant having changes of approximately 80 Hz per half millimeter of bone loss and changes of approximately 100 Hz per half millimeter for the 4 mm implant at an interface stiffness of 1 GPa. Model simulations with and without a flange indicated that for a number of patients in the *in vivo* study, the flange does not appear to contribute to the implant stability.

The *in vivo* tests utilizing the impact test and the analytical model provided longitudinal interface stiffness and damping values for twelve patients fitted with BAHA® implants. Model results based on the determination of $k$ from the measured fundamental frequency show good overall agreement with the measured accelerometer responses for the patients. The damping of the implant interface from the model results was determined to be relatively low, below 5% in the second mode. The damping ratio varied between approximately 1 and 5% longitudinally. The average bone-implant interface stiffness determined at the twelve month measurement was 9.01 GPa for the men and 5.75 GPa for the women. From the interface stiffness values determined longitudinally, the initial three month period appears to be when the implants have the lowest interface stiffness. The lower stiffness values at this stage may be due to the modelling/remodelling of the bone around the implant. Based on the lower interface stiffness values determined in the first three months, the current practice of processor connection and implant loading after three months for the patients in the study appear reasonable.

## 7.2 Conclusions

- A non-invasive, rapid and relatively inexpensive impact technique was developed based on a un-filtered (raw) accelerometer signal obtained from a Periotest® handpiece.
- The raw accelerometer signal was shown to accurately reflect the true contact time of the system, while the conditioned signal is not a true representation of the motion.
- A measurement protocol and calibration block was developed to increase the precision of the impact technique.

- An analytical four degree of freedom model was developed which could evaluate the interface stiffness and damping properties of implants based on raw accelerometer impact measurements.
- The analytical model demonstrated that the internal stiffness components in the system could not be ignored and had to be included to accurately reflect the system dynamics.
- The model results demonstrated that the high frequency term found in the accelerometer signal was a second mode of vibration of the system.
- *In vitro* experiments demonstrated that the impact technique and four degree of freedom model could provide consistent interface measurements over a range of different Brånemark implant and abutment systems.
- Model simulations demonstrated that for interface stiffness values greater than 5 GPa the fundamental frequency becomes less sensitive to changes in the interface stiffness.
- The impact technique and analytical model were shown to be appropriate for use in evaluating the interface properties of 12 BAHA® patients in a longitudinal clinical study.
- The flange present on the extraoral BAHA® implant did not appear to provide significant support to the implant.
- The magnitude of changes in the damping ratio of the interface between patient visits was found to be small.
- The interface stiffness properties of the BAHA® patients varied considerably within the first three months. The minimum interface stiffness values for 11 of the 12 patients occurred during this interval.
- Overall, the smallest variations in interface stiffness between patient visits occurred between the six and twelve month measurements.

The developed impact testing technique is shown to be accurate and sensitive in the measurement of interface properties both *in vitro* and *in vivo*. The analytical model provides a method to extract basic mechanical properties of the interface from the impact measurements. Ultimately, the testing method is shown to have clinical significance as it provides a means to track the mechanical properties of the bone-implant interface in a noninvasive way in patients.

## 7.3 Future Considerations

### 7.3.1 *In Vitro* Testing on an Implant Placed in Self Polymerising Resin

Studies by Meredith, N. et al. (1996b) and Elias, J. et al. (1996) tested the resonant frequency properties of implants placed in a self curing resin. Longitudinal impact measurements on an implant placed in self curing resin would provide raw accelerometer data of changing interface properties. The analytical model could then be compared to the measurements to evaluate how well the model predicts the effects of changing interface stiffness as the resin cures.

### 7.3.2 Verifying Damping Properties of Bone *In Vivo*

The damping properties of BAHA® implants predicted by the model were found to be low (less than approximately 5%). Further tests to confirm the damping properties could be done with a strain-gauged abutment. By striking the strain-gauged abutment the damping properties could be estimated by monitoring the decay of the strain response over time. This damping ratio could then be compared to the analytical model results to determine the accuracy of the predicted damping ratio.

### 7.3.3 Model with Multi-Layered Supporting Tissue

Depending on the implant location, the bone supporting the implant may not exist as a single layer of one type of bone. The analytical model as presented assumes a uniform interface along the length of the implant. For those implants that have multiple layers of different types of bone the model may require multiple interface stiffness "layers". This extension of the model is relatively simple, as it does not change the solution method but is achieved through changes to the stiffness matrix [K]. For cases involving multiple stiffness layers, both the fundamental and second mode frequency measurements may be required to determine the multiple interface stiffness values.

### 7.3.4 Testing on Fixed Dental Restorations

As a large number of dental restorations utilize fixed or cemented tooth prosthesis, there is a need for a method of testing these implants. The developed impact technique may be well suited for this testing, as the impact could occur on the prosthetic tooth. Changes to the internal mass and stiffness properties

to match the tooth prosthesis would allow for an estimation of the interface properties of the implant.

### 7.3.5 Further *In Vivo* Testing of Implants

The *in vivo* tests with the proposed method completed to date were all on BAHA® implants in good quality bone. There were no recorded implant failures during this time. Further testing needs to be completed to compare model results with measurements on patients with intraoral as well as other types of extraoral implants. Tests on implants in poor quality bone, or implants that are failing may produce raw accelerometer signals significantly different than those measured to date. For these signals the modal participation factors, second mode frequency and damping properties may be significantly different than those found in healthy implants.

### 7.3.6 Additional Operator Use Testing

While some multi-user testing has been done, further testing to quantify the affects of a user holding the Periotest® handpiece needs to be completed. *In vitro* tests could be completed to compare the measured accelerometer response from tests done using the handpiece stand to those of an operator holding the Periotest® handpiece. These tests would help to quantify any differences between the two signals. Additional clinical testing could determine the variability caused from multiple users testing an implant in a patient.

### 7.3.7 Modification of the Model for Use with the Osstell®

The model could be adapted for use with the Osstell® by replacing the mass of the Periotest® rod with the Osstell® transducer, and increasing the stiffness of $K_I$ so that the mass is rigidly connected to the abutment. Resonant frequency values from the Osstell® could then be used with the model to determine the interface stiffness.

# References


*Dental Implants: Benefit and Risk. NIH Consensis Statement Online*, June 13-14 1978.

Adell, R., Lekholm, V., Rockler, B.R., and Branemark, P-I. A 15-year study of osseointegrated implants in the treatment of the edentulous jaw. *International Journal of Oral Surgery*, **10**:387–416, 1981.

Aparicio, C. The use of the periotest value as the initial success criteria of an implant: 8-year report. *The International Journal of Periodontics and Restorative Dentistry*, **17**(2):150–161, 1997.

Bischof, M., Nedir, R., Szmukler-Moncler, S., Bernard, J-P., and Samson, J. Implant stability measurement of delayed and immediately loaded implants during healing. *COIR*, **15**:pp. 529–539, 2004.

Brånemark, P-I., Zarb, G.A., and Albrektsson, T. *Tissue-Integrated Prostheses:Osseointegration in Clinical Dentistry.* Quintessence Publishing Co, 1985.

Brunski, J.B. In vivo bone response to biomechanical loading at the bone/dental-implant interface. *Advances in Dental Research*, **13**:99–119, 1999.

Carr, A.B., Papzoglou, E., and Larsen, P. The relationship of periotest values, biomaterials, and torque to failure in adult baboons. *International Journal of Prosthodontics*, **8**:pp. 15–20, 1995.

Cowin, S. *Bone Mechanics Handbook.* CRC Press, 2001.

Cowin, S. and Guo, X. *Bone Mechanics Handbook.* CRC Press, 2001.

Derhami, K., Wolfaardt, J., Faulkner, G., and Grace, M. Assessment of periotest device in baseline mobility measurements of craniofacial implants. *International Journal of Oral and Maxillofacial Implants*, **10**:221–229, 1995.

Elias, J. *A noninvasive method for assessing the dental implant-bone interface.* Doctorate thesis, Rensselaer Polytechnic Institute, 1994.

Elias, J., Brunski, J.B., and Scarton, H. A dynamic modal testing technique for noninvasive assessment of bone-dental implant interfaces. *International Journal of Oral and Maxillofacial Implants*, **11**(6):pp. 728–734, 1996.

Faulkner, G., Giannitsios, D., Lipsett, W., and Wolfaardt, J. The use and abuse of the periotest for 2-piece implant/abutment systems. *International Journal of Oral and Maxillofacial Implants*, **16**(4):pp. 486–494, 2001.

Faulkner, G., Wolfaardt, J., and Chan, A. Measuring abutment/implant joint integrity with the periotest instrument. *International Journal of Oral and Maxillofacial Implants*, **14**:681–688, 1999a.

Faulkner, G., Wolfaardt, J.F., and Chan, A. Measuring abutment/implant joint integrity with the periotest instrument. *International Journal of Oral and Maxillofacial Implants*, **14**:681–688, 1999b.

Friberg, B., Sennerby, L., Linden, B., Gröndahl, K., and Lekholm, U. Stability measurements of one-stage branemark implants during healing in mandibles. *International Journal of Oral and Maxillofacial Surgery*, **28**:pp. 266–272, 1999.

Giannitsios, D. *Dynamic Modeling of the Periotest® Method.* Master's thesis, University of Alberta, 2001.

Glauser, R., Sennerby, L., Meredith, N., Rée, A., Lundgren, A., Gottlow, J., and Hämmerle, C.H.F. Resonance frequency analysis of implants subjected to immediate or early functional occlusal loading. *COIR*, **15**:pp. 428–434, 2004.

Huang, H.-M., Chiu, C.-L., Yeh, C.-Y., Lin, C.-T., Lin, L.-H., and Lee, S.-Y. Early detection of implant healing process using resonance frequency analysis. *Clinical Oral Implants Research*, **14**:pp. 437–443, 2003.

Huang, H.-M., Lee, S.-Y., Yeh, C.-Y., and Lin, C.-T. Resonance frequency assessment of dental implant stability with various bone qualities: A numerical approach. *Clinical Oral Implants Research*, **13**:pp. 65–74, 2002.

Hurst, S. *Investigation of Periotest® and Osstell® Instruments for Measuring Craniofacial Implant Integrity.* Master's thesis, University of Alberta, 2002.

Jafari, A., Sadashiva Shetty, K., and Kumar, M. Study of stress distribution and displacement of various craniofacial structures following application of transverse orthopedic forces - a three-dimensiounal fem study. *Angle Orthodontist*, **73**:12–20, 2003.

Jones, S. *Simulation of Impact Testing of Implant/Abutment System.* Master's thesis, University of Alberta, 2005.

Kaneko, T.M. Relationship between the stiffness of the dental implant-bone system and the duration of the implant-tapping rod contact. *Medical Engineering & Physics*, **16**:pp. 310–315, 1994.

Lukas, D. and Schulte, W. Periotest - a dynamic procedure for the diagnosis of the human periodontium. *Clinical Physics and Physiological Measurement*, **11**:pp. 65–75, 1990.

Meredith, N. *On the Clinical Measurement of Implant Stability and Osseointegration.* PhD thesis, Göteborg University, 1997.

Meredith, N., Alleyne, D., and Cawley, P. Quantitative determination of the stability of the implant-tissue interface using resonance frequency analysis. *COIR*, **7**:pp. 261–267, 1996a.

Meredith, N., Alleyne, D., and Cawley, P. Quantitative determination of the stability of the implant-tissue interface using resonance frequency analysis. *Clinical Oral Implants Research*, **7**:pp. 261–267, 1996b.

Meredith, N., Book, K., Friberg, B., Jemt, T., and Sennerby, L. Resonance frequency measurements of implant stability *in vivo*. *COIR*, **8**:pp. 226–233, 1997.

Nedir, R., Bischof, M., Szmukler-Moncler, S., Bernard, J-P., and Samson, J. Predicting osseointegration by means of implant primary stability. *COIR*, **15**:pp. 520–528, 2004.

Olivé, J. and Aparicio, C. The periotest method as a measure of osseointegrated oral implant stability. *International Journal of Oral and Maxillofacial Implants*, **5**(4):pp. 390–400, 1990.

Oppenheim, A.V., Willsky, A.S., and Young, I.T. *Signals and Systems.* Prentice Hall, 1983.

Pattijn, V., Van Lierde, C., Van der Perre, G., Naert, I., and Vander Sloten, J. The resonance frequencies and mode shapes of dental implants: Rigid body behavior versus bending behaviour. a numerical approach. *Journal of Biomechanics*, **39**:pp. 939–947, 2006.

Raghavendra, S., Wood, M.C., and Taylor, T.D. Early wound healing around endosseous implants: A review of the literature. *International Journal of Oral and Maxillofacial Implants*, **20**:pp. 425–431, 2005.

Rao, S.S. *Mechanical Vibrations.* Addison-Wesley, 1995.

Roberts, W.E. Fundamental principles of bone physiology, metabolism and loading. In Worthington, P., Naert, I., and van Steenberghe, D., editors, *Osseointegration in Oral Rehabilitation*, pages 157–170. Quintessence Publications, 1993.

Sundén, S., Gröndahl, K., and Gröndahl, H.-G. Accuracy and precision in the radiographic diagnosis of clinical instability in brånemark dental implants. *Clinical Oral Implants Research*, **6**:220–226, 1995.

Thomson, W.T. and Dahleh, M.D. *Theory of Vibration with Applications 5th Edition.* Prentice Hall, 1998.

van Steenberghe, D. and Quirynen, M. Reproducibility and detection threshold of peri-implant diagnostics. *Adv Dent Res*, **7**:191–195, 1993.

van Steenberghe, D., Tricio, J., Naert, I., and Nys, M. Damping characteristics of bone-to-implant interfaces; a clinical study with the periotest device. *Clinical Oral Implants Research*, **6**:pp. 31–39, 1995.

# Appendix A

# Four Degree of Freedom Model

The presented analytical model is composed of two rigid bodies, the implant with mass $m_I$ and mass moment of inertia $J_I$, an abutment with mass $m_A$ and mass moment of inertia $J_A$. The impact rod was treated as a point mass with mass $m_R$. The implant and abutment are connected by a pin and torsional spring of stiffness $K_T$. During the time that the abutment and impacting rod are in contact, the dynamic response of the system is described using the coordinates $X_1$ (displacement of the impacting rod), $X_2$ (displacement of a point, O, along the centre of the abutment at the same height as the striking rod), $\Theta_1$ (rotation of the abutment) and $\Theta_2$ (rotation of the implant) as shown in Figure 4.1. The bone implant interface is represented by a series of distributed horizontal and vertical springs with stiffnesses per unit length ($k$) of the supporting tissue. To maintain an analytical solution, the damping is assumed to be proportional to the stiffnesses. This leads to a set of 4 coupled equations;

$$[M]\begin{Bmatrix} \ddot{X}_1 \\ \ddot{X}_2 \\ \ddot{\Theta}_1 \\ \ddot{\Theta}_2 \end{Bmatrix} + \beta[K]\begin{Bmatrix} \dot{X}_1 \\ \dot{X}_2 \\ \dot{\Theta}_1 \\ \dot{\Theta}_2 \end{Bmatrix} + [K]\begin{Bmatrix} X_1 \\ X_2 \\ \Theta_1 \\ \Theta_2 \end{Bmatrix} = \{0\}. \tag{A.1}$$

The mass and stiffness matrices are derived through the use of stiffness and inertia influence coefficients and are:

$$[M] = \begin{bmatrix} M_{11} & M_{12} & M_{13} & M_{14} \\ M_{21} & M_{22} & M_{23} & M_{24} \\ M_{31} & M_{32} & M_{33} & M_{34} \\ M_{41} & M_{42} & M_{43} & M_{44} \end{bmatrix} \tag{A.2}$$

with;

$$[M_{11}] = m_R;$$

$$[M_{12}] = [M_{21}] = [M_{13}] = [M_{31}] = [M_{14}] = [M_{41}] = 0;$$

$$[M_{22}] = m_A + m_I;$$

$$[M_{23}] = [M_{32}] = -(m_A h_1 + m_I(\frac{l_A}{2} + h_1));$$

$$[M_{24}] = [M_{42}] = -m_I \frac{l_I}{2};$$

$$[M_{33}] = J_A + m_A {h_1}^2 + m_I(\frac{l_A}{2} + h_1)^2;$$

$$[M_{34}] = [M_{43}] = m_I(\frac{l_A}{2} + h_1)\frac{l_I}{2};$$

$$[M_{44}] = J_I + m_I(\frac{l_I}{2})^2;$$

and;

$$[K] = \begin{bmatrix} K_{11} & K_{12} & K_{13} & K_{14} \\ K_{21} & K_{22} & K_{23} & K_{24} \\ K_{31} & K_{32} & K_{33} & K_{34} \\ K_{41} & K_{42} & K_{43} & K_{44} \end{bmatrix} \tag{A.3}$$

with;

$$[K_{11}] = K_I;$$

$$[K_{12}] = [K_{21}] = -K_I;$$

$$[K_{13}] = [K_{31}] = [K_{14}] = [K_{41}] = 0;$$

$$[K_{22}] = K_I + 2k(l_I - l_C);$$

$$[K_{23}] = [K_{32}] = -2k(l_I - l_C)(\frac{l_A}{2} + h_1);$$

$$[K_{24}] = [K_{42}] = -k({l_I}^2 - {l_C}^2);$$

$$[K_{33}] = 2k(l_I - l_C)(\frac{l_A}{2} + h_1)^2 + K_T;$$

$$[K_{34}] = [K_{43}] = k(\frac{l_A}{2} + h_1)({l_I}^2 - {l_C}^2) - K_T;$$

$$[K_{44}] = \frac{2}{3}k({l_I}^3 - {l_C}^3) + 2kb^2(l_I - l_C) + K_T + r^2 K_F.$$

For the mass matrix, implant masses ($m_I$) were measured and found to be 0.1538 and 0.647 gm for the 4 mm and 10 mm implant, respectively. Abutment

masses ($m_A$), were measured as 0.228, 0.333, 0.448, 0.647 gm for the 4, 5.5, 7, 10 mm abutments. Both implants and abutments were considered as uniform solid cylinders for calculation of the moment of inertia values, with centres of mass located at the mid-point of the cylinder. In the stiffness matrix the values of $K_I$, $K_T$ and $K_F$ were found through *in vitro* experimentation, leaving the only unknown in the matrix as $k$.

To solve (A.1) we first examine the un-damped case ($\beta = 0$) and assume a solution in the form;

$$\begin{Bmatrix} X_1(t) \\ X_2(t) \\ \Theta_1(t) \\ \Theta_2(t) \end{Bmatrix} = \begin{Bmatrix} \bar{X}_1 \\ \bar{X}_2 \\ \bar{\Theta}_1 \\ \bar{\Theta}_2 \end{Bmatrix} \sin(p_r t + \phi) \tag{A.4}$$

where $\bar{X}_1$, $\bar{X}_2$, $\bar{\Theta}_1$, $\bar{\Theta}_2$ are magnitudes of the resulting motion. Substituting this solution into equation (A.1) we get the following formula;

$$[K] \begin{Bmatrix} \bar{X}_1 \\ \bar{X}_2 \\ \bar{\Theta}_1 \\ \bar{\Theta}_2 \end{Bmatrix} = p_r^2 [M] \begin{Bmatrix} \bar{X}_1 \\ \bar{X}_2 \\ \bar{\Theta}_1 \\ \bar{\Theta}_2 \end{Bmatrix}. \tag{A.5}$$

If $k$ is known, equation (A.5) is a standard Eigenvalue/Eigenvector problem in which the Eigenvalues are the resonant frequency values $p_r$ (there are a number of resonant frequency solutions, "$r$", equal to the number of degrees of freedom of the system) and the Eigenvectors are the mode shapes $[u]$. If the first mode resonant frequency ($p_1$) is known, but $k$ is not known, $k$ can be found by multiplying both sides of (A.5) by $[M]^{-1}$ and re-arranging such that;

$$[[M]^{-1}[K] - \Lambda] \begin{Bmatrix} \bar{X}_1 \\ \bar{X}_2 \\ \bar{\Theta}_1 \\ \bar{\Theta}_2 \end{Bmatrix} = 0 \tag{A.6}$$

where,

$$\Lambda = \begin{bmatrix} p_1^2 & 0 & 0 & 0 \\ 0 & p_2^2 & 0 & 0 \\ 0 & 0 & p_3^2 & 0 \\ 0 & 0 & 0 & p_4^2 \end{bmatrix}.$$

To solve, set the $det[[M]^{-1}[K] - \Lambda] = 0$, and this results in an equation with only one unknown, $k$ that can be solved. Once $k$ is determined, equation

(A.5) can be used to get the remaining resonant frequency values and the mode shapes.

Once $p_r$ and $[u]$ are known, the damped solution to equation (A.1) can be found. The first step is defining $\beta$ such that

$$\beta = \frac{2(\nu_r)}{p_r} \tag{A.7}$$

where $\nu_r$=damping ratio for each mode and $p_r$=resonant frequency for each mode. The value for $\beta$ was found by setting $r = 2$ and choosing the damping ratio $\nu_2$ to match the *in vitro* measurements. Once $\beta$ is known, equation (A.7) can be re-arranged and $\nu_r$ can be solved for each mode.

The next step is to normalize the modal matrix such that the normalized modal matrix $[\mu]$ satisfies the condition

$$[\mu]^T[M][\mu] = [I] \tag{A.8}$$

where $[I]$ is the identity matrix. The only requirement for this is that the mass matrix $[M]$ is a symmetric matrix. To simplify the normalization process, both the $[\mu]$ and $[u]$ matrices can be expressed as a set of column vectors, such that

$$[u] = [\{u\}_1\{u\}_2....\{u\}_r],$$

and

$$[\mu] = [\{\mu\}_1\{\mu\}_2....\{\mu\}_r].$$

Using the column vectors, equation (A.8) will be satisfied if the normalized column vectors are defined as

$$\{\mu\}_r^T[M]\{\mu\}_r = 1. \tag{A.9}$$

A normalization constant, $\alpha$ can now be defined for each column so that

$$\{\mu\}_r = \alpha_r\{u\}_r. \tag{A.10}$$

Substituting this into equation (A.9), and solving for $\alpha_r$

$$\alpha_r = \frac{1}{\sqrt{\{u\}_r^T[M]\{u\}_r}}.$$

This now gives an $\alpha_r$ value for each column and with the use of equation (A.10) allows construction of the normalized modal matrix $[\mu]$. Besides having the property of equation (A.8), the normalized modal matrix has two other important characteristics.

1) The column vectors of the normalized modal matrix have the property,

$$\{\mu\}_i^T[M]\{\mu\}_j = \delta_{ij} \tag{A.11}$$

so that $\delta_{ij} = 0$ if $i \neq j$ and $\delta_{ij} = 1$ when $i = j$.

2) If the assumed solution in (A.4) is multiplied by the normalized modal matrix $[\mu]$ and substituted into the un-damped equation (A.1), then multiplied by $[\mu]^T$ we get

$$[\mu]^T[K][\mu] = \Lambda[\mu]^T[M][\mu] = \Lambda.$$

To solve (A.1), let the solution

$$\left\{ \begin{array}{c} X_1(t) \\ X_2(t) \\ \Theta_1(t) \\ \Theta_2(t) \end{array} \right\} = \{x(t)\} = [\mu]\{\eta(t)\} \tag{A.12}$$

If the results of (A.12) are substituted into equation (A.1) and the resulting equation is multiplied by $[\mu]^T$

$$[\mu]^T[M][\mu]\{\ddot{\eta}(t)\} + \beta[\mu]^T[K][\mu]\{\dot{\eta}(t)\} + [\mu]^T[K][\mu]\{\eta(t)\} = \{0\}. \tag{A.13}$$

Using the previously defined properties of the normalized modal matrix along with equation (A.7), the equation (A.13) becomes a set of un-coupled equations in the form

$$\ddot{\eta}_r + 2\nu_r p_r \dot{\eta}_r + p_r^2 \eta_r = 0. \tag{A.14}$$

The solution to this set of un-coupled equations is in the form:

$$\eta_r = G_r e^{s_r t}$$

where $G_r$ is a constant. This result can be substituted into equation (A.14), and the roots for $s_r$ can be determined such that;

$$\eta_r = e^{-\nu_r p_r t}\left[C_r \cos(\sqrt{1-\nu_r^2}p_r t) + D_r \sin(\sqrt{1-\nu_r^2}p_r t)\right] \tag{A.15}$$

where $C_r$ and $D_r$ are constants.

Since

$$\{x(t)\} = [\mu]\{\eta(t)\} = \sum_{r=1}^{n} \eta_r \{\mu\}_r$$

with $n$=the number of degrees of freedom of the system, equation (A.15) can be re-written as

$$\{x(t)\} = \sum_{r=1}^{n}\left[e^{-\nu_r p_r t}(C_r \cos(\sqrt{1-\nu_r^2}p_r t) + D_r \sin(\sqrt{1-\nu_r^2}p_r t)\right]\{\mu\}_r. \tag{A.16}$$

From this, we can solve for $C_r$ and $D_r$ using the initial conditions.

$$\{x(0)\} = \sum_{r=1}^{n} C_r \{\mu\}_r \tag{A.17}$$

and

$$\{\dot{x}(0)\} = \sum_{r=1}^{n} p_r (D_r - \nu_r C_r) \{\mu\}_r \tag{A.18}$$

where $\{x(0)\}$ and $\{\dot{x}(0)\}$ are the initial displacements and velocities. To solve for $C_r$ and $D_r$, multiply each side of equations (A.17) and (A.18) by $[\mu]_s^T[M]$ to give

$$\{\mu\}_s^T[M]\{x(0)\} = \{\mu\}_s^T[M] \sum_{r=1}^{n} C_r \{\mu\}_r$$

and

$$\{\mu\}_s^T[M]\{\dot{x}(0)\} = \{\mu\}_s^T[M] \sum_{r=1}^{n} p_r (D_r - \nu_r C_r) \{\mu\}_r.$$

Using the normalized matrix property from (A.11) and solving for $C_r$ and $D_r$ we get:

$$C_r = \{\mu\}_r^T[M]\{x(0)\}$$

and

$$D_r = \frac{1}{p_r}\{\mu\}_r^T[M]\{\dot{x}(0)\} + \nu_r \{\mu\}_r^T[M]\{x(0)\}.$$

For the four degree of freedom model analyzed, $n = 4$, and the initial displacement $\{x(0)\} = \{0\}$ which causes $C_r = 0$. Substituting these results, and $D_r$ into equation (A.16) results in

$$\{x(t)\} = \sum_{r=1}^{4} e^{-\nu_r p_r t} \left[ \frac{1}{p_r} \{\mu\}_r^T[M]\{\dot{x}(0)\} \sin\left(\sqrt{1-\nu_r^2}\, p_r t\right) \right] \{\mu\}_r. \tag{A.19}$$

The acceleration response can be obtained from (A.19) by taking $\frac{d^2\{x\}}{dt^2}$ to give

$$\{\ddot{x}(t)\} = \sum_{r=1}^{4} (3\nu_r^2 - \nu_r^4 - 1) p_r e^{-\nu_r p_r t} \left[ \{\mu\}_r^T[M]\{\dot{x}(0)\} \sin\left(\sqrt{1-\nu_r^2}\, p_r t\right) \right] \{\mu\}_r. \tag{A.20}$$

Knowing that the initial velocity of the system

$$\{\dot{x}(0)\} = \begin{Bmatrix} v_o \\ 0 \\ 0 \\ 0 \end{Bmatrix}$$

with $v_o = 0.2$ m/s, equation (A.20) can be solved to determine the acceleration of the striking rod $X_1$ which can be compared to the measured accelerometer signal on the rod.

# Appendix B

# *In vivo* First Mode Frequency Measurements

This appendix contains the *in vivo* longitudinal first mode frequency plots for all 12 patients.

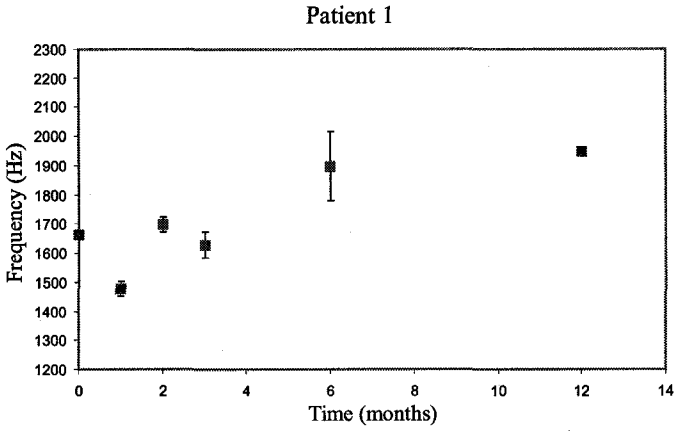


Figure B.1: Longitudinal first mode frequency measurements for Patient 1 (Female).

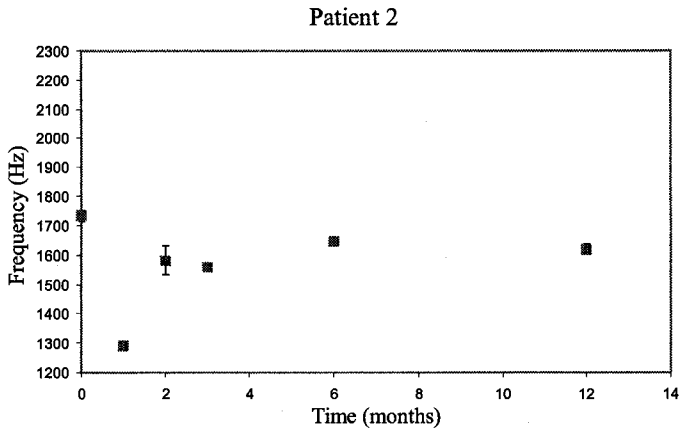


Figure B.2: Longitudinal first mode frequency measurements for Patient 2 (Female).

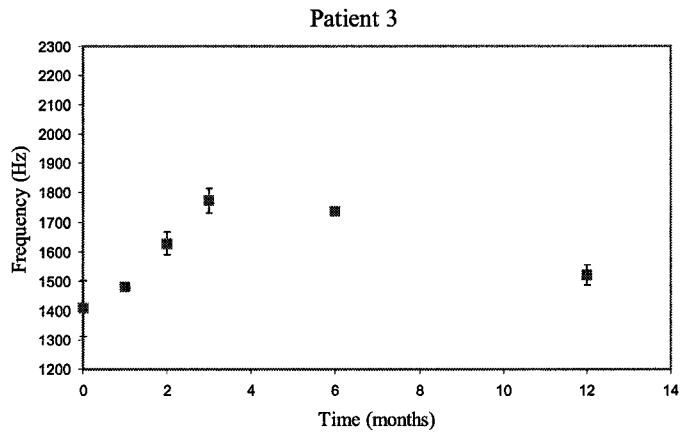


Figure B.3: Longitudinal first mode frequency measurements for Patient 3 (Male).

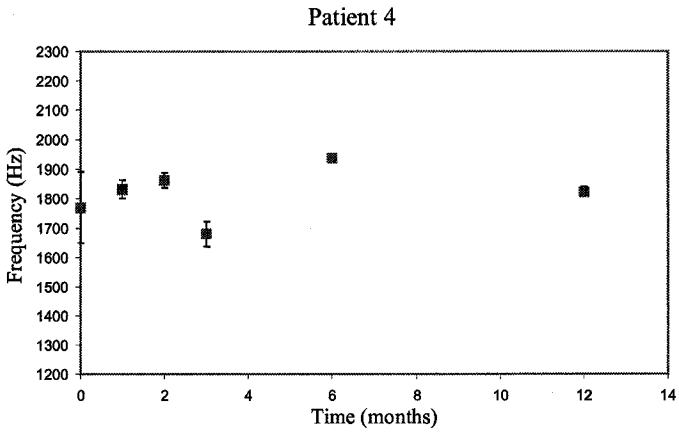


Figure B.4: Longitudinal first mode frequency measurements for Patient 4 (Male).

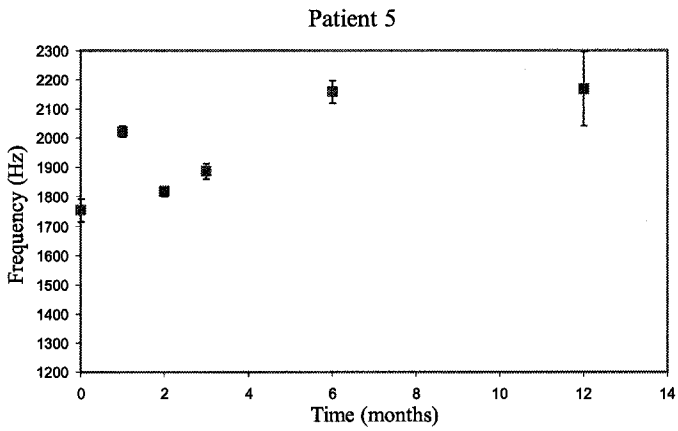


Figure B.5: Longitudinal first mode frequency measurements for Patient 5 (Male).

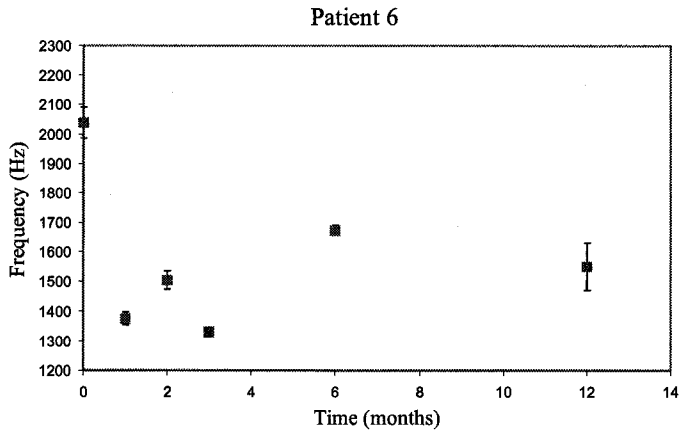


Figure B.6: Longitudinal first mode frequency measurements for Patient 6 (Male).

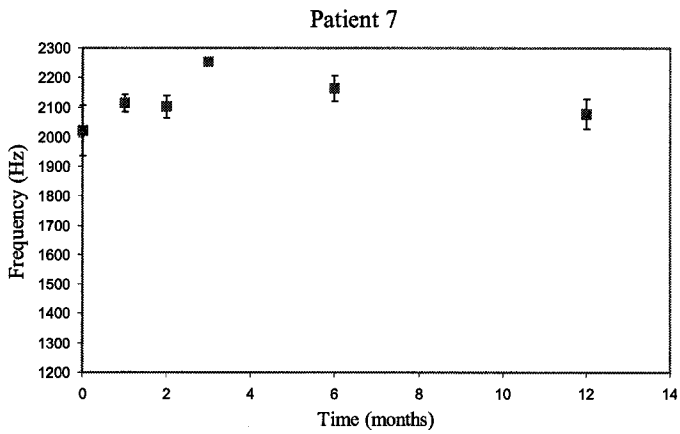


Figure B.7: Longitudinal first mode frequency measurements for Patient 7 (Male).

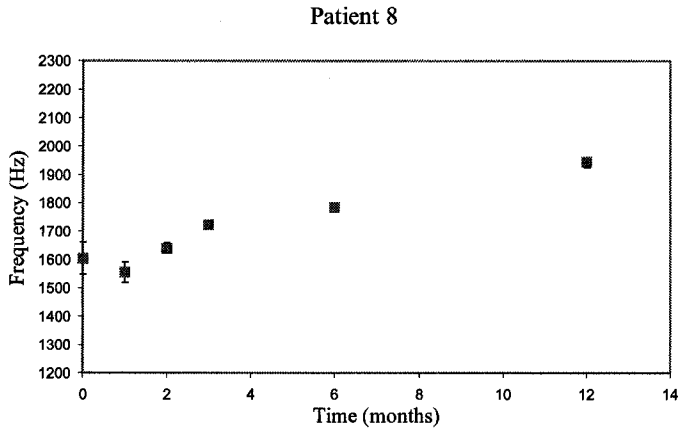


Figure B.8: Longitudinal first mode frequency measurements for Patient 8 (Female).

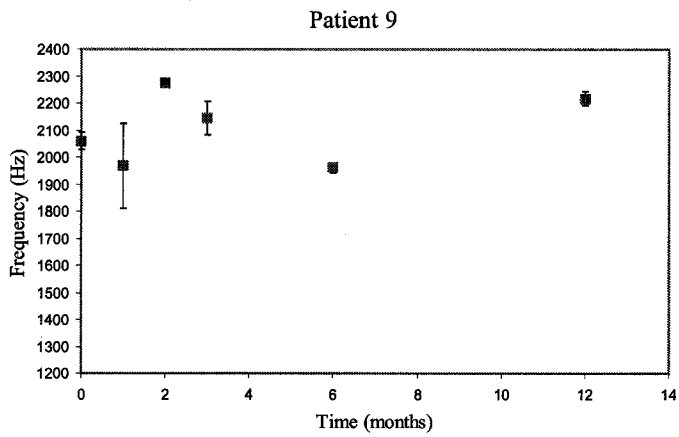


Figure B.9: Longitudinal first mode frequency measurements for Patient 9 (Male).

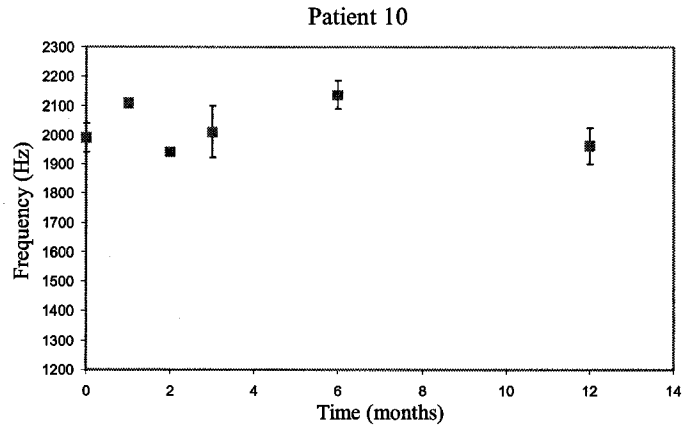


Figure B.10: Longitudinal first mode frequency measurements for Patient 10 (Male).

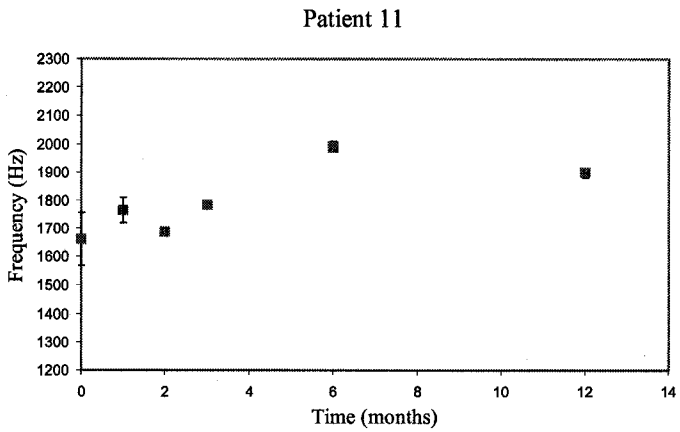


Figure B.11: Longitudinal first mode frequency measurements for Patient 11 (Female).

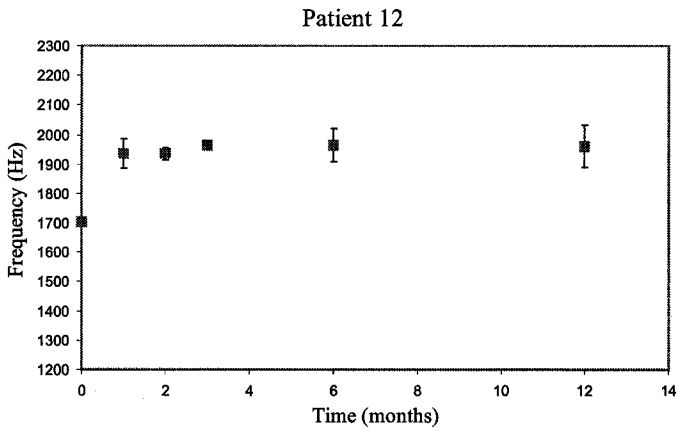


Figure B.12: Longitudinal first mode frequency measurements for Patient 12 (Male).

# Appendix C

# Patient Predicted Acceleration Response Compared to Measurements

This appendix contains the raw accelerometer response and the predicted four degree of freedom analytical response for the 12 BAHA® patients in the *in vivo* study. The interface stiffness, $k$, used in the model for each plot are the average values listed in Tables 6.3a and 6.3b. The $K_I$ and $K_T$ values were for a 5.5 mm abutment, which was used in the measurements.

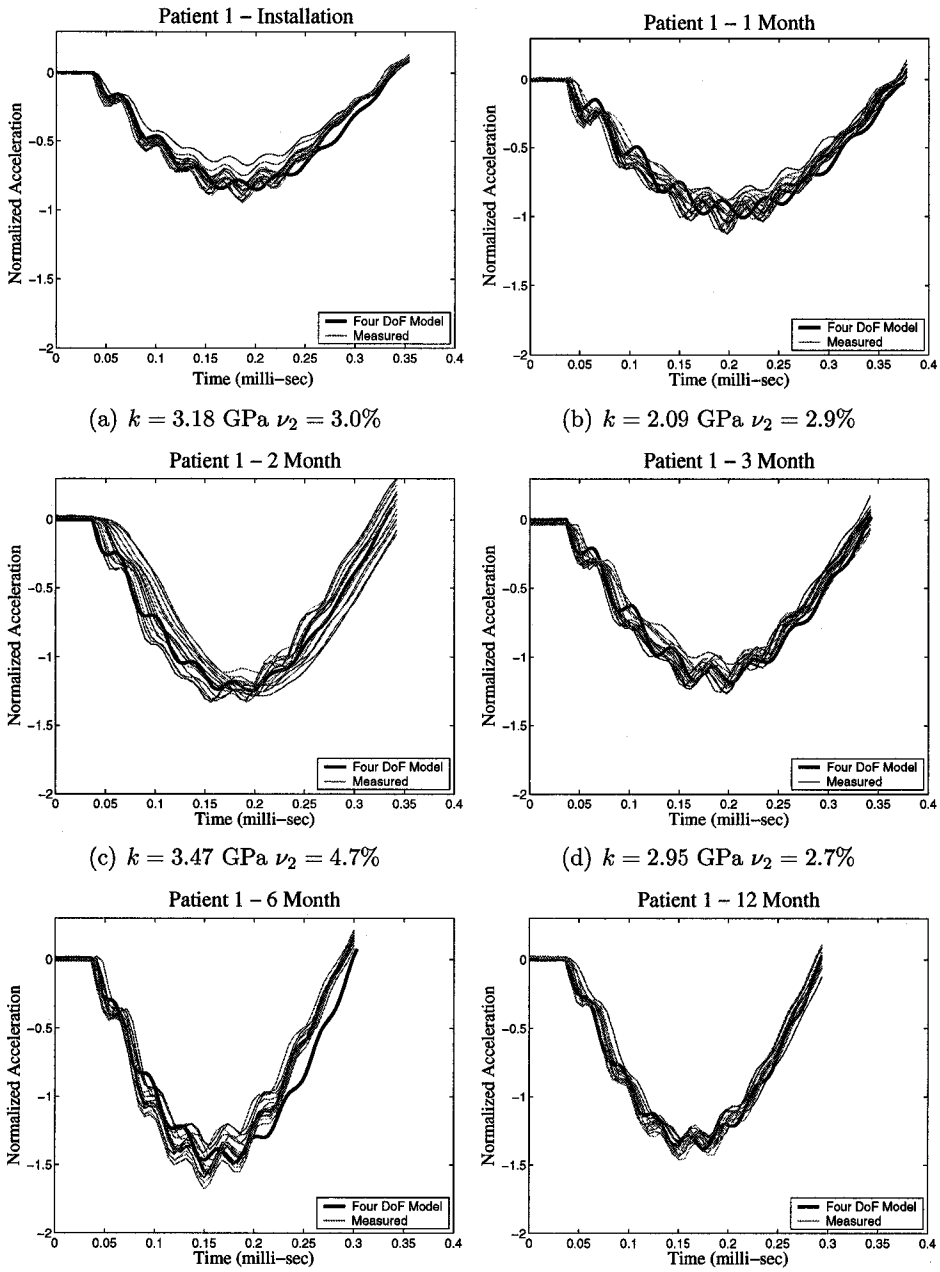


(a) $k = 3.18$ GPa $\nu_2 = 3.0\%$

(b) $k = 2.09$ GPa $\nu_2 = 2.9\%$

(c) $k = 3.47$ GPa $\nu_2 = 4.7\%$

(d) $k = 2.95$ GPa $\nu_2 = 2.7\%$

(e) $k = 5.80$ GPa $\nu_2 = 1.9\%$

(f) $k = 6.71$ GPa $\nu_2 = 1.5\%$

Figure C.1: Patient 1 acceleration measurement compared to predicted model response at different patient visits.

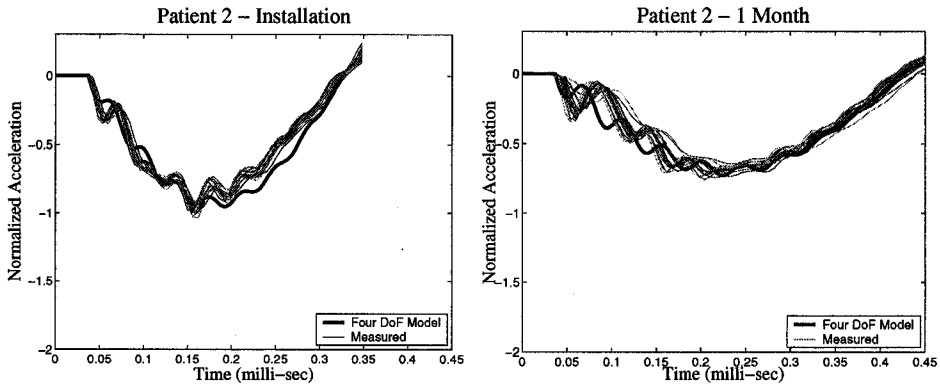


(a) $k = 4.98$ GPa $\nu_2 = 3.0\%$




(b) $k = 1.85$ GPa $\nu_2 = 4.0\%$

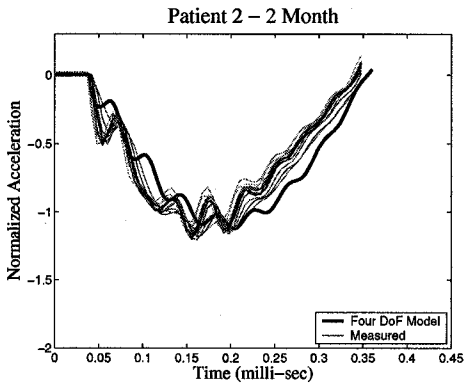


(c) $k = 3.49$ GPa $\nu_2 = 3.3\%$

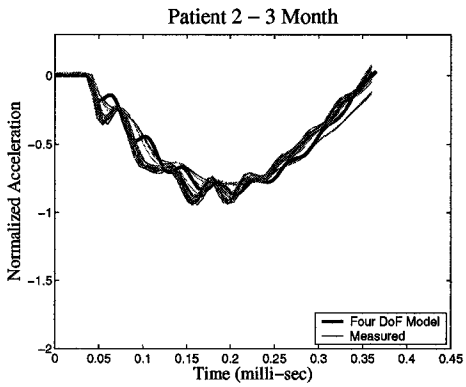


(d) $k = 3.31$ GPa $\nu_2 = 3.4\%$

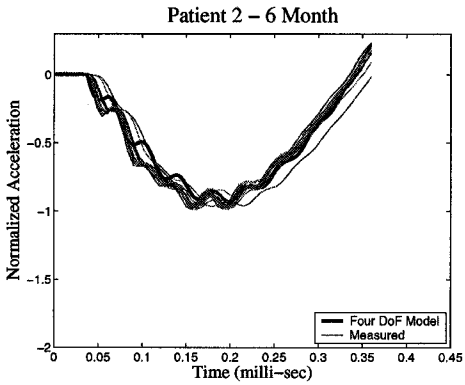


(e) $k = 4.05$ GPa $\nu_2 = 3.2\%$

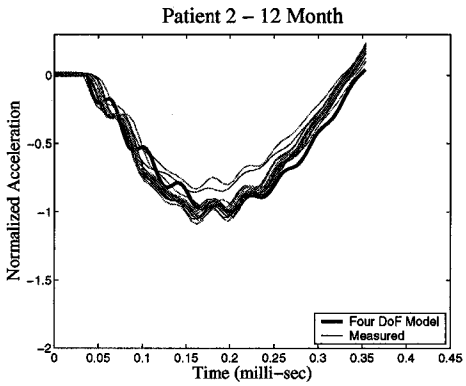


(f) $k = 3.80$ GPa $\nu_2 = 3.2\%$

Figure C.2: Patient 2 acceleration measurement compared to predicted model response at different patient visits.

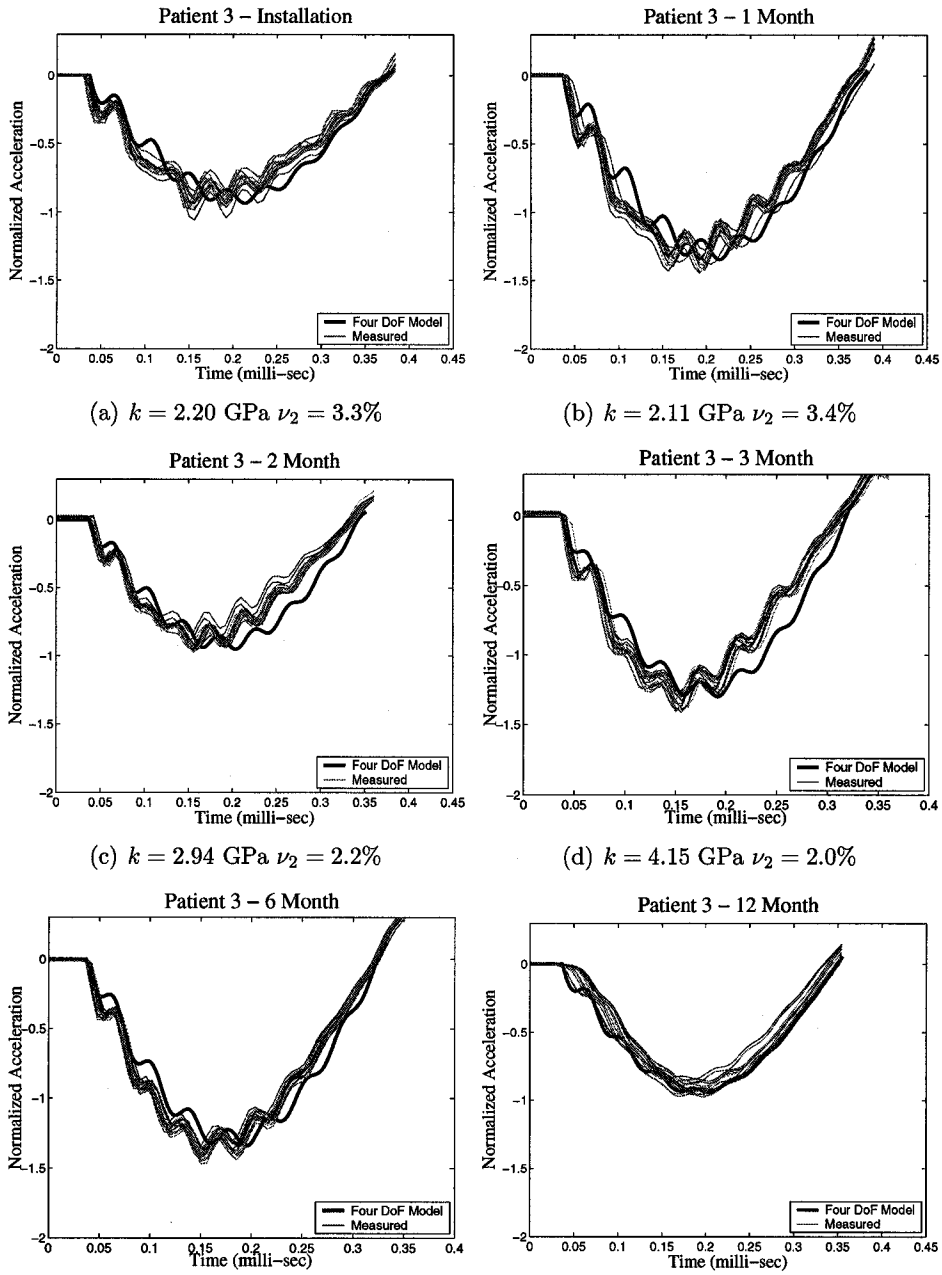


(a) $k = 2.20$ GPa $\nu_2 = 3.3\%$

(b) $k = 2.11$ GPa $\nu_2 = 3.4\%$

(c) $k = 2.94$ GPa $\nu_2 = 2.2\%$

(d) $k = 4.15$ GPa $\nu_2 = 2.0\%$

(e) $k = 3.80$ GPa $\nu_2 = 2.1\%$

(f) $k = 2.80$ GPa $\nu_2 = 6.7\%$

Figure C.3: Patient 3 acceleration measurement compared to predicted model response at different patient visits.

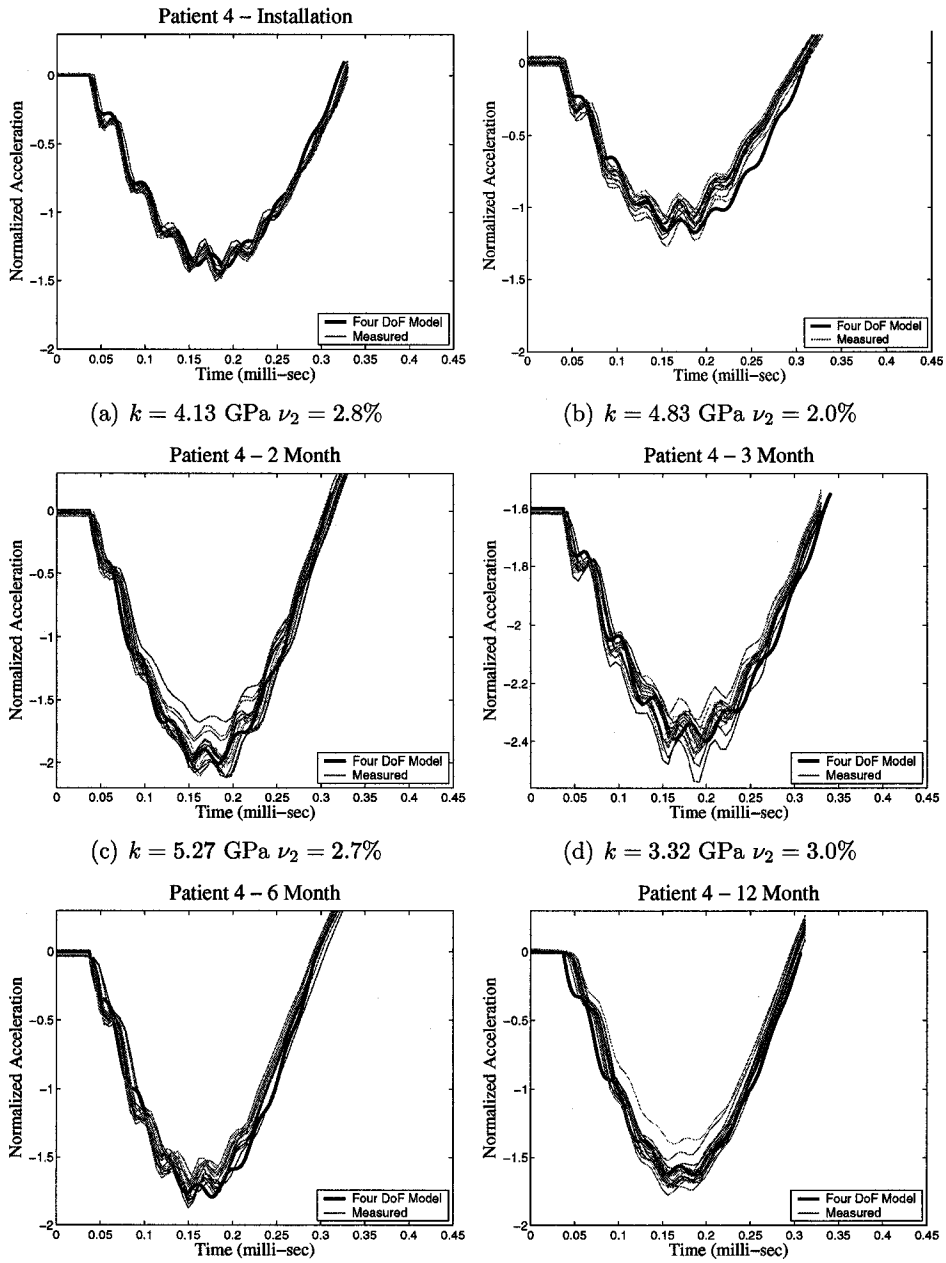


(a) $k = 4.13$ GPa $\nu_2 = 2.8\%$

(b) $k = 4.83$ GPa $\nu_2 = 2.0\%$

(c) $k = 5.27$ GPa $\nu_2 = 2.7\%$

(d) $k = 3.32$ GPa $\nu_2 = 3.0\%$

(e) $k = 6.52$ GPa $\nu_2 = 2.6\%$

(f) $k = 4.73$ GPa $\nu_2 = 3.9\%$

Figure C.4: Patient 4 acceleration measurement compared to predicted model response at different patient visits.

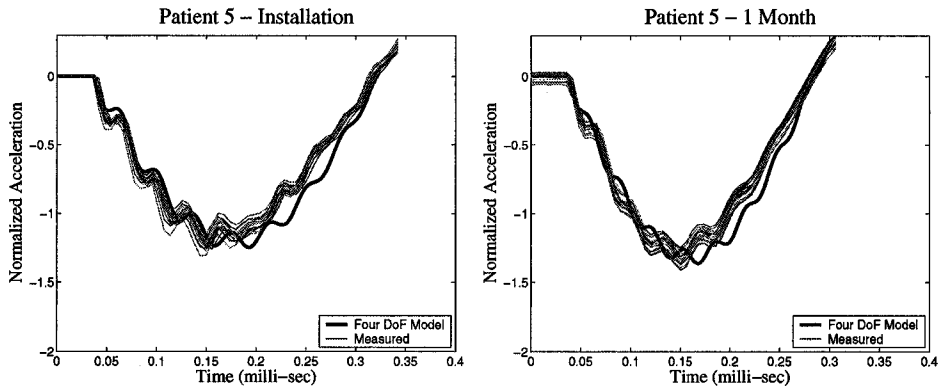


(a) $k = 3.96$ GPa $\nu_2 = 2.1\%$




(b) $k = 8.64$ GPa $\nu_2 = 2.1\%$

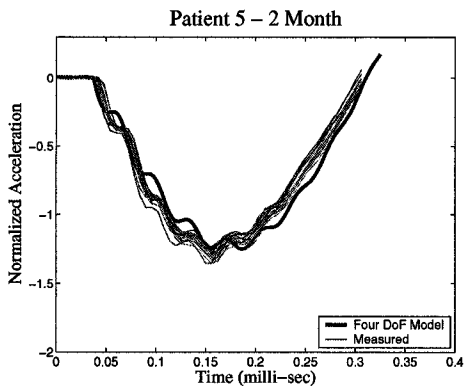


(c) $k = 4.68$ GPa $\nu_2 = 3.2\%$

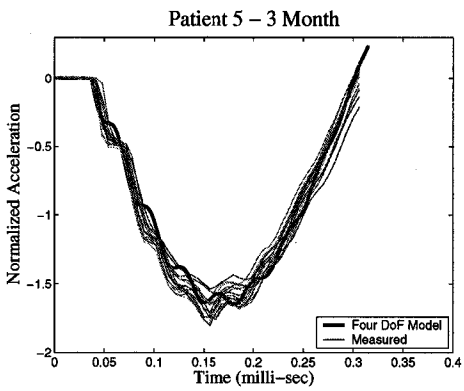


(d) $k = 5.65$ GPa $\nu_2 = 3.0\%$

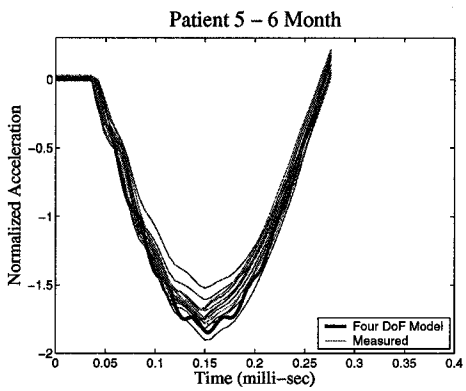


(e) $k = 15.2$ GPa $\nu_2 = 1.5\%$

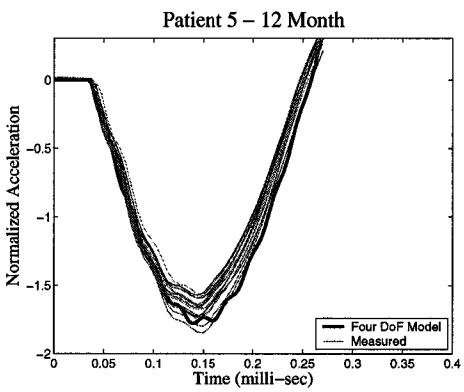


(f) $k = 32.0$ GPa $\nu_2 = 1.0\%$

Figure C.5: Patient 5 acceleration measurement compared to predicted model response at different patient visits.

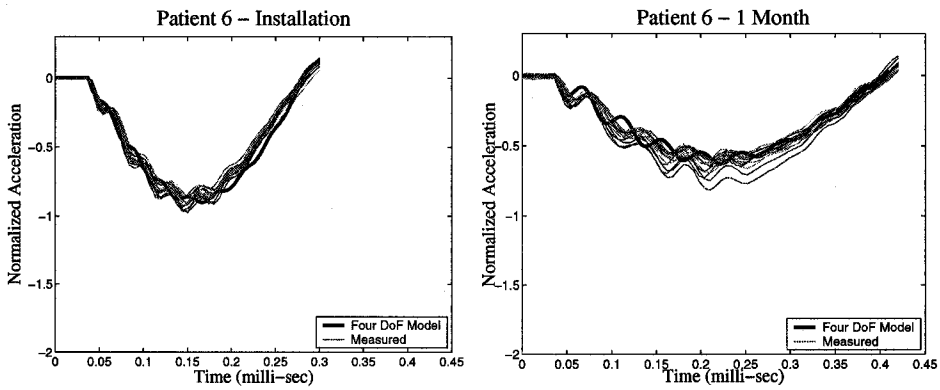


(a) $k = 9.11$ GPa $\nu_2 = 2.4\%$




(b) $k = 1.67$ GPa $\nu_2 = 3.6\%$

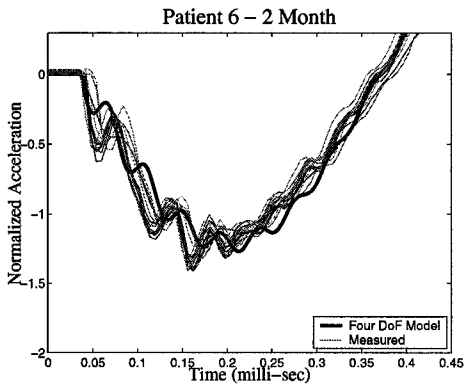


(c) $k = 2.23$ GPa $\nu_2 = 3.4\%$

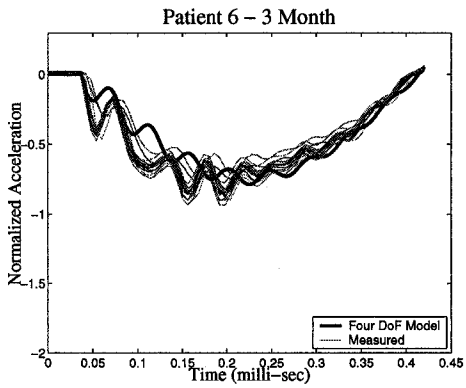


(d) $k = 1.53$ GPa $\nu_2 = 3.7\%$

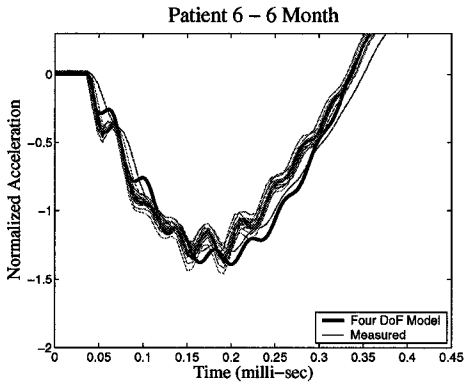


(e) $k = 3.27$ GPa $\nu_2 = 3.0\%$

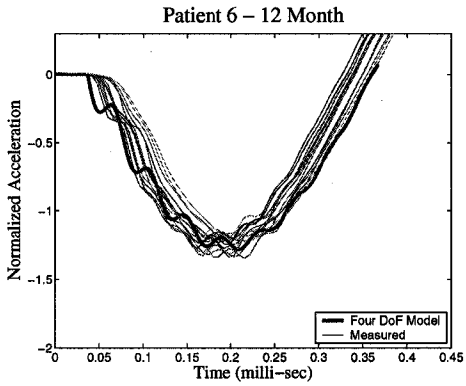


(f) $k = 2.47$ GPa $\nu_2 = 4.7\%$

Figure C.6: Patient 6 acceleration measurement compared to predicted model response at different patient visits.

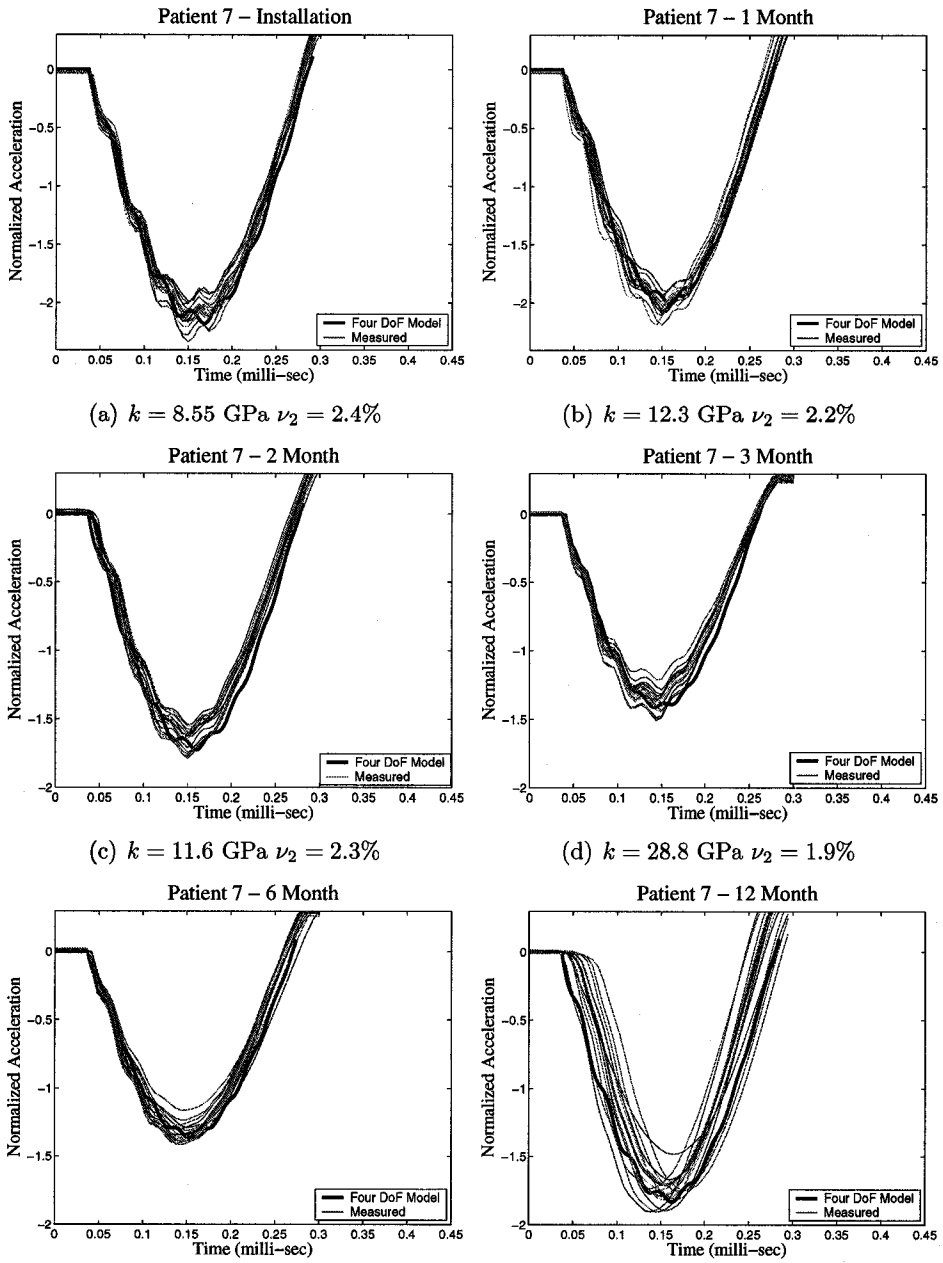


(a) $k = 8.55$ GPa $\nu_2 = 2.4\%$

(b) $k = 12.3$ GPa $\nu_2 = 2.2\%$

(c) $k = 11.6$ GPa $\nu_2 = 2.3\%$

(d) $k = 28.8$ GPa $\nu_2 = 1.9\%$

(e) $k = 15.6$ GPa $\nu_2 = 2.1\%$

(f) $k = 10.6$ GPa $\nu_2 = 3.3\%$

Figure C.7: Patient 7 acceleration measurement compared to predicted model response at different patient visits.

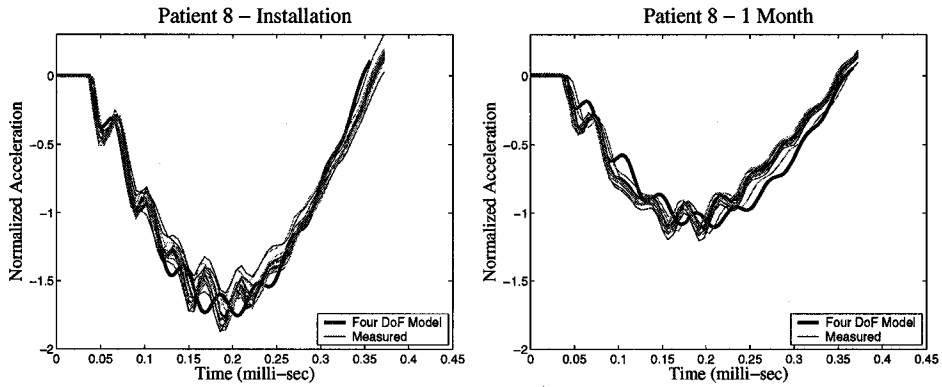


(a) $k = 2.79$ GPa $\nu_2 = 3.2\%$




(b) $k = 2.49$ GPa $\nu_2 = 3.3\%$

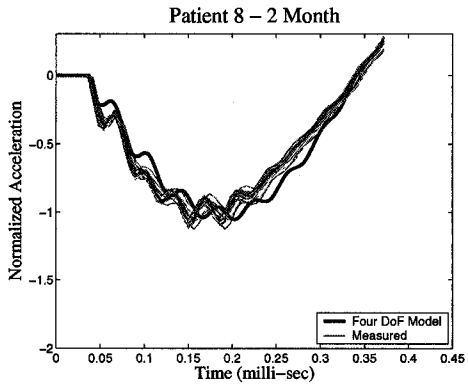


(c) $k = 3.02$ GPa $\nu_2 = 3.1\%$

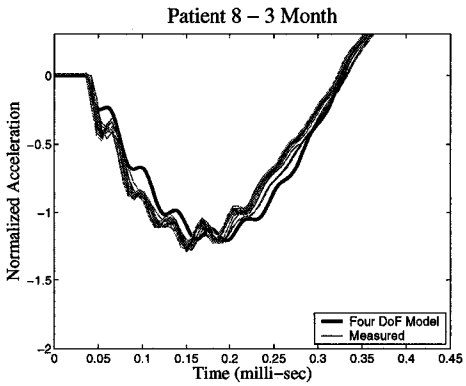


(d) $k = 3.66$ GPa $\nu_2 = 2.9\%$

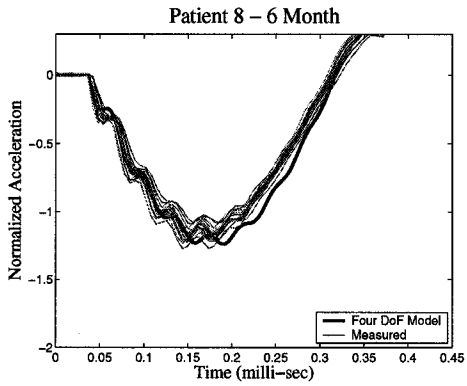


(e) $k = 4.29$ GPa $\nu_2 = 3.6\%$

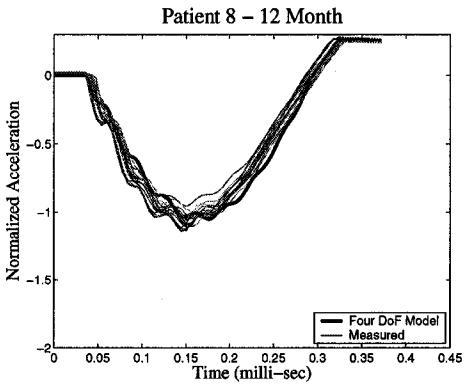


(f) $k = 6.66$ GPa $\nu_2 = 3.3\%$

Figure C.8: Patient 8 acceleration measurement compared to predicted model response at different patient visits.

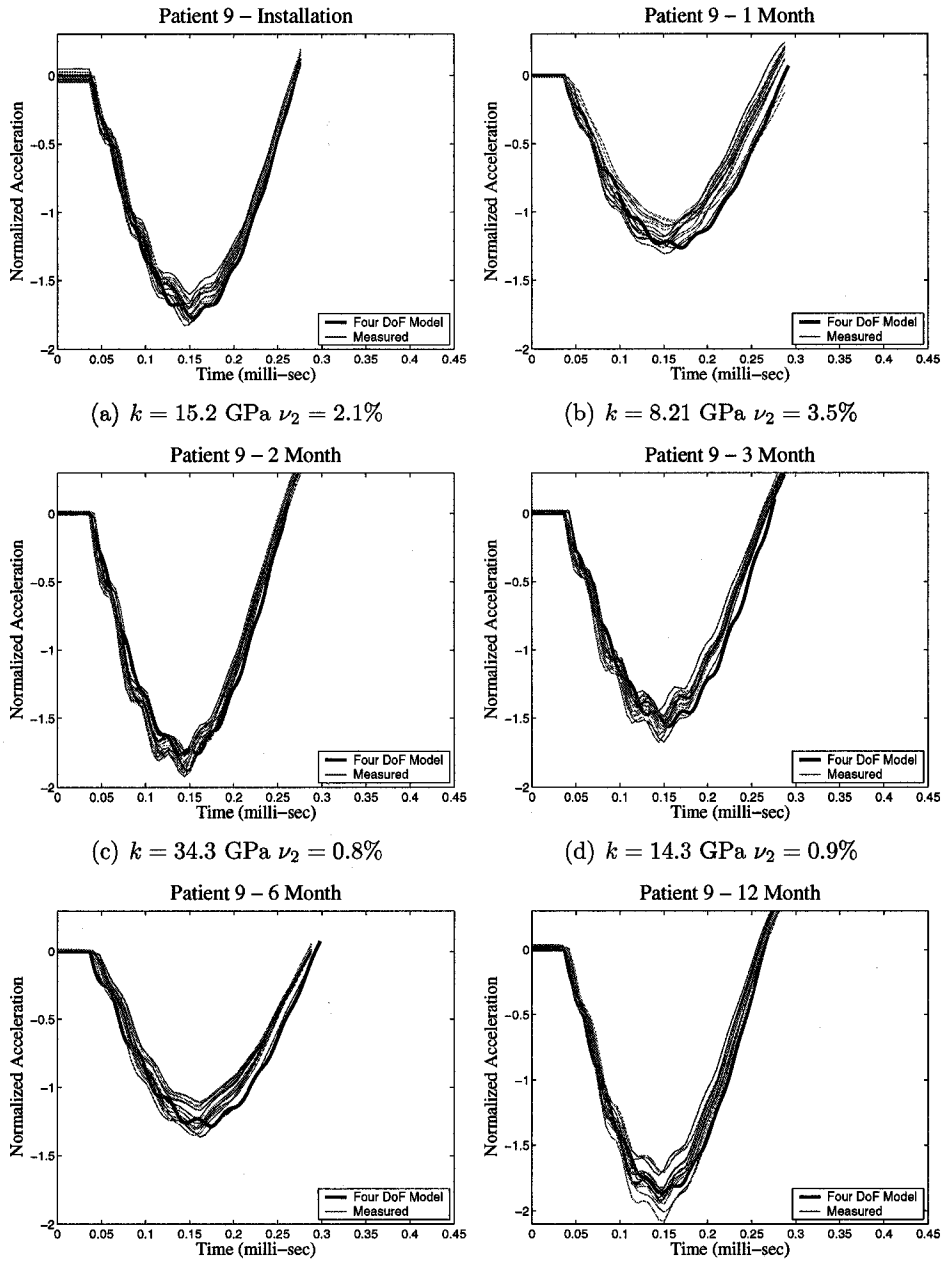


(a) $k = 15.2$ GPa $\nu_2 = 2.1\%$

(b) $k = 8.21$ GPa $\nu_2 = 3.5\%$

(c) $k = 34.3$ GPa $\nu_2 = 0.8\%$

(d) $k = 14.3$ GPa $\nu_2 = 0.9\%$

(e) $k = 7.05$ GPa $\nu_2 = 3.2\%$

(f) $k = 21.6$ GPa $\nu_2 = 2.6\%$

Figure C.9: Patient 9 acceleration measurement compared to predicted model response at different patient visits.

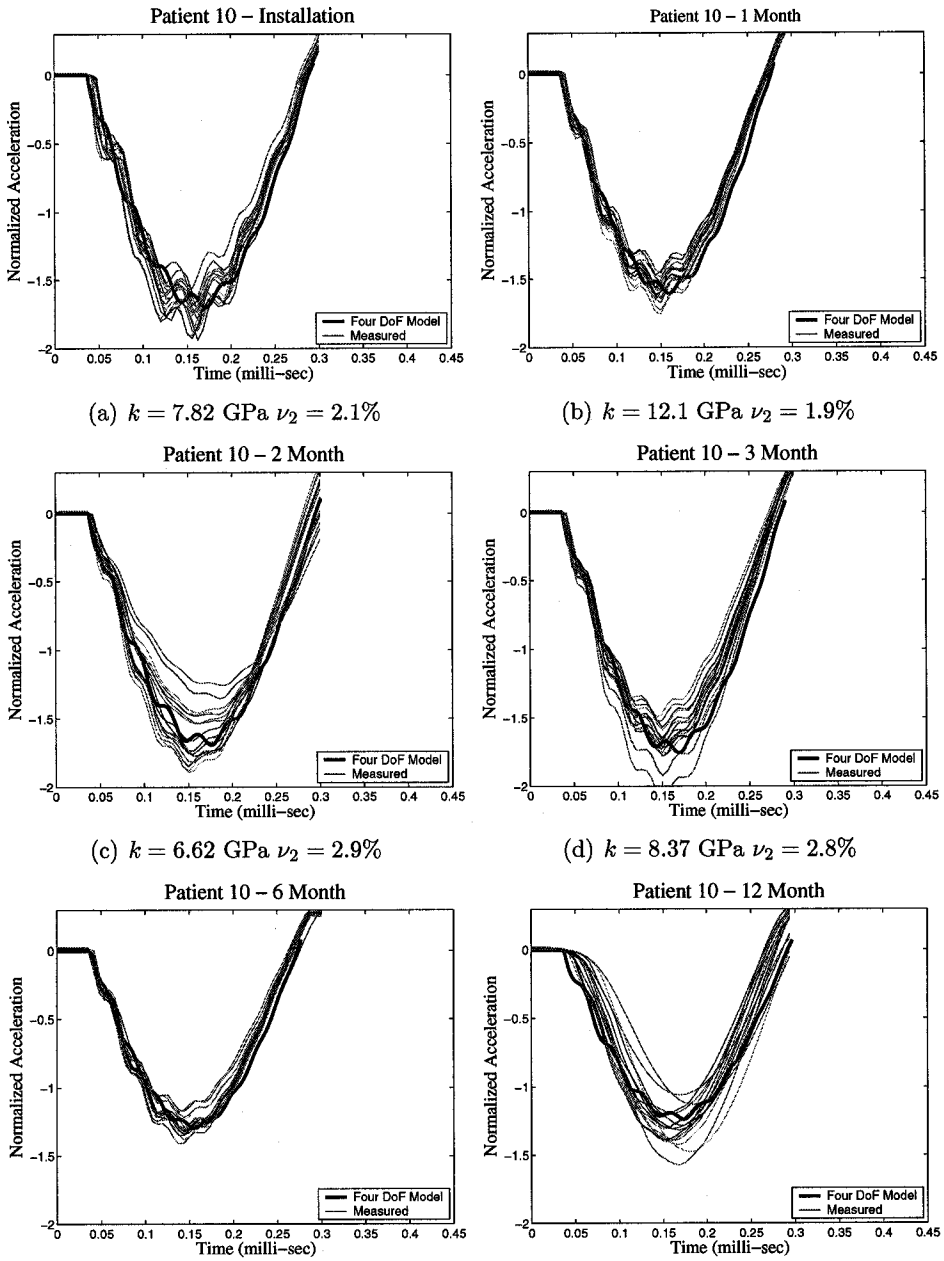


(a) $k = 7.82$ GPa $\nu_2 = 2.1\%$

(b) $k = 12.1$ GPa $\nu_2 = 1.9\%$

(c) $k = 6.62$ GPa $\nu_2 = 2.9\%$

(d) $k = 8.37$ GPa $\nu_2 = 2.8\%$

(e) $k = 13.8$ GPa $\nu_2 = 2.5\%$

(f) $k = 7.21$ GPa $\nu_2 = 3.6\%$

Figure C.10: Patient 10 acceleration measurement compared to predicted model response at different patient visits.

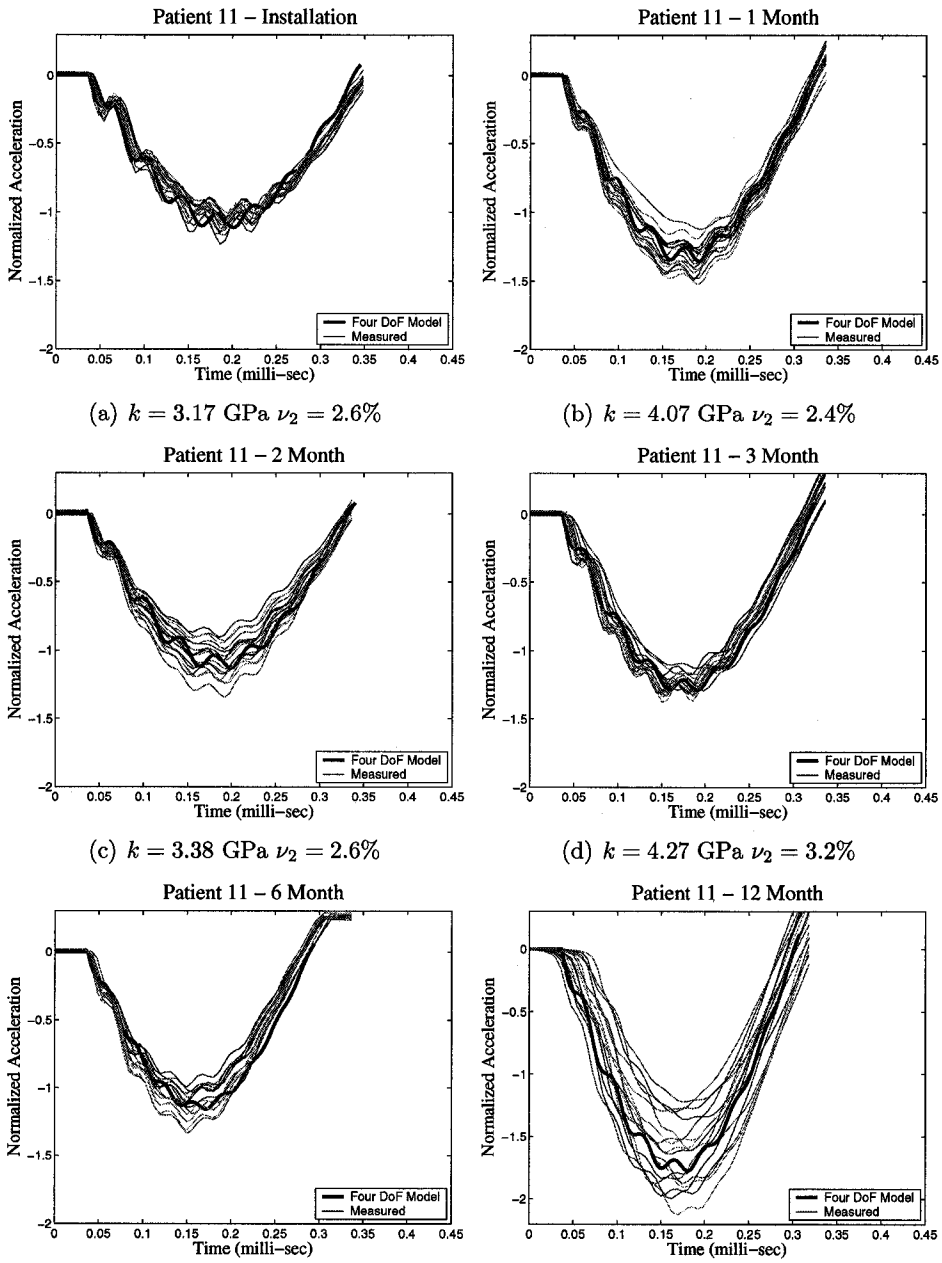


(a) $k = 3.17$ GPa $\nu_2 = 2.6\%$

(b) $k = 4.07$ GPa $\nu_2 = 2.4\%$

(c) $k = 3.38$ GPa $\nu_2 = 2.6\%$

(d) $k = 4.27$ GPa $\nu_2 = 3.2\%$

(e) $k = 7.72$ GPa $\nu_2 = 2.8\%$

(f) $k = 5.81$ GPa $\nu_2 = 3.0\%$

Figure C.11: Patient 11 acceleration measurement compared to predicted model response at different patient visits.

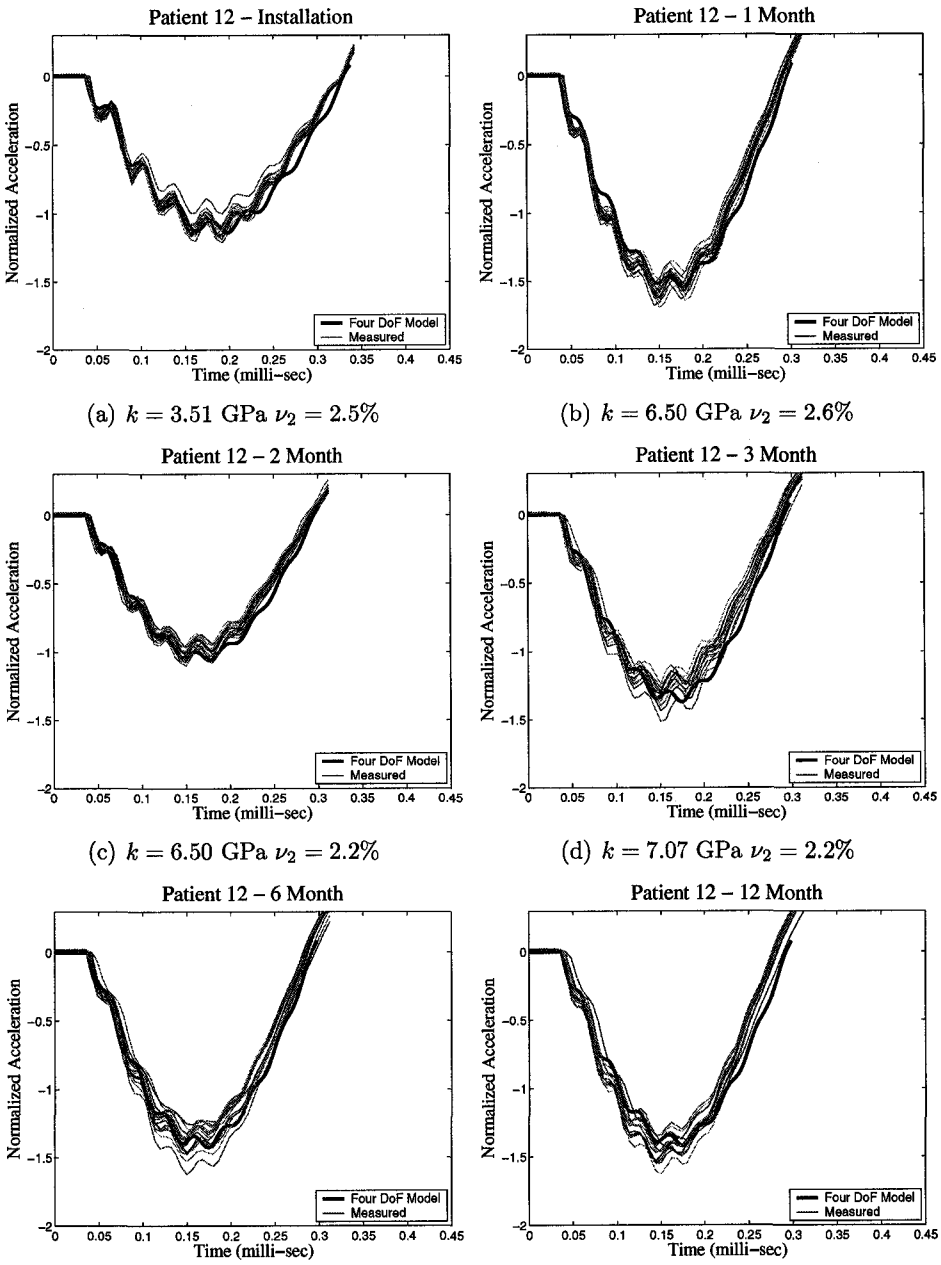


(a) $k = 3.51$ GPa $\nu_2 = 2.5\%$

(b) $k = 6.50$ GPa $\nu_2 = 2.6\%$

(c) $k = 6.50$ GPa $\nu_2 = 2.2\%$

(d) $k = 7.07$ GPa $\nu_2 = 2.2\%$

(e) $k = 7.12$ GPa $\nu_2 = 2.2\%$

(f) $k = 7.03$ GPa $\nu_2 = 2.2\%$

Figure C.12: Patient 12 acceleration measurement compared to predicted model response at different patient visits.